

134
11/2/80

DR. 463

ornl

ORNL/TM-6729

**OAK
RIDGE
NATIONAL
LABORATORY**



MASTER

**Oak Ridge TNS Program:
Study of Fueling Techniques
in Support of TNS
Development**

William Simpson

**OPERATED BY
UNION CARBIDE CORPORATION
FOR THE UNITED STATES
DEPARTMENT OF ENERGY**

DISTRIBUTION OF THIS DOCUMENT IS UNLIMITED

DISCLAIMER

This report was prepared as an account of work sponsored by an agency of the United States Government. Neither the United States Government nor any agency Thereof, nor any of their employees, makes any warranty, express or implied, or assumes any legal liability or responsibility for the accuracy, completeness, or usefulness of any information, apparatus, product, or process disclosed, or represents that its use would not infringe privately owned rights. Reference herein to any specific commercial product, process, or service by trade name, trademark, manufacturer, or otherwise does not necessarily constitute or imply its endorsement, recommendation, or favoring by the United States Government or any agency thereof. The views and opinions of authors expressed herein do not necessarily state or reflect those of the United States Government or any agency thereof.

DISCLAIMER

Portions of this document may be illegible in electronic image products. Images are produced from the best available original document.

Printed in the United States of America. Available from
National Technical Information Service
U.S. Department of Commerce
5285 Port Royal Road, Springfield, Virginia 22161
NTIS price codes—Printed Copy: A06 Microfiche A01

This report was prepared as an account of work sponsored by an agency of the United States Government. Neither the United States nor any agency thereof, nor any of their employees, makes any warranty, expressed or implied, or assumes any legal liability or responsibility for any third party's use or the results of such use of any information, apparatus, product or process disclosed in this report, or represents that its use by such third party would not infringe privately owned rights.

ORNL/TM-6729
Dist. Category UC-20 d

Contract No. W-7405-eng-26

FUSION ENERGY DIVISION

OAK RIDGE TNS PROGRAM: STUDY OF FUELING TECHNIQUES

IN SUPPORT OF TNS DEVELOPMENT

William Simpson
Advanced Energy Systems
Grumman Aerospace Corporation
Bethpage, New York 11714

Date Published: December 1979

DISCLAIMER
This book was prepared as an account of work sponsored by an agency of the United States Government. Neither the United States Government nor any agency thereof, nor any of their employees, makes any warranty, express or implied, or assumes any legal liability or responsibility for the accuracy, completeness, or usefulness of any information, apparatus, product, or process disclosed, or represents that its use would not infringe privately owned rights. Reference herein to any specific commercial product, process, or service by trade name, trademark, manufacturer, or otherwise, does not necessarily constitute or imply its endorsement, recommendation, or favoring by the United States Government or any agency thereof. The views and opinions of authors expressed herein do not necessarily state or reflect those of the United States Government or any agency thereof.

Prepared by the
OAK RIDGE NATIONAL LABORATORY
Oak Ridge, Tennessee 37830
operated by
UNION CARBIDE CORPORATION
for the
DEPARTMENT OF ENERGY

DISTRIBUTION OF THIS DOCUMENT IS UNLIMITED *rb*

THIS PAGE
WAS INTENTIONALLY
LEFT BLANK

CONTENTS

ABSTRACT	v
ACKNOWLEDGMENTS	vii
1. INTRODUCTION AND SUMMARY	1
2. FUELING DEVICES — INJECTION VELOCITY LIMITATIONS	7
2.1 GAS INJECTION (PUFFING)	9
2.2 GAS DYNAMIC	9
2.3 PNEUMATIC GUN	12
2.4 LIQUID JET	12
2.5 ROTATING HELIX	15
2.6 CENTRIFUGAL PELLET INJECTOR	18
2.7 HYPERVELOCITY ACCELERATORS	20
3. PELLET CHARACTERISTICS	25
3.1 MECHANICAL PROPERTIES	25
3.2 DETERMINING PELLET CAPABILITIES	31
3.2.1 Material Testing	32
3.2.2 Physical Tests with Accelerating Devices	33
3.3 ANALYSIS OF PELLET LOADS — CENTRIFUGAL PELLET INJECTOR	35
3.3.1 Dynamic Loads	35
3.3.2 Strain Rate	36
3.3.3 Interrelation of Materials	36
3.3.4 Friction Effects	36
3.3.5 Pellet Performance Summary	37
3.4 PELLET DELIVERY RATES	39
4. CANDIDATE INJECTORS	43
4.1 CENTRIFUGAL PELLET INJECTOR EVALUATION	45
4.2 PNEUMATIC GUN INJECTOR EVALUATION	49
4.3 LIQUID JET INJECTOR EVALUATION	52
4.4 MAINTENANCE	57
4.5 RELIABILITY	58
4.6 OPERATING REDUNDANCY	58
4.7 SAFETY	59

5. RECOMMENDATIONS	61
5.1 CENTRIFUGAL PELLET INJECTOR	61
5.2 PNEUMATIC GUN	61
5.3 FLUID INJECTOR	62
5.4 MATERIALS TESTING	62
5.5 TEST PROGRAM	63
REFERENCES	65
APPENDIX A — BIBLIOGRAPHY OF HYPERVELOCITY ACCELERATORS	67
APPENDIX B — CRYOGENIC PROPERTIES OF H, D, and T	69
APPENDIX C — FUEL PELLET INJECTION IMPACT FORCE	75
APPENDIX D — STRAIN RATE ASSESSMENT	81
APPENDIX E — STATIC PELLET LOADS	87
APPENDIX F — DYNAMIC ANALYSES FOR TWO ROTATING PARTICLE ACCELERATING DEVICES	91

ABSTRACT

To successfully refuel a magnetically confined plasma, the fuel must be delivered to the device in precise quantities with controlled quality. The fuel must also penetrate the plasma to a sufficient depth to be assimilated by the plasma while the individual injected fuel elements must be small enough to prevent unacceptably large, local plasma cooling. The fuel injector itself must be capable of continuous operation in a radioactive environment and compatible with the D-T fuel material. These general requirements serve as the criteria for this survey by establishing the range of allowable parameters for pellet mass and velocity and injector design.

The objective of this study was to survey fueling techniques and determine which approaches were compatible with the TNS requirements. Specifically, the following tasks were undertaken: survey of existing fueling concepts for use in TNS, determination of available physical properties for D-T fuel pellets, performance of preliminary load analysis of selected pellet acceleration machines, preparation of conceptual designs, and recommendations for follow-on work.

Based on the results of the review, three generic systems which met TNS requirements were recommended for further development. They are: the centrifugal pellet injector, the pneumatic gun, and the pressurized fluid injector. None of these systems is presently capable of meeting all of the TNS requirements; engineering problems still remain to be solved. There is some question as to the ability to scale these systems to deliver large D-T pellets at the required velocity.

The scope of the study did not permit detailed design or analyses of the recommended injector systems, but serious thought was given to recommended development areas pertinent to each device. The installation requirements have been outlined as well as design recommendations on maintainability and reliability.

THIS PAGE
WAS INTENTIONALLY
LEFT BLANK

ACKNOWLEDGMENTS

The author wishes to acknowledge the helpful assistance of Dr. P. Clark Souers (Lawrence Livermore Laboratory), Dr. R. J. Turnbull (University of Illinois), Dr. R. Flagg and Dr. J. Knowles (Physics International), and Dr. S. Milora, Dr. C. Foster, and J. Mayhall (Oak Ridge National Laboratory) in the preparation of this report.

R. Bullis, R. Botwin, T. Carpenter, I. Ojalvo, and A. Levy of Grumman contributed to this study and report.

1. INTRODUCTION AND SUMMARY

To successfully refuel a magnetically confined plasma, the fuel must be delivered to the device in precise quantities with controlled quality. The fuel must also penetrate the plasma to a sufficient depth to be assimilated by the plasma while the individual injected fuel elements must be small enough to prevent unacceptably large, local plasma cooling. The fuel injector itself must be capable of continuous operation in a radioactive environment and compatible with the D-T fuel material. These general requirements serve as the criteria for this survey by establishing the range of allowable parameters for pellet mass and velocity and injector design.

The objective of this study was to survey fueling techniques and determine which approaches are compatible with the TNS requirements. Specifically, the following tasks were undertaken:

- Survey of existing fueling concepts for use in TNS
- Determination of available physical properties for D-T fuel pellets
- Performance of preliminary load analysis of selected pellet acceleration machines
- Preparation of conceptual designs
- Recommendations for follow-on work.

While the TNS requirements have not been finalized, the following specifications were established for the study based on Ref. 1:

- Velocity 1-3 km/sec
- Pellet diameter 0.3-0.6 cm
- Pellet injection frequency 20-30 pellets/sec
- Fuel composition 50/50 mix deuterium/tritium
- Fuel density 0.25 g/cm⁻³ at 12K
0.26 g/cm⁻³ at 4K

Figure 1-1 shows the study plan. Initially the full spectrum of injector types was reviewed and the pellet requirements recorded. Parallel with this effort, available physical property data were

OBJECTIVE:
SURVEY FUELING
TECHNIQUES IN
SUPPORT OF TNS

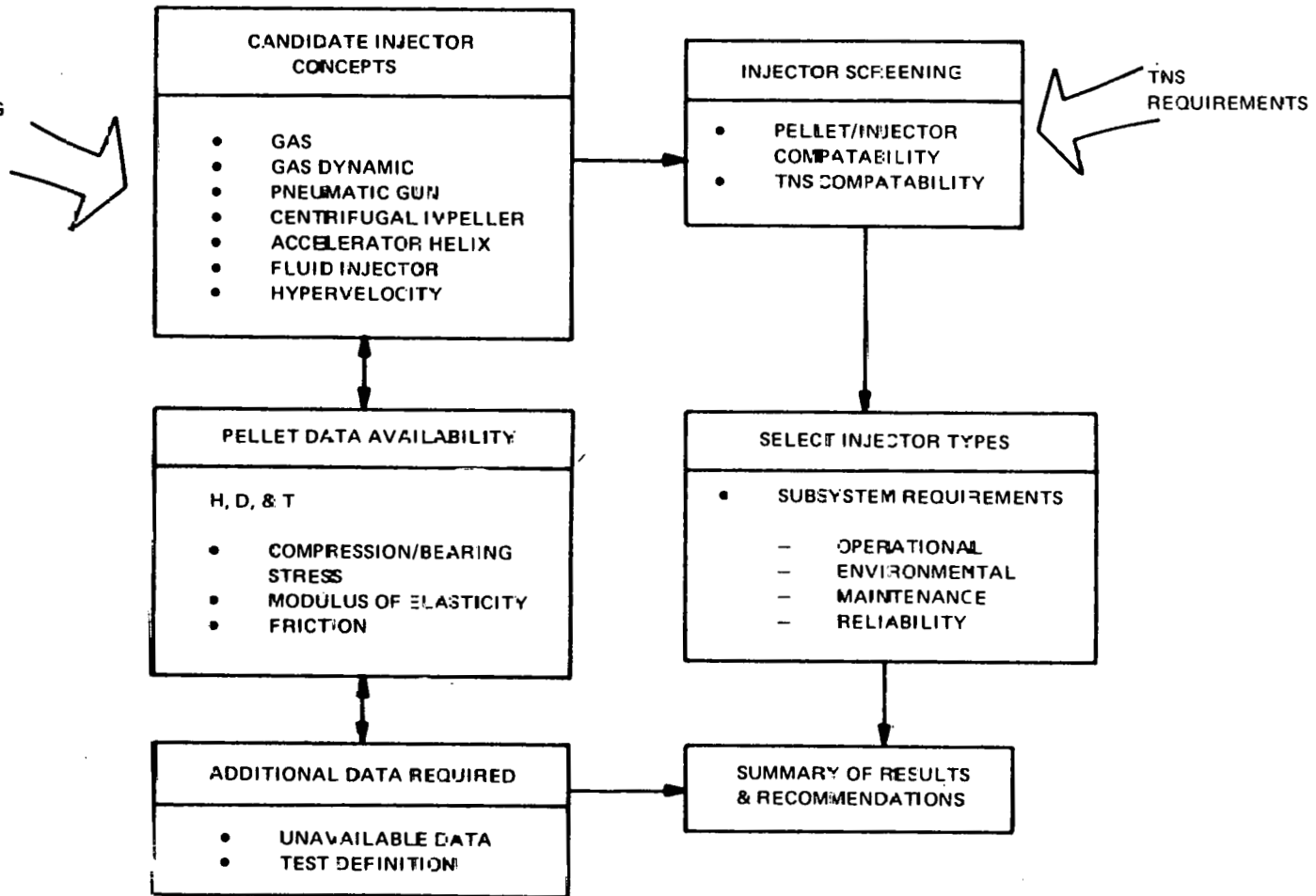


Fig. 1-1. Study plan - fueling techniques.

accumulated for H, D, and T pellets. A test program was outlined for the pellet data required but not available in the literature.

The study reviewed a number of potential fuel pellet injection systems. Additional injector types exist, but they were not considered since they have been discounted in other studies (e.g., Ref. 2). Utilizing the TNS requirements, the pellet injection systems were screened, and those not compatible with the TNS requirements were eliminated. For the surviving systems, a more detailed evaluation was made of injector subsystems including maintenance and reliability requirements.

Based on the results of the review (summarized in Fig. 1-2), three generic systems which met TNS design requirements were recommended for further development. They are:

- the centrifugal pellet injector
- the pneumatic gun
- the pressurized fluid injector.

Because these systems are in an early stage of investigation, all of their advantages and limitations are not well defined, and more development work is planned (subject to funding limitations). To date, there has been no combined testing for repetition rate, pellet velocity, and pellet size. Pellet velocities up to 1 km/sec and repetition rates of 150 pellets/sec have been attained in individual tests. The existing test designs use H and D pellets with injectors that deliver small pellets because 1 mm is the present limit for existing tokamaks. None of these systems is presently capable of meeting all of the TNS requirements; engineering problems still remain to be solved. There is some question as to the ability to scale these systems to deliver large D-T pellets at the required velocity. (This is particularly true for the pressurized fluid injector.)

The inherent lack of strength of D-T pellets limits the acceleration forces they can tolerate, thereby increasing the time required to reach injection velocity and increasing their thermal exposure in transit. It is strongly recommended that the essential mechanical properties of D-T be investigated so that injectors can be built which do not require excessive future modifications because of inaccurate material data.

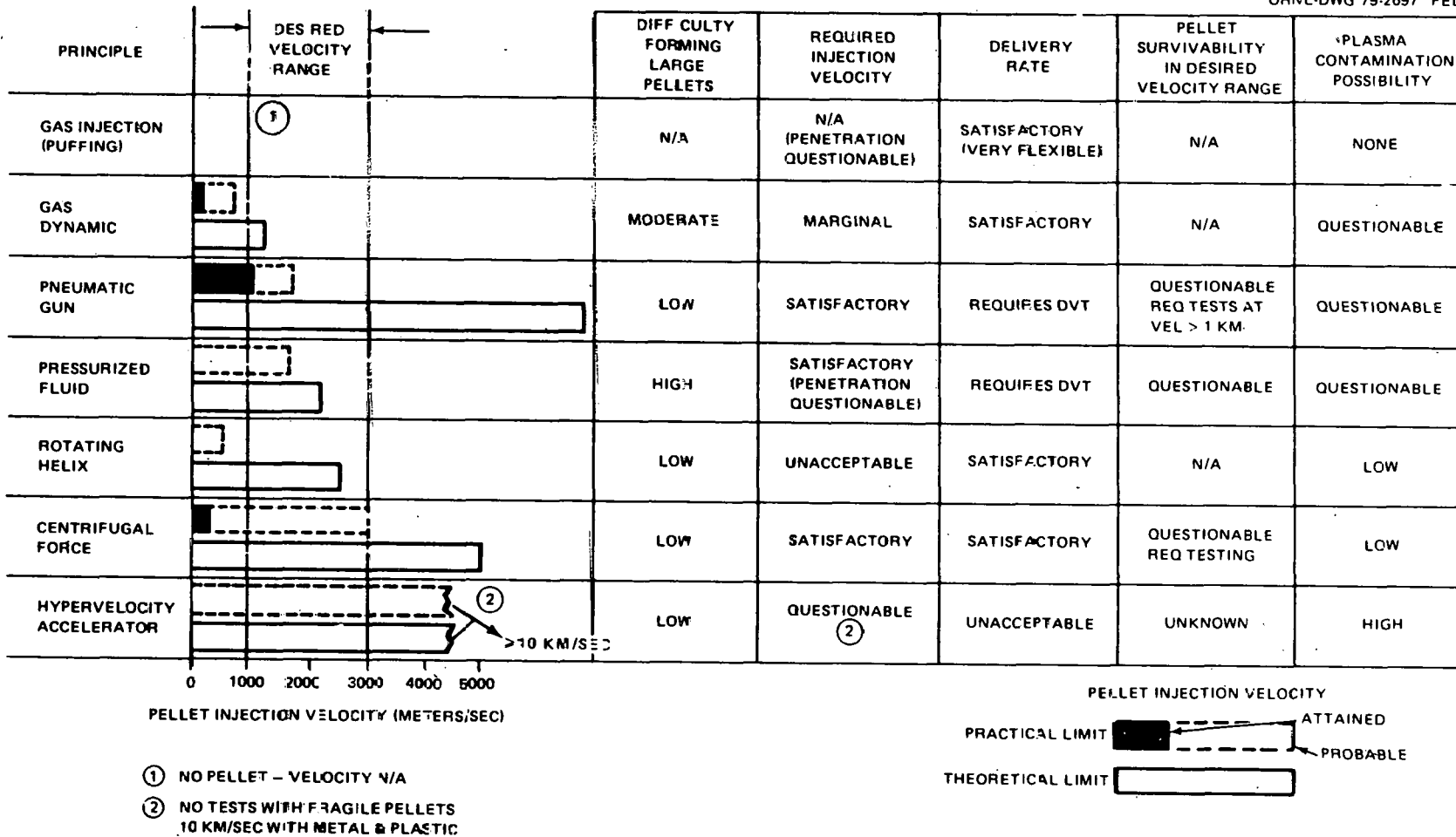


Fig. 1-2. Fuel injector comparisons.

The scope of the study did not permit detailed design or analyses of the recommended injector systems, but serious thought was given to recommended development areas pertinent to each device. The installation requirements have been outlined as well as design recommendations on maintainability and reliability.

While fueling is a serious concern, the effort for tokamaks is less than \$1 million per year, and a significant effort has existed for only three years. The recommendations of this report do not appear to be compatible with the present funding level for fueling.

THIS PAGE
WAS INTENTIONALLY
LEFT BLANK

2. FUELING DEVICES — INJECTION VELOCITY LIMITATIONS

Refueling processes at present are confined to initial fill or replenishing pumping losses. The means for continuous refueling will become important for experimental machines planned to operate in the next five to six years with actual 1-60-sec burn times which will require replenishment of lost fuel during the burn cycle.

Pellet injection experiments have been conducted on tokamaks to determine refueling requirements. This includes tests on ORMAK, ISX, and Pulsator, and more tests are anticipated in the future.

In the past, many theories were proposed which purported to establish the relation between pellet size, pellet velocity, and required plasma penetration. These theories disagreed in many cases by an order of magnitude or more. Recent theoretical and experimental work resulted in much better correlations. Typical of this are the results presented in Ref. 3.

The only present tokamak planned for D-T operations is the TFTR; other near-term machines are hydrogen-fueled. TNS is the planned test device for fusion power machines combining long duration burns using D-T fuel as well as systems aimed at solving the practical problems of extracting heat in a usable manner. While this study is directed to TNS objectives, an examination of the systems' hardware and the experience of other past and future experiments provides a perspective and background.

Hardware for solid fuel (H) pellets has been produced by several organizations, notably by the University of Illinois (gas dynamics). ORNL is developing a mechanical method using a centrifugal injector and a pneumatic gun. Fluid injection is being pursued by Physics International of San Leandro, California under a DOE contract. Pellet designs for inertial confinement machines have been pursued by many organizations, i.e., LLL, LASL, Battelle, University of Illinois et al., but the pellet construction is complex, and the containment shells of the fuel pellet (D-T) introduce undesirable impurities into a tokamak plasma. Figure 2-1 shows the injection devices that have been tested or are in hardware development.

TYPE	LOCATION	STATUS
GAS DYNAMIC	U. OF ILLINOIS/CRNL	TESTED ON ORMAK
PNEUMATIC GUN	ORNL	TESTED ON ISX-A & B
MECHANICAL SLINGER	ORNL	IN DEVELOPMENT
LIQUID JET	MAX-PLANCK INSTITUTE	IN DEVELOPMENT
PNEUMATIC GUN	MAX-PLANCK INSTITUTE	IN DEVELOPMENT
MECHANICAL SLINGER	MAX-PLANCK INSTITUTE	IN DEVELOPMENT
EXTRUSION/SOLID	MAX-PLANCK INSTITUTE	IN USE-STELLEFATOR AND PULSATOR
EXTRUSION/SOLID	EURATOM-RISO NAT'L LAB	IN USE-PUFFATRON

Fig. 2-1. Plasma fueling experiments/concepts.

Devices used to replenish lost fuel may be divided into three categories: those injecting pressurized fuel directly, those using pressurized neutral gas to propel a frozen pellet of D-T, and those using mechanical means to propel a frozen pellet of D-T.

The various fluid and pneumatic injection systems were evaluated to determine their theoretical velocity limitations and assess their practical limitations.

2.1 GAS INJECTION (PUFFING)

Injection of gas into a vacuum is one of the simplest, most flexible methods of fueling or refueling a tokamak. In essence, the system consists of a pressurized supply of gaseous fuel, a control valve which either meters a selected quantity of gas or modulates a continuous flow, and a tube or pipe leading to the plasma chamber. The pressurized gas reaches sonic or near-sonic velocities as it enters the plasma chamber. Figure 2-2 depicts the basic elements. In theory the system is simple and versatile, but a real installation is quite complex as shown in Fig. 2-3, the TFTR Gas Injection System. While this is the easiest method of refueling tokamaks, the mechanism is not fully understood and there are real questions whether gas injection will work in larger plasma devices such as TNG.⁴

2.2 GAS DYNAMIC

Gas dynamic injectors are typified by the device used for the pellet injection studies on ORMAK.⁵ A continuous stream of subcooled liquid hydrogen, formed by condensing hydrogen gas in helium-cooled heat exchangers, flows from a nozzle and is broken into uniform droplets by acoustic excitation. The individual droplets freeze and are accelerated by a rapid gas dynamic expansion through an acceleration tube.

Theoretically, these injectors can attain the sonic velocity of hydrogen, ~ 1300 m/sec. Practically, this type of injector is limited by the pressure difference across the acceleration tube and a reasonable length for the acceleration tube. ORMAK studies with a device built by

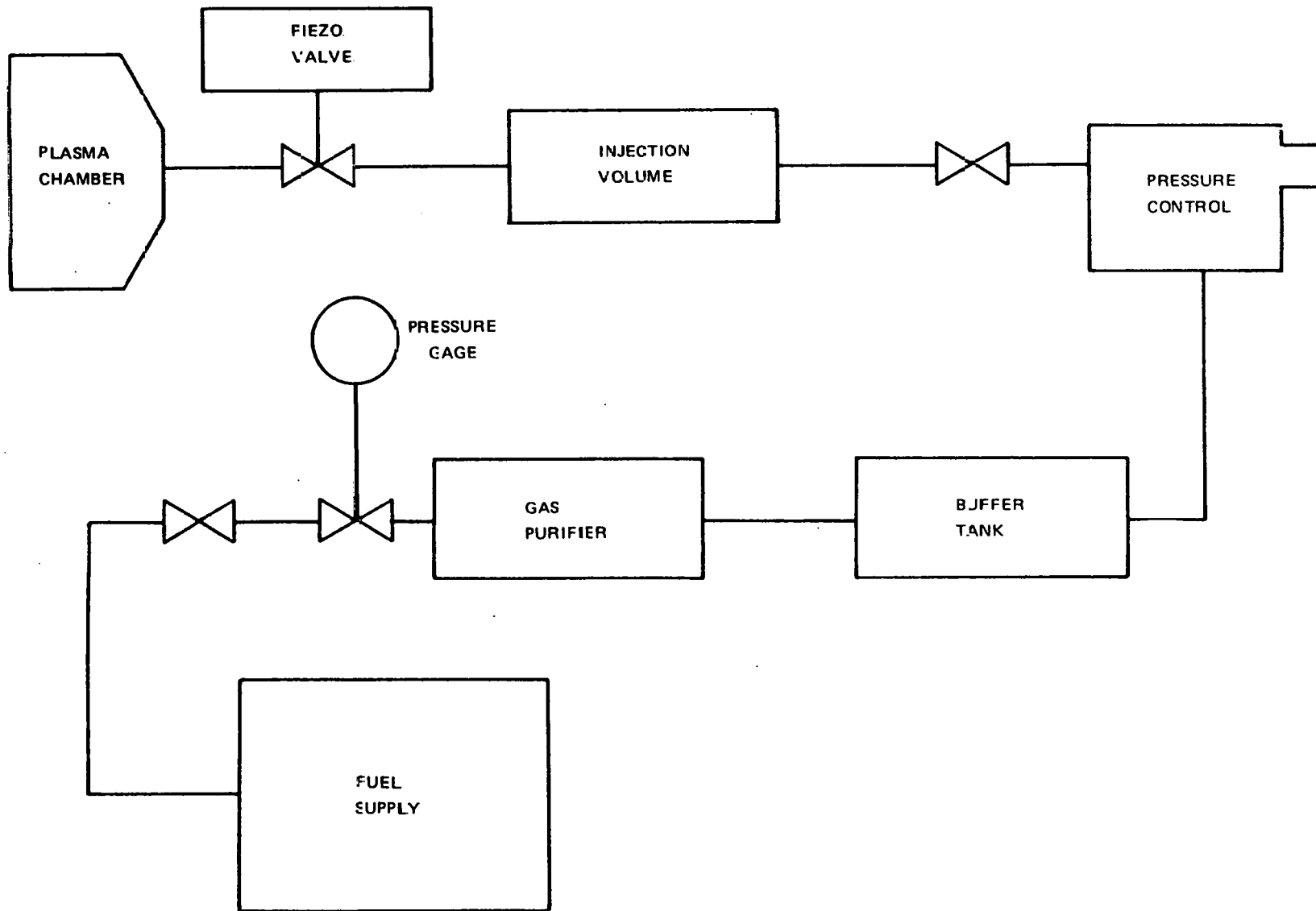


Fig. 2-2. Gas injection system.

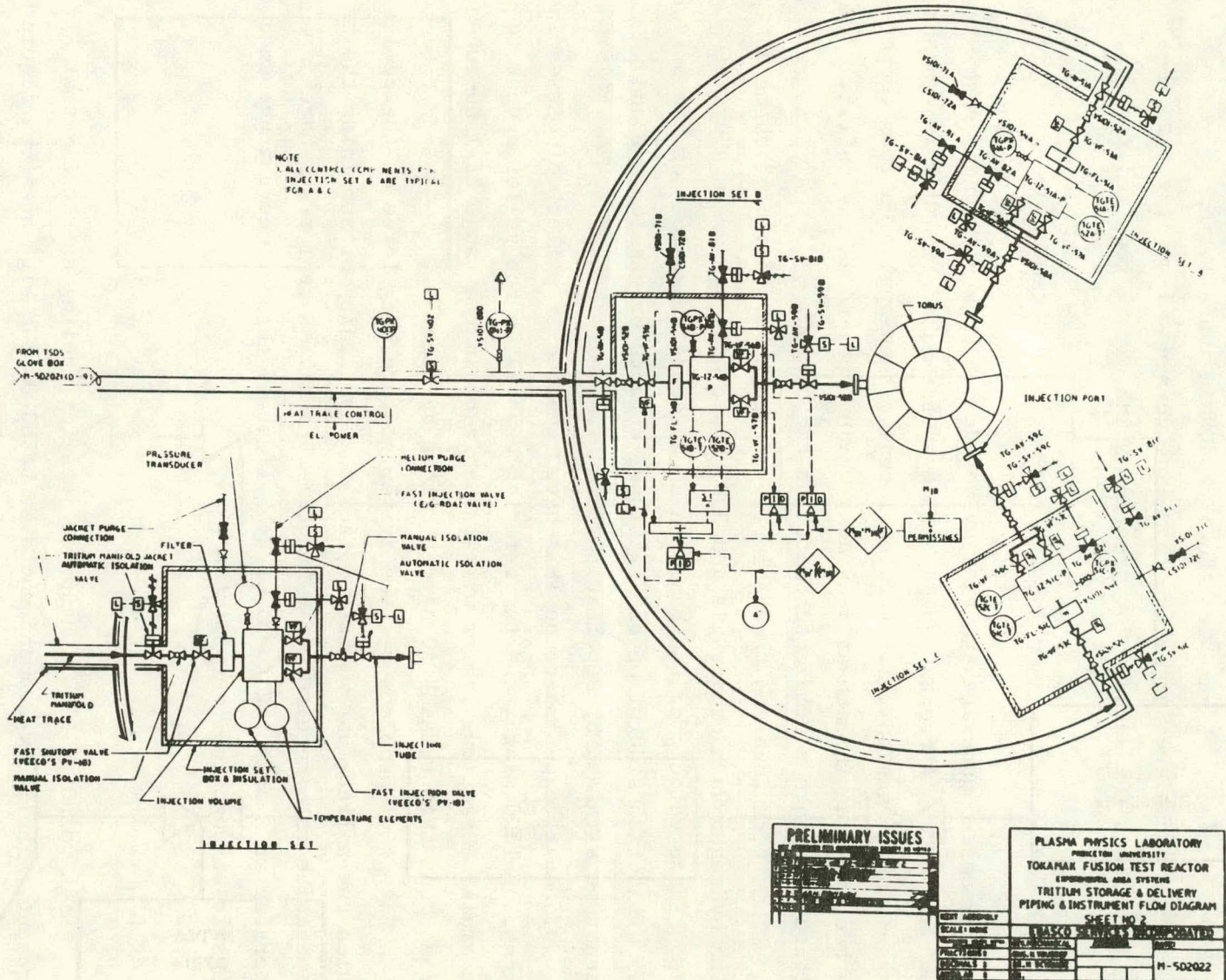


Fig. 2-3. TFTR gas injection system.

the University of Illinois have already obtained 100 m/sec pellet velocities, and practical limitations will probably result in velocities of 300-500 m/sec. Figure 2-4 shows the ORMAK installation.

This technique for pellet formation does not lend itself to the large pellets (0.5-cm diam or greater) which may be required for TNS.

2.3 PNEUMATIC GUN

Pneumatic guns are typified by the device presently under development at ORNL.⁶ A frozen, solid pellet is formed of liquid hydrogen and loaded into a gun barrel. A solenoid valve then applies a room temperature driver gas (helium at 8-29 atm) which accelerates the pellet. Figure 2-5 shows a simple schematic of the system.

This technique can theoretically attain a velocity of 6500 m/sec with hydrogen as a driver gas and 3000 m/sec with helium as a driver gas. These velocities are based on an unsteady expansion⁷ of the driver gas without consideration of frictional effects or gas leakage and cannot be attained by a pellet.

To date, experiments on ISX⁶ have resulted in pellet velocities in excess of 1000 m/sec, and the friction effects on the pellet appear to be small. Practical limits will probably be in the range of 1500-2000 m/sec, but this remains to be determined by test.

Potential problems are the driver gas crushing force on the pellet which the pellet must withstand, and the difficulty of attaining the repetition rate required (\sim 20-30 pellets/sec). Recent tests have operated at a crushing force of approximately three times the presumed tensile strength of the pellet.

2.4 LIQUID JET

High velocity liquid hydrogen jets for fueling do not exist at present. Their development would be based on the high pressure liquid jet technology presently being used in diesel fuel injectors.⁸ Typically, an injector would be fed liquid hydrogen at a pressure of \sim 7 atm and would then inject it at a pressure of 1500 atm or more. Expansion

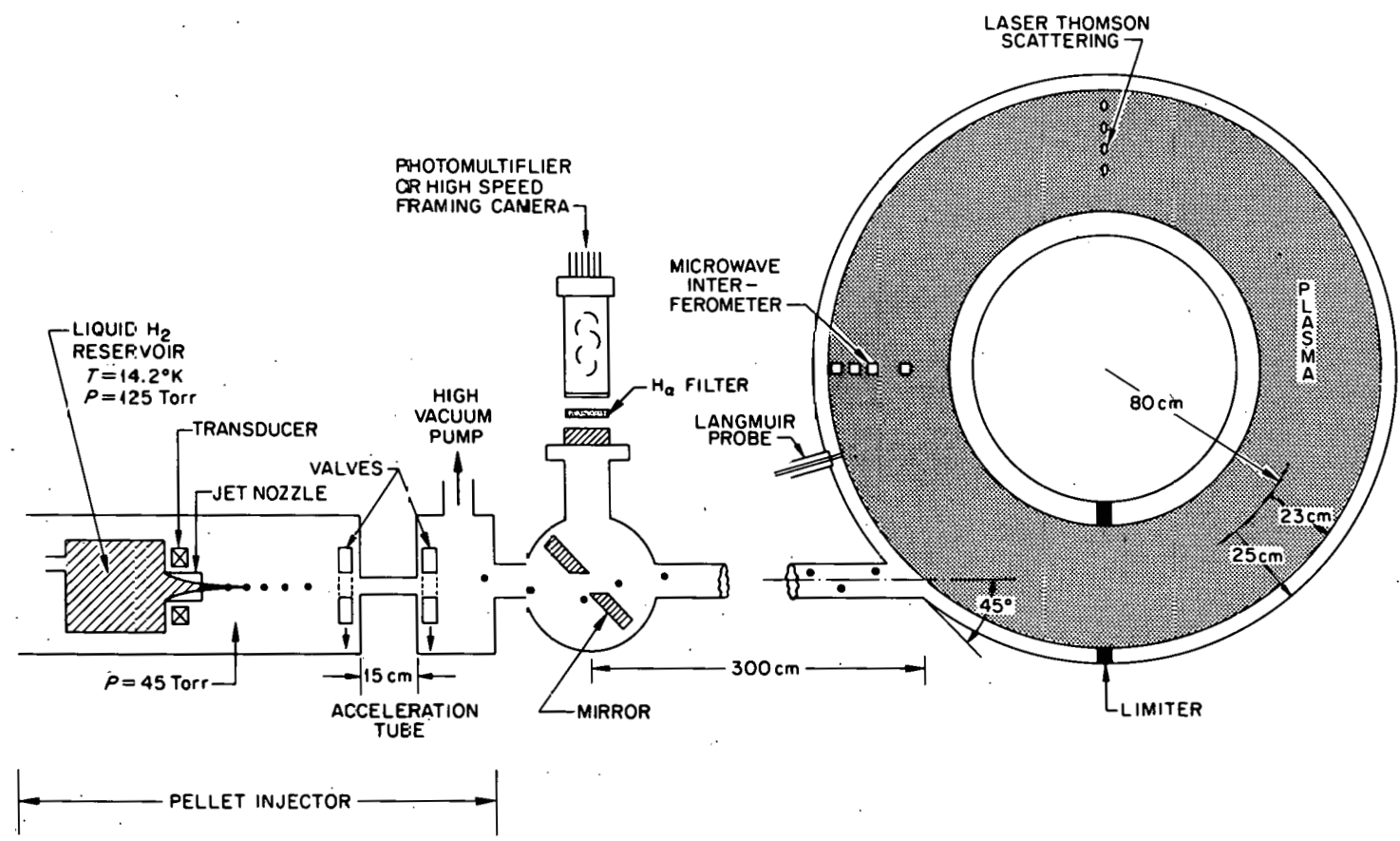
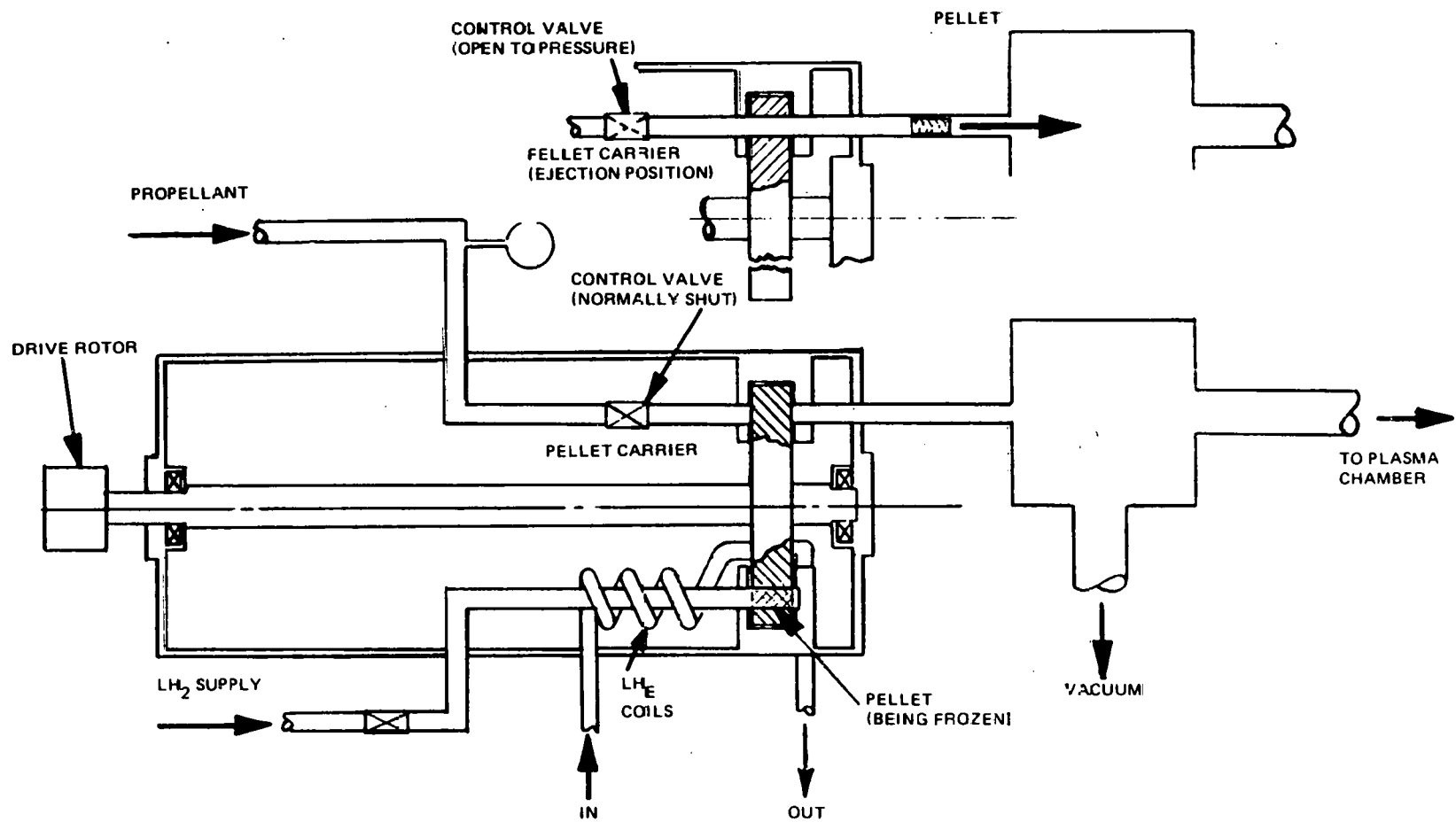


Fig. 2-4. Gas dynamic pellet injector (ORMAK).



14

Fig. 2-5. Pneumatic gun.

through a short nozzle would cause the pressure energy to accelerate the hydrogen to over 1500 m/sec. The jet would be broken into uniform droplets by acoustic excitation.

Theoretically, jet velocities ≥ 2000 m/sec can be achieved with pressures ≥ 2000 atm. Practically, the attainable velocity is questionable since adiabatic compression data for hydrogen is scarce in the high pressure range of interest.

Preliminary studies of this class of liquid jet indicate that pellets of 0.1-cm diam are attainable. However, this technique does not lend itself to the formation of large pellets (~ 0.5 -cm diam or greater) which may be required for TNS.⁹ Figure 2-6 depicts the principles of the liquid injector.

2.5 ROTATING HELIX

A mechanical pellet accelerator that theoretically can produce pellet velocities in the range desired (> 2000 km/sec) was suggested.¹⁰ The device, illustrated diagrammatically in Fig. 2-7, consists of a tubular housing containing a linear groove whose depth is one-half of the pellet diameter and a rotating roller fitted closely to the tubular housing. The roller has a helix cut into its surface with a constantly increasing pitch and a groove depth one-half the pellet diameter. A spherically shaped pellet was assumed so the grooves in both the housing and roller are semicircularly shaped. When the pellet is introduced into the housing groove and mated with the roller groove, rotation of the roller forces the pellet to move axially along the housing groove. The propelling action is produced by the roller helix angle force vector as the roller rotates, and the constantly increasing helix pitch accelerates the pellet. The proper combination of roller diameter, roller helix angle and angular velocity, and maximum practical helix angle (15 - 20°) governs the pellet acceleration.

The device has many favorable aspects: the pellet is positively controlled, timing can be accurately set, pellet mass and friction do not affect the machine operation, the exit trajectory is accurate, and the device produces no extraneous gases or wear materials that can

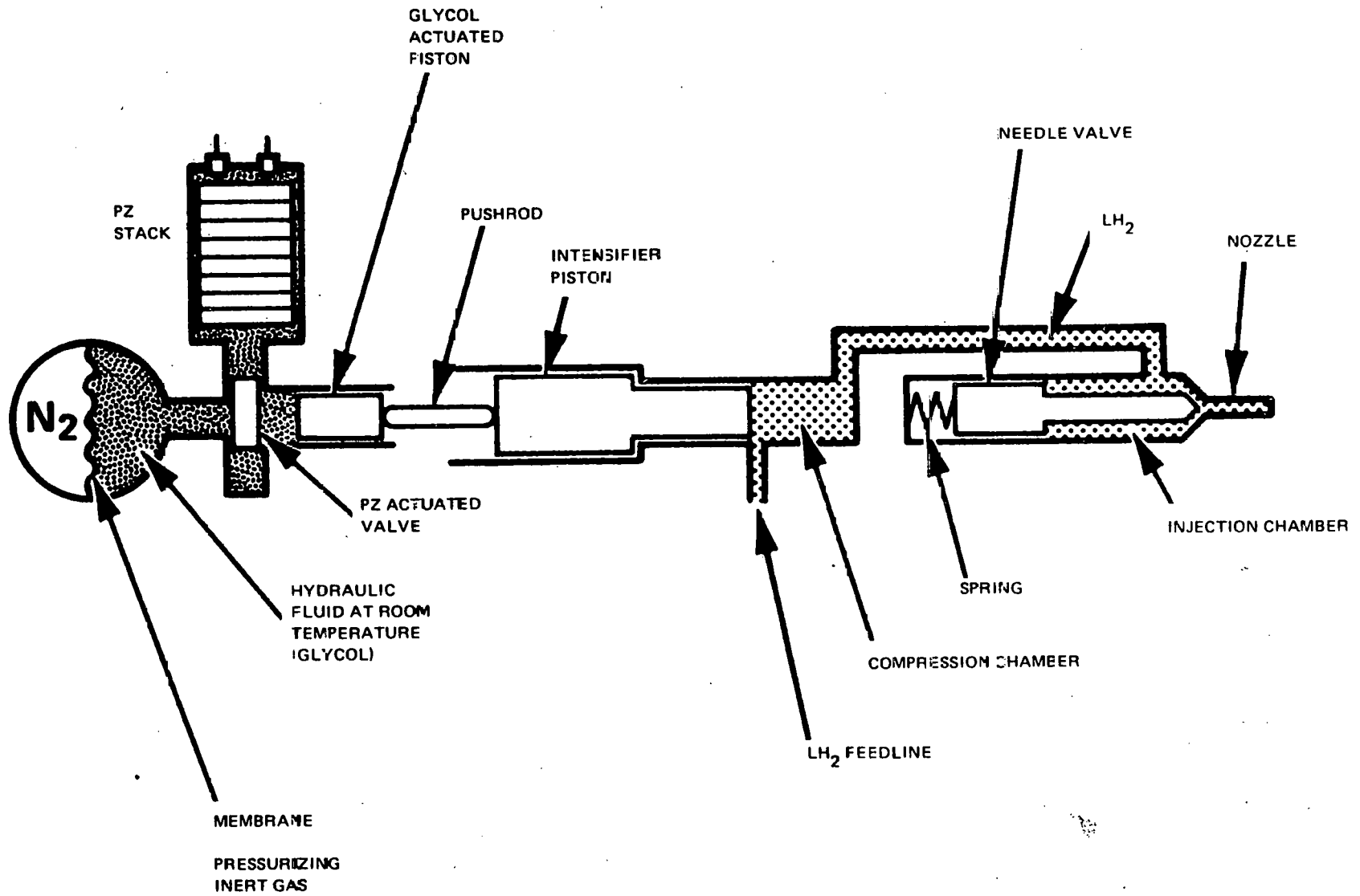
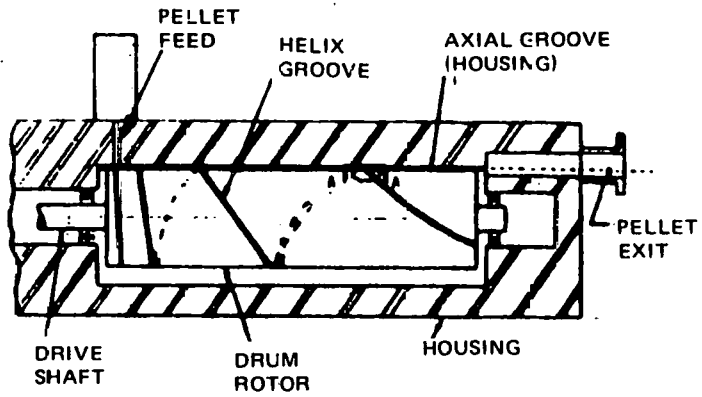
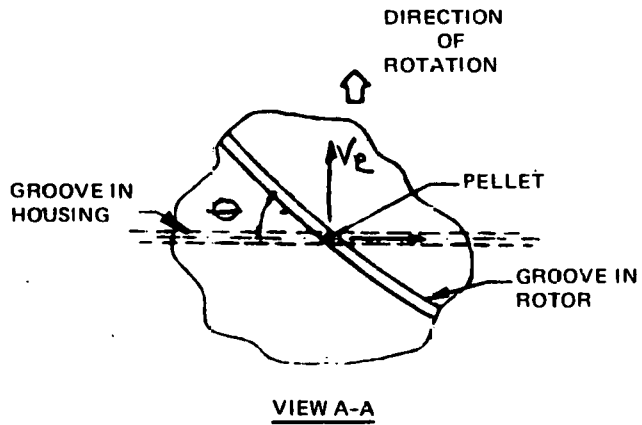
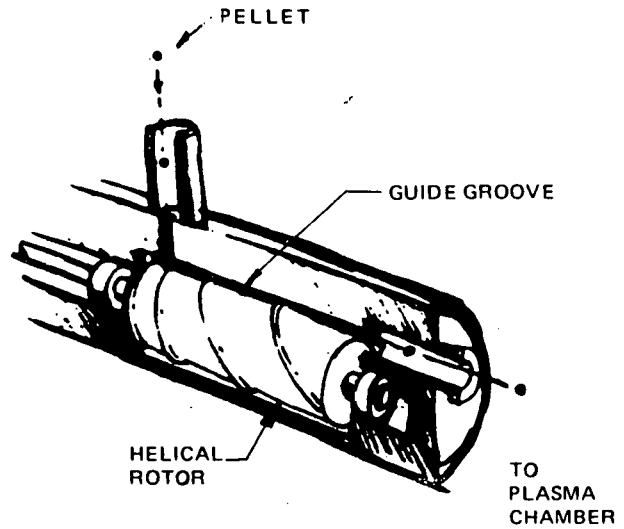


Fig. 2-6. Simplified sketch of LH₂ injector.



ACCELERATOR CROSS SECTION



VIEW A-A

Fig. 2-7. Accelerating helix injector.

migrate to the plasma chamber. The major objection to the device concerns the pellet, which can withstand only low forces. Time to accelerate is high, and the groove length is long (20 m). Therefore, pellet ablation and deformation due to rubbing and wear is a concern.

2.6 CENTRIFUGAL PELLETT INJECTOR

This injector mechanism provides the desired injection velocity by exerting centrifugal force on a fuel pellet. One concept involves a rapidly rotating disc spinning on a vertical axis. A formed track mounted on its upper face captures the fuel pellet, which is introduced to the upper face of the disc close to the central hub. The pellet is accelerated along the track by centrifugal force and leaves the disc through a tube connected to the plasma chamber. The rotational speed of the disc, disc diameter, track geometry, and pellet characteristics such as friction coefficient govern the ejection velocity and trajectory. Principal subassemblies of the injector mechanism are the rotating disc with its drive and the device that forms the solid (frozen) D-T pellets, as shown in Fig. 2-8.

The entire assembly is housed in a vacuum tight container with a tube that connects the main unit with the plasma chamber and serves as a clear passage for pellet entrance to the plasma chamber. The theoretical velocity of the rotating impeller disc, hence the pellet injection velocity, is limited by the strength of the impeller. With advanced composite materials and optimum conditions, a 5000-m/sec velocity can be achieved. With high strength-to-weight metals, 3500 m/sec may be the limit. These theoretical pellet velocity limits may be reduced due to friction effects and pellet strength limitations.

Proof of concept experiments conducted at ORNL have resulted in pellet velocities of 290 m/sec with 1-mm-diam pellets and a repetition rate of 150 pellets/sec. Other centrifugal injector concepts are presently under investigation, including an approach in which the impeller shears off the extruded pellet, which is deposited directly into the track.

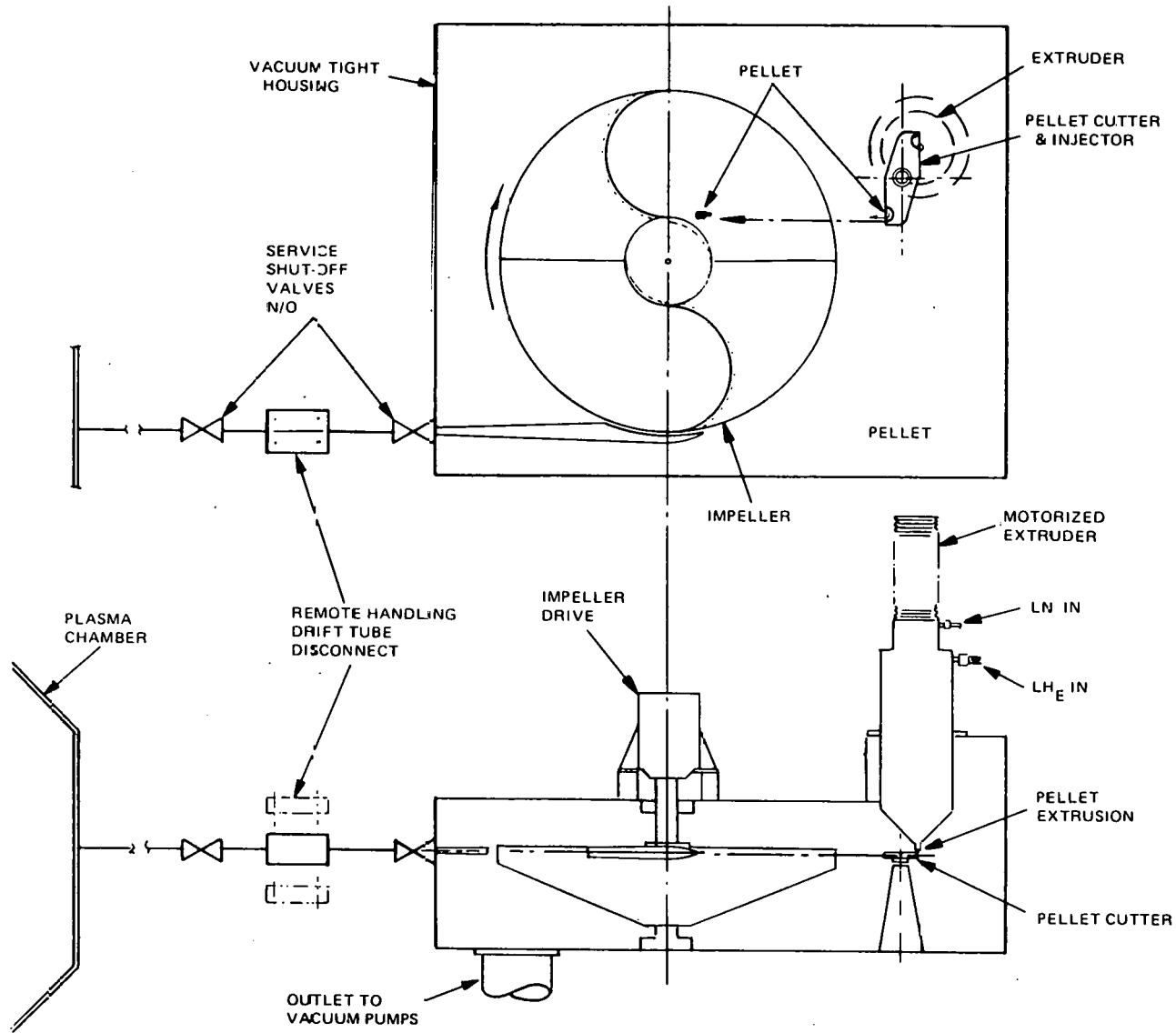


Fig. 2-8. ORNL centrifugal pellet injector.

2.7 HYPERVELOCITY ACCELERATORS

Hypervelocity accelerators or "light gas guns" have been developed for many applications including NASA sponsored studies of micrometeorite effects. Basically, a propellant or low temperature, high pressure gas is used to compress a driver gas to high temperature and pressure. The driver gas then pushes on the base of the projectile and expels it from a launch tube.

An extensive literature survey of hypervelocity accelerators was made and resulted in approximately 2000 different listings. Selected listings are presented in Appendix A.

The more commonly used light gas guns fall into two basic classifications. The first is a gun where gas is compressed adiabatically and isentropically by a slowly accelerated heavy piston. At a predetermined chamber pressure a break valve opens and the gas accelerates the projectile down the barrel. In early versions the tapered transition section was very short, and the piston was decelerated by the gas pressure in the pump tube or by jamming in the short taper. Significant advances in capability were achieved when the transition section was made a gentle taper as shown in Fig. 2-9. The heavy piston is of a readily deformable, low compressibility material (such as plastic) which is extruded through the taper and into the valve. A very high compression ratio is achieved, and the light gas reservoir is given a significant velocity component which is unavailable in other types of guns. This type of gun approaches the ideal — one in which the projectile base pressure is held constant, just below the projectile design limit, during the launch cycle.

The second is the adiabatic, nonisentropic compression gun. The reservoir of high enthalpy gas is produced by single or multiple reflections of a strong shock wave within the pump tube. Figure 2-10A shows a no-piston type making use of a single shock wave reflection. If a lightweight piston is used, multiple shock reflections occur between the front face of the piston and the pump tube, resulting in a higher temperature reservoir of gas. This is used in a three-stage shock heated gun (Fig. 2-10B) which, in effect, uses a light gas gun to accelerate the piston. The disadvantage of this type is that it does not approach

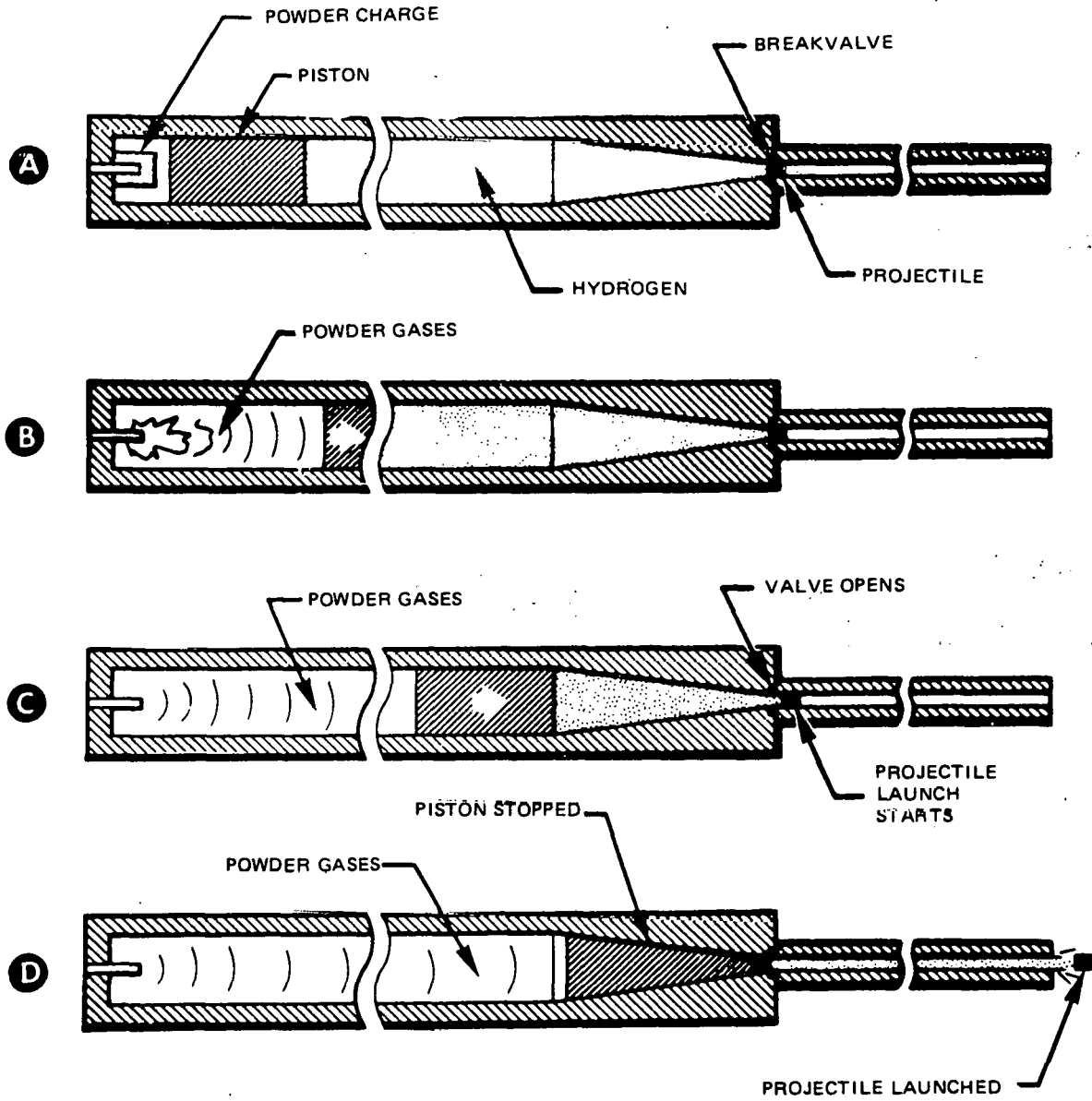
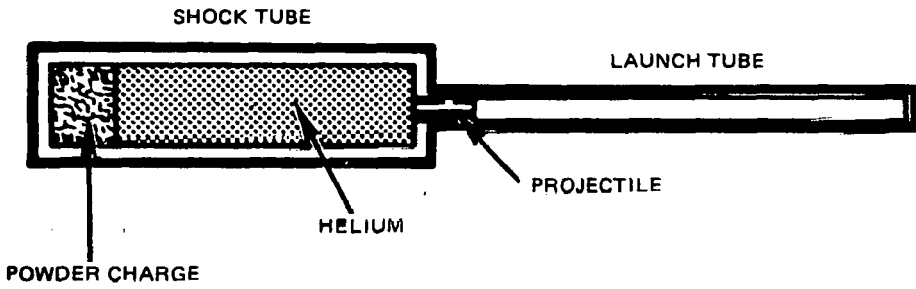


Fig. 2-9. Accelerated reservoir light gas gun.

A



B

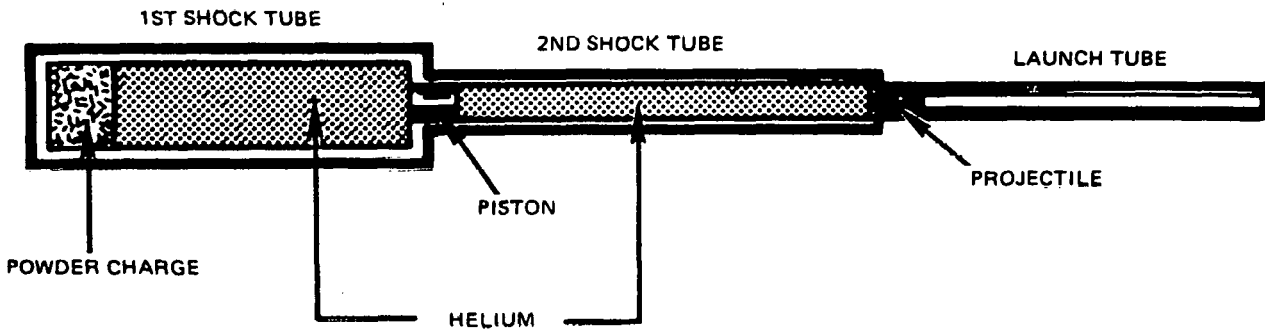


Fig. 2-10. Shock compression light gas gun.

ideal gun performance, and the strong shock waves make it difficult to launch sophisticated projectiles.

Hypervelocity accelerators are capable of handling the velocity and pellet mass combinations needed for TNS with high strength (metallic or plastic) pellets. This is readily seen in the evaluation by R. Flagg of Physics International which is presented as Fig. 2-11. However, the use of frozen hydrogen or D-T as a pellet presents serious pellet integrity concerns for this type of injector due to pellet shock, acceleration, and frictional heating in the barrel.

These devices are basically single-shot injectors. Even with multiple guns it is not apparent that the TNS repetition rate can be attained. A variation suggested by Flagg⁷ is the use of multiple injectors (e.g., six or seven tubes) driven by a single gun which could provide multiple pellets in a "burst" mode. Multiples of this type could be employed. However, even this approach does not appear to have the capability of satisfying TNS, which will require a constant stream of pellets.

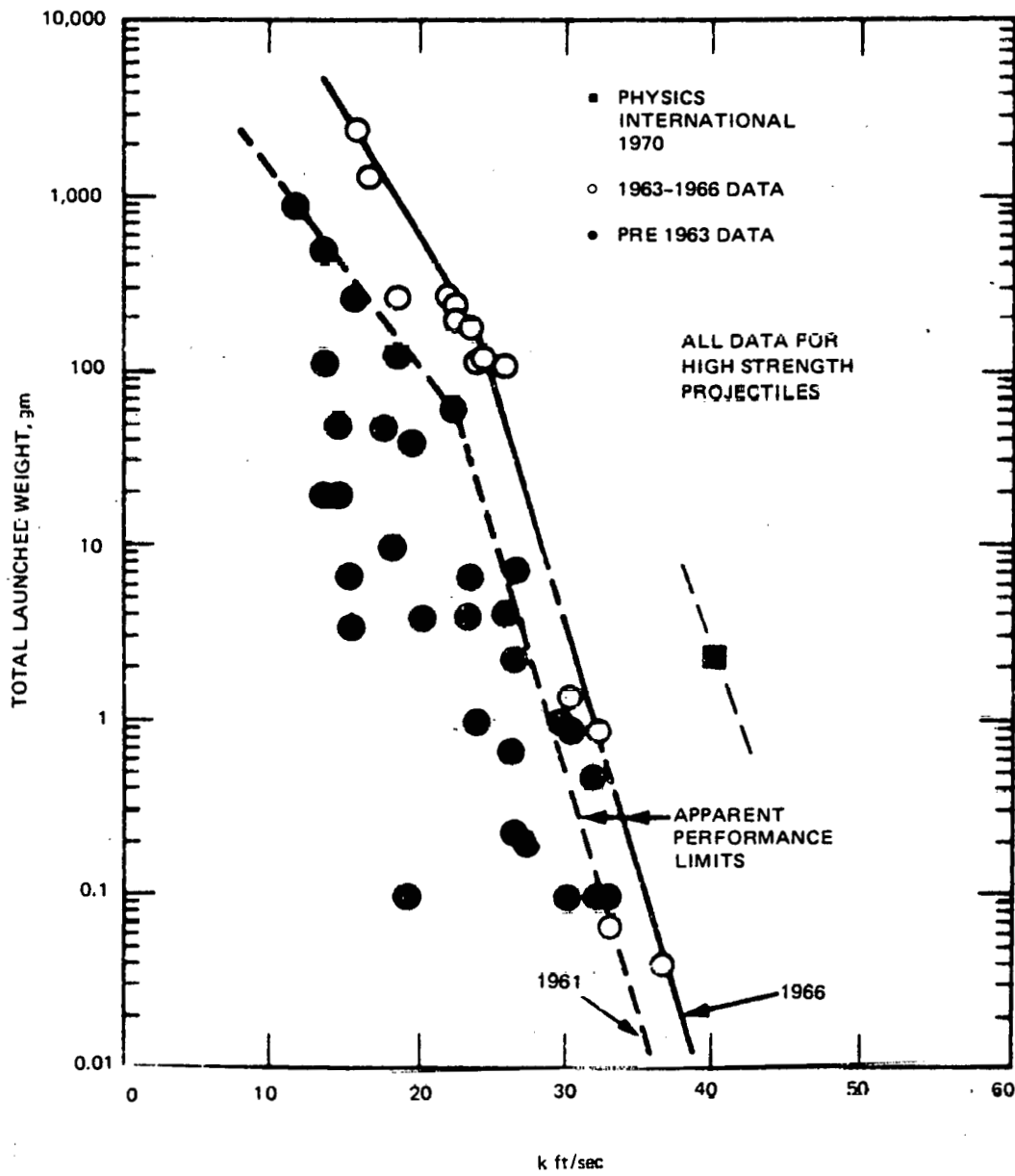


Fig. 2-11. Maximum launch velocities and weights.

3. PELLET CHARACTERISTICS

3.1 MECHANICAL PROPERTIES

Analysis of various injection devices used to accelerate and inject solid fuel pellets at high velocities has shown that their successful operation is highly dependent on the physical properties of the pellet. Therefore, it is necessary to know the properties of the pellet and of materials contacting the pellet. Near-term experimental tokamaks are to be fueled by solid hydrogen pellets. Fusion demonstration projects and actual power generators will use frozen D-T. Many of the pellet mechanical properties are untested, and hydrogen and D-T pellets are suspected to be relatively fragile. Since the proposed devices seem to impose relatively high loads on the pellets, velocities may have to be reduced to limit loads. The use of these devices is relatively new, and investigations of devices and methods of accelerating pellets to the proposed velocities have illustrated the lack of information concerning material properties that influence analysis and tend to reduce confidence in designs. Figure 3-1 tabulates the desired mechanical properties and illustrates the large areas where information is lacking.

It was beyond the scope of the study to investigate all material properties, but the literature search performed plus personal contacts with individuals and centers concerned with fuel pellets and fueling — notably LLL and LASL — have substantially covered areas where the major gaps occur.

One of the few sources describing mechanical properties of frozen hydrogen based on experimental results was found in Ref. 11. Figure 3-2 illustrates some of the tested properties of hydrogen and deuterium at cryogenic temperatures, all made on tensile specimens.

Appendix B describes the vapor pressure, compressibility, density, and heat of sublimation for H, D, T, and D-T (estimated) based on correlations with known data as compiled by P. C. Souers of LLL.¹²

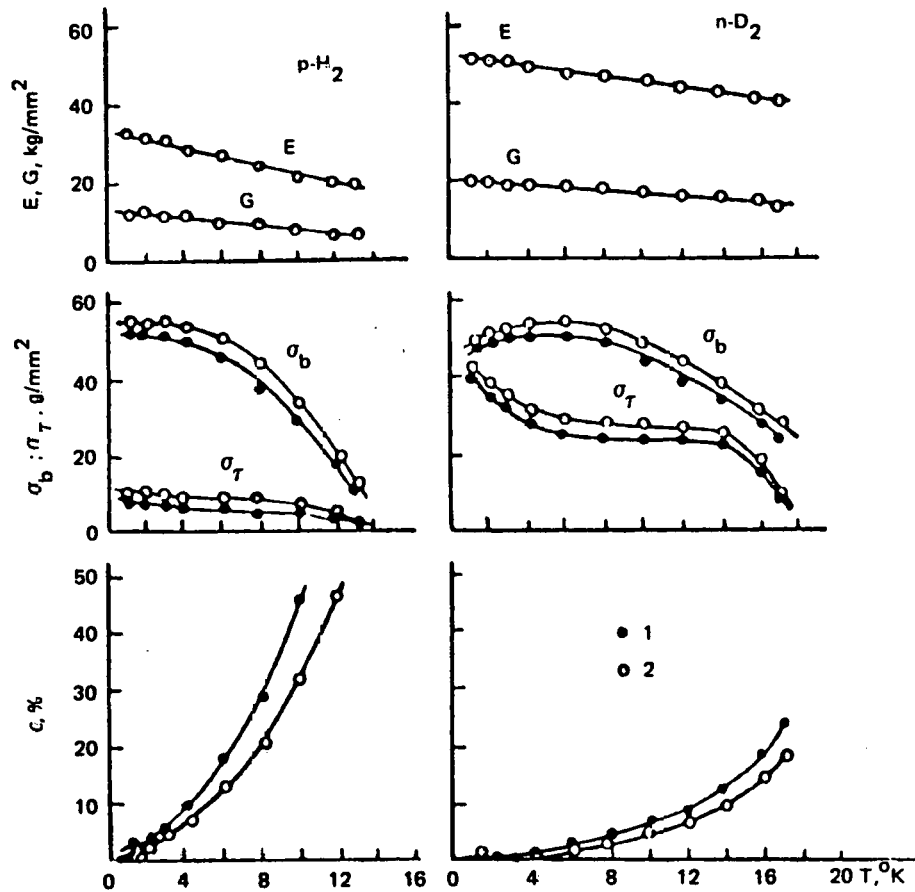
Due to the lack of information on D-T properties, the experimental deformation characteristics of solid D₂ have been studied from 1.4–16.4K (Ref. 13). In Fig. 3-3 we summarize that data. Figure 3-4 is included

ORNL-DWG 79-2714 FED

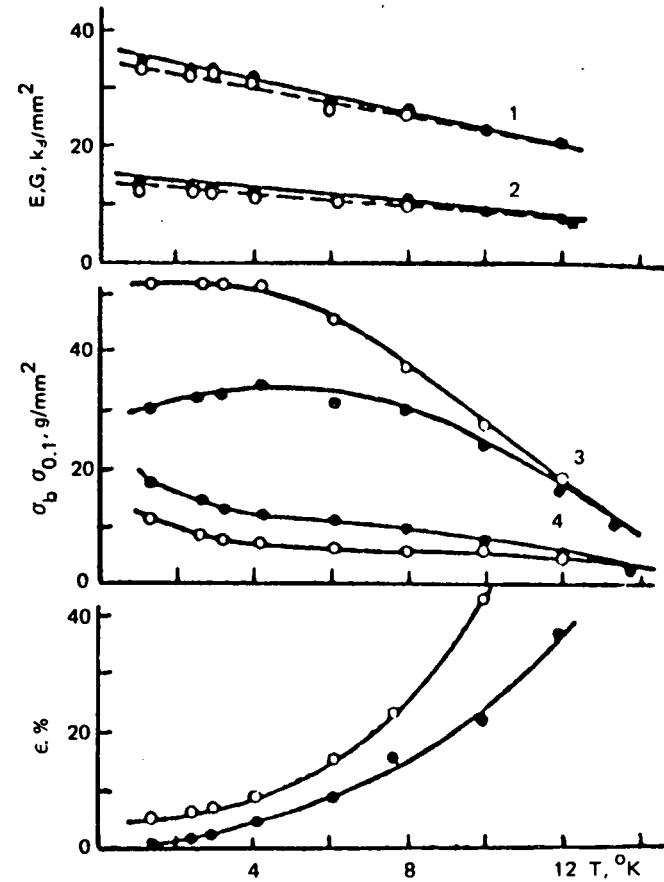
PROPERTIES	PELLET MATERIALS		
	H	D	D-T
DENSITY (δ)	✓	✓	ESTIMATED
TRIPLE POINT	✓	✓	ESTIMATED
TENSILE STRENGTH	✓	✓	
SHEAR STRENGTH			
COMPRESSION			
BEARING STRENGTH			
MODULUS OF ELASTICITY (E)	✓	✓	
COEFFICIENT OF FRICTION (μ)			

✓ - DATA EXISTS

Fig. 3-1. Availability of published physical properties data - frozen pellet materials.



DEPENDENCE OF YOUNG'S MODULUS E, THE SHEAR MODULUS G, THE TENSILE STRENGTH σ_b , THE YIELD STRESS σ_T , AND THE RELATIVE ELONGATION ϵ ON TEMPERATURE. STRAIN RATE SEC^{-1} ; 1) $4.8 \cdot 10^{-5}$; 2) $4.4 \cdot 10^{-3}$.



TEMPERATURE DEPENDENCES OF YOUNG'S MODULUS E (1), THE SHEAR MODULUS G (2), TENSILE STRENGTH σ_b (3), NOMINAL YIELD STRESS $\sigma_{0.1}$ (4), AND RELATIVE ELONGATION ϵ OF n-H₂ AND p-H₂, BLACK DOTS REPRESENT n-H₂ AND OPEN CIRCLES, p-H₂.

Fig. 3-2. Tested material properties of hydrogen and deuterium.

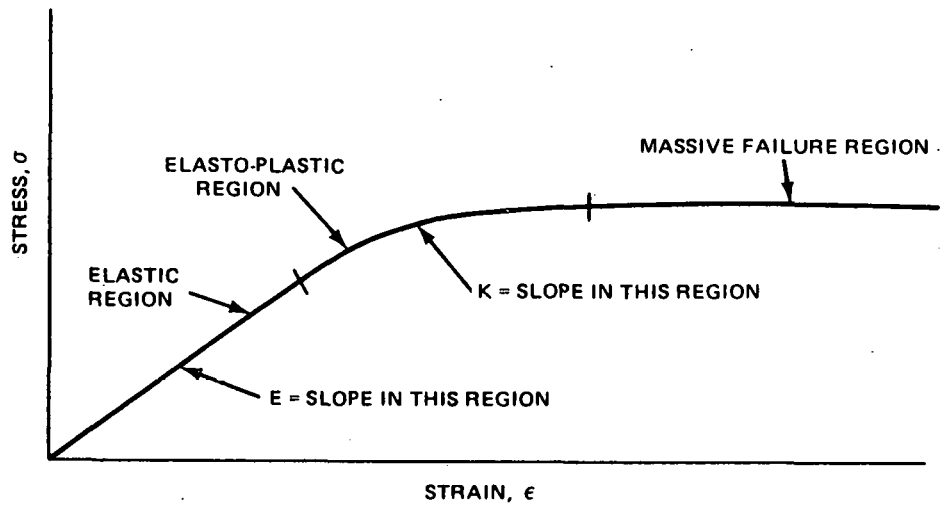
ELASTIC REGION			ELASTO-PLASTIC REGION			MASSIVE FAILURE REGION		
TEMPERATURE, K	FRACTIONAL YIELD STRAIN, ϵ_s	YIELD STRESS σ_s , ATM.	YOUNG'S MODULUS, E, ATM.	K: COEF. FICIENT OF HARDENING AT $2\epsilon_s$, ATM.	FRACTIONAL NECKING STRAIN, ϵ_B	NECKING STRESS, σ_B ATM.	MAXIMUM OBSERVED STRAIN, FRACTIONAL	APPARENT END-POINT STRESS ATM.
1.4	0.001	4.2	4200	400 (?)	0.005	5.5	0.006	4.2
4.2	0.001	3.0	3000	900	0.008	5.3	0.010	5.2
8.0	0.0015	2.0	1300	400	0.012	4.8	0.030	4.4
11.6	0.0015	1.7	1100	500	0.014	4.6	0.062	4.2
15.6	0.002	1.2	600	150	0.020	2.9	0.130	2.8
16.4	0.002	0.9	450	100	0.020	2.3	0.223	2.1

NOTE: Within error, yield strain and strain at the limit of proportionality are the same. At the necking point, $\Delta\sigma / \Delta\epsilon = 0$.

BOL'SHUTKIN
SOVIET PHYS-SOLID
STATE, 12, 119 (1970)

Fig. 3-3. Mechanical properties of solid D₂ under tension.

ORNL-DWG 79-2705 FED

Fig. 3-4. Deformation characteristics of D₂.

to illustrate the behavior regions the material undergoes as the strain is increased. The first region is the elastic region, in which the strain is proportional to stress, and all effects are reversible. From Fig. 1 in the reference, we have extracted the yield strain (the longitudinal deformation), ϵ_3 , and yield stress, σ_s . We may take these values as the end points of the elastic region, although strictly speaking, the yield points are slightly further on.¹⁴ Also included is Young's modulus for the entire elastic region, E , in which

$$E = \frac{d\sigma}{d\epsilon} \sim \frac{\sigma_s}{\epsilon_s}$$

where ϵ and σ are the strain and stress at any other point in the elastic region. Young's modulus is the amount of pressure needed to cause a fractional deformation of 1 (100% extension) if the elastic region extended to such large elongations. For D_2 , it does not — the elastic region is ended after only 0.001–0.002 fractional length change. Young's modulus is also confusing in that it describes the stress as a function of the strain. Actually, of course, the stress is the pressure that causes the deformation of the strain.

Beyond the elastic region is the elastoplastic region. Here, the derivative $d\sigma/d\epsilon$ is a function of ϵ and is now called the coefficient of hardening, K . We have

$$E \geq K = 0 \text{ for } \epsilon_s \leq \epsilon \leq \epsilon_B$$

where ϵ_B is the necking strain marking the end of the elastoplastic region. The equation indicates that it requires less stress to produce more strain. When the stress is reduced to zero, moreover, the strain does not fully disappear but reduces to the value $\epsilon - \epsilon_s$ (permanent set). Figure 3-3 lists the properties for this region for solid D_2 (see also Fig. 1 of the reference). The value of K at $2\epsilon_s$ is at the same point relative to ϵ_s for each temperature, and it shows that indeed $K < \epsilon$. The necking strain and stress mark the end of this region, where K has fallen to zero. The realm of massive failure comes next.

In the massive failure region, the derivative $d\sigma/d\epsilon$ becomes negative, meaning that the sample continues to deform as long as any stress at all is applied. The final strain and stress values in the D₂ experiment are taken to be the "relative elongation" and "strength" from Table 1 of the reference. The 1.4-4.2K samples apparently shattered at the limit of the maximum observed strain. Microscopic cracks appeared in the 8.0-11.6K samples but the 15.6K and 16.4K samples simply continued to neck down.

3.2 DETERMINING PELLET CAPABILITIES

The analyses of pellet loads encountered during injection were performed parametrically because of the uncertainty of the actual physical properties of the frozen D-T and its response to applied loads. For instance, one assumption could be that the pellet would respond to a dynamically applied load and deform to match a contacting surface, thereby reducing bearing stresses. A preliminary examination showed that the pellets must undergo high strain rates and enter the plastic deformation region to conform to this assumption. This strain may cause increases or decreases in the material allowables, depending on load application. D-T appeared relatively ductile at temperatures of 12-16K, but the pellet may also shatter or shear off small sections because of its undefined crystalline infrastructure. Other factors, such as pellet groove shapes and loads applied to a pellet closely fitted within a pneumatic tube and exposed to near explosive dynamic gas pressure, tend to affect the rate of strain deflection and the actual unit stresses.

The study examined the effects of friction. If significant coefficients of friction are applied, reduced pellet velocities will result, or the timing injection of the accelerated pellet may be erratic or intermittent due to frictional contacts. Basic data must become available before success of solid pellet injection mechanisms can be confidently predicted.

Two methods for deducing some properties are actual testing to determine the desired physical properties and testing the reactions of pellets in actual injection devices. Properly conducted material tests

together with analysis can speed results and ultimately reduce costs. Analysis alone cannot accurately predict the design performance of pellet injectors.

In order to determine the ability of the D-T fuel to withstand the accelerations necessary to achieve the assumed injection velocities, an attempt was made to research existing physical properties data of solid deuterium and tritium. In addition, an extensive literature search was implemented for physical properties data on cryogenic D-T. We are grateful for prepublication material on the estimated properties of D-T (Appendix B) that Dr. P. C. Souers of LLL has supplied for this report. As of this date, no actual tests have been performed to verify the estimates.

In summary, we have discovered little actual test data on physical properties of frozen D-T. These properties can only be deduced from hydrogen and deuterium tests and extrapolation of calculated values of known chemical properties of D-T.

3.2.1 Material Testing

The various devices used to accelerate pellets have been reviewed. Force is always required to impart motion; how this force is applied and the time of application are critical. For example, the muzzle velocity of a high powered rifle is approximately 1 km/sec, and the study requested a review of devices producing up to 10 km/sec. The projectile material involved is a frozen gas, either hydrogen, deuterium, a mixture of deuterium and tritium, or perhaps two projectiles with one gun delivering deuterium and the other tritium. All of these materials are physically weak and, below 12K, probably brittle. Section 3.1.1 discusses, as an example, the behavior of deuterium under load.

We assessed the requirements to test for strain rates, one of the more critical D-T physical properties, and describe a promising method of performing the tests. Pellets are impulsively loaded in compression, but the only data found during the study was generated for tensile specimens. Knowing material mechanical properties can greatly simplify the design of pellet accelerators and reduce costly mechanical tests and

machine modifications. A method of determining the stress-strain relation of materials when stresses are applied for times of the order of 20 μ sec is outlined. It is based on a technique for the measurement of internal dynamic stresses in rods using explosive shock waves. Figure 3-5 illustrates the principal test components required. The transducer (piezoelectric-quartz-crystal disc) is sandwiched with epoxy adhesive in a Hopkinson pressure bar arrangement to compare its output from the center electrode area with surface mounted strain gages. Test methods that would be employed for tensile, compressive, and friction tests (which must be done at cryogenic temperatures in vacuum) are not simple, but are well within present capabilities.

It appears that T and D-T tests will be similar but not identical because of the uncertain nature of granular structure of deuterium and tritium in mixed frozen gas. D-T is expected to be more brittle and fracture prone than pure hydrogen or deuterium, but this assumption is subject to test.

3.2.2 Physical Tests with Accelerating Devices

Because ORNL has built and tested a pneumatic gun and a centrifugal pellet injector, it is quite possible that these devices will provide data that will remove some doubts about pellet behavior.

Scaling up pellet size and weight and closely controlling dimensions can, with changes of barrel length and driving pressure, provide trending data on friction and pellet reaction to a compressive load. Actual exit muzzle velocity can be compared to theoretical calculations, and with the use of a gas other than hydrogen for a driver, pellet losses due to friction or fracture can be chemically tracked. Recent evaluations of pneumatic gun data⁶ showed pellet velocities approximately 20% less than predicted by an idealized constant area expansion process.

The centrifugal slinger can also be employed by making modest changes of track geometry and pellet size (to simulate D-T pellet masses), and by varying the rotational speed of the impeller. High speed photography can be used on either unit to photograph pellet behavior under loads.

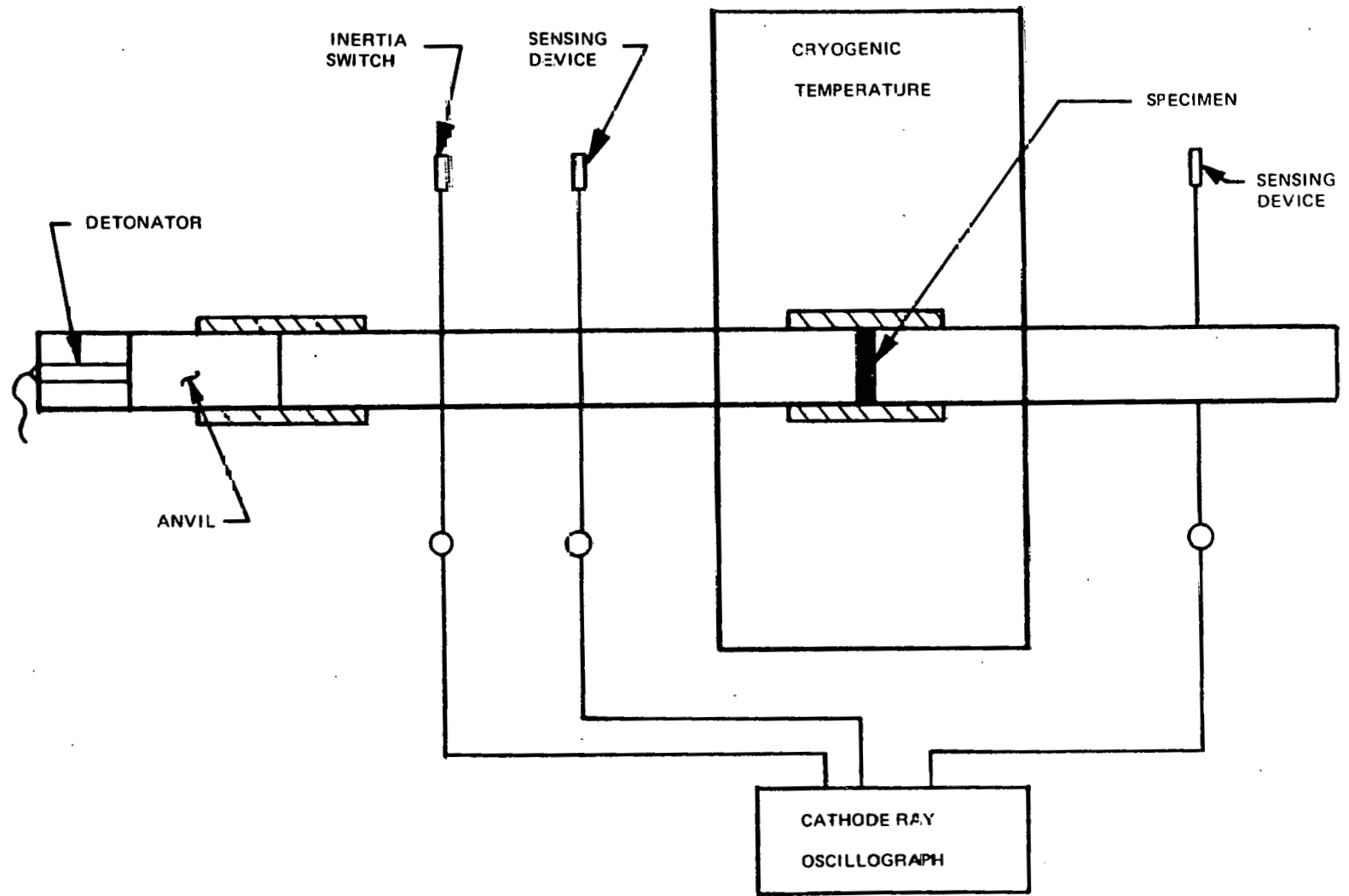


Fig. 3-5. General arrangement of modified Hopkinson pressure bar.

3.3 ANALYSIS OF PELLETS LOADS - CENTRIFUGAL PELLETS INJECTOR

In the initial phases of the study and from preliminary analyses to prove machine feasibility, it was shown that pellet loading for TNS applications was indeed severe and could conceivably govern or limit permissible acceleration forces. For the purpose of establishing trends and scoping loads encountered by pellet accelerating devices, the ORNL centrifugal pellet injector was used as an example in the following analyses. Since the pellet is subjected to impact loads, high strain rates, and sliding forces on tracks, loads and effects of friction were calculated using probable material properties and changing impeller spin speeds.

3.3.1 Dynamic Loads

For the ORNL geometry, the pellet is initially delivered to the impeller from the cutter at ~ 14 m/sec and at $\sim 45^\circ$ to the impeller disc. The design pellet exit velocity (V_e) is 940 m/sec. It was assumed that the pellet trajectory leaving the cutter would not be perfect; therefore, the dynamic loads encountered by the pellet as it was struck by the rapidly moving surface of the impeller track were calculated for "miss" distances of 0.5 and 1.0 cm from the hub, as well as for the design contact point in the hub groove. Certain simplifying assumptions were made as to the orientation of the pellet in relation to the groove geometry of the impeller. The analysis is included in Appendix C. Results indicate that the pellet initially received an impact load of ~ 550 psi when perfectly placed and loads of ~ 4650 - 8400 psi if it "missed" by 0.5 to 1.0 cm. Although some of the simplifying assumptions of initial contact geometry were subsequently revised, the imposed stresses are still extremely high in relation to those assumed allowable for D-T (60-80 psi).

3.3.2 Strain Rate

Pellet loads were investigated for two types of strain, those associated with static or low rates of strain and those associated with impact or high rates of strain. At high strain rates, materials may not respond to the applied load, thereby exhibiting apparently higher stress allowables than in static load application situations. Since no data was discovered on either static or dynamic compressive strain D-T allowables, an analysis (Appendix D) was performed to determine the strain rate and its effect. The analysis considered the behavior of a material in relation to its modulus of elasticity, E, and the time constant of load. For the examples used, the initial impact load results indicate that the material is subjected to strain rates of $\sim 10^3$ - 10^4 in./in./sec. In that range it behaves in an elastic manner and "sees" the applied load. The analysis implies that the pellet will behave in traditional fashion and will deform under the applied load.

3.3.3 Interrelation of Materials

Local stresses of contacting bodies are governed by the geometry of the contacting surfaces and the relative modulus of elasticity of the two contacting materials. The contact stresses (Hertzian) of a H pellet with an impeller track that presumes low clearance between pellet and groove were calculated. Kevlar, a high strength/weight plastic material, was used for the track as an example. Kevlar is soft in relation to any metals considered, but analysis shows that the pellet is so soft in relation to any probable contacting material that relative track deformation is negligible. The analysis and rationale are detailed in Appendix E.

3.3.4 Friction Effects

In all of the devices examined, the frozen pellet slides on a surface, usually under significant load. Friction can retard acceleration, resulting in lower injection velocities, or generate heat, which raises the surface temperature and causes some ablation. The actual

coefficient of friction of contacting surfaces has not been measured for H, D, or, most importantly, frozen D-T pellets. An analysis of the ORNL impeller disc was made assuming that 0.4-cm-diam cylindrical D-T pellets were used to calculate the effect of friction and to gage the reduction of pellet injection velocity. Figure 3-6 shows the calculated exit velocity of the centrifugal injector with assumed coefficients of friction. The analysis uses the modified ORNL pellet cutter and a higher initial delivery velocity ($V_{in} = 100$ m/sec) to the impeller. A loop configuration was also used in this study for geometric comparison purposes. Computer analysis results show a significant reduction in pellet exit velocity with increasing friction. It must be noted that the loop originates at the center of the disc, and therefore a finite injection velocity must be imparted to start accelerating the pellet. In Fig. 3-6, $V_{in} = 11$ m/sec is assumed for the loop.

It has been postulated that the pellets will ablate, generate a thin gas blanket, and thus be insulated from contacting surfaces. If this occurs, the resultant viscous drag coefficient of friction will be very low. If, however, the contact forces are higher than the pressure generated by the ablation gas blanket, then contact between material surfaces will occur with a friction coefficient yet to be determined. Based on test results, the present system does not seem to be affected at low speeds.

3.3.5 Pellet Performance Summary

The test cases examined in our analysis led to these conclusions.

- The mechanical physical properties of D-T will be essentially the same as those of H or D. LLL expects that the frozen D-T will be slightly stronger than H or D and probably less ductile.
- Application of the strain rates that we have calculated shows that the rates of strain application, even in the dynamic impact load applications, are not high enough to provide higher dynamic strength allowables partly because of the assumed low

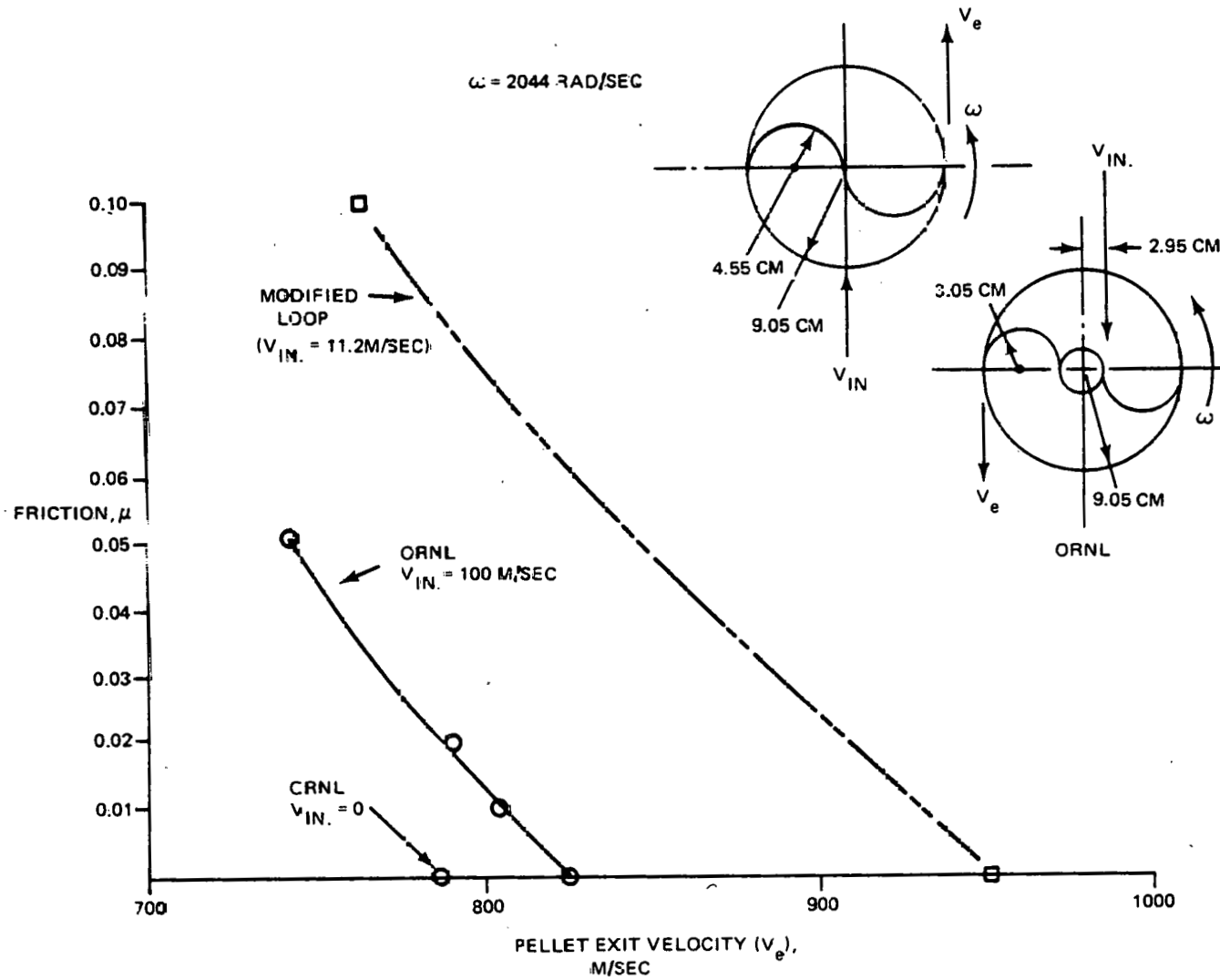


Fig. 3-6. Frictional effects on exit velocity.

E of the D-T. Our load analyses are nonconservative in that we did not consider Hertzian contact stresses but assumed full area contact in all cases.

- Friction can be a problem in injection devices in which the pellet contacts the accelerating device.

3.4 PELLETT DELIVERY RATES

During the study, the estimated TNS requirements provided guidelines which influenced injector capabilities, installation, and sizing of fuel storage capacities.

Fuel delivery during ignition steady state is estimated at $\cong 0.21$ gm/sec. Approximately 20% of this quantity is absorbed in the plasma and consumed in the fusion process. The remainder is collected by the divertors or scraped off by the plasma limiters and removed by the vacuum pump to be separated from unwanted materials by recycling systems and then reinjected.

Pellet sizes suitable for TNS application range from 0.3-0.6-cm diam. Generally, the larger the pellet, the lower the injection velocity required to penetrate a given distance into a plasma, a situation which eases machine design requirements. However, there are limits to the physical size of a pellet that can be introduced into a plasma without extensively cooling or quenching it. The present mass limit for TNS pellets, based on quantity of lost and consumed fuel, is approximately 10-15% of the total fuel in the plasma chamber.

Two methods of producing frozen pellets from liquid gases are common. One method manufactures pellets by freezing D-T material, extruding the material through a properly sized nozzle, and then mechanically cutting the extruded stream into predetermined lengths. The other method requires forcing liquid D-T at the triple point temperature ($\sim 20\text{K}$) through a nozzle into a high vacuum chamber. The liquid stream is broken into droplets by various means and the droplets, by the mechanism of surface tension, tend to form a spherical shape. Each droplet cools to the freezing point by surface evaporation and conduction from within the surface. This method has been successfully employed in

forming frozen spherical pellets up to ~ 0.3 cm, but it is not certain that larger pellets can be produced in this fashion. The practicality and necessity of solidly freezing larger droplets in a reasonable time are also questionable. A sufficiently thick frozen shell may provide for adequate penetration.

Figure 3-7 presents the weight of various size pellets and the number of pellets/sec needed to satisfy a D-T fuel requirement of 0.20 gm/sec. Figure 3-8 illustrates this delivery rate for both cylindrical and spherical pellets. It also illustrates the high delivery rate required for small pellets and implies the high injection velocities that would be required. Lower delivery rates reduce impeller or pneumatic gun requirements, and increasing the pellet weight has a negligible effect on machine performance. The difficulty of providing continuous rapid delivery rates greatly influences the effectiveness of candidate injector systems.

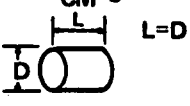
PELLET DIA (CM)	VOLUME CM ⁻³ 	WEIGHT (D-T) = 0.25 GM/CM ³		DELIVERY RATE (0.200 GM/SEC) PELLETS/SEC	PELLET DIA EQUIV SPHERE
		GM.	LB		
0.05	0.000098	2.45×10^{-5} 5.40×10^{-8}		8149	0.0572
0.10	0.000785	1.98×10^{-4} 4.32×10^{-7}		1019	0.114
0.20	0.00628	1.571×10^{-3} 3.468×10^{-6}		127	0.229
0.30	0.0212	5.30×10^{-3} 1.170×10^{-5}		37.7	0.343
0.40	0.0503	1.257×10^{-2} 2.774×10^{-5}		15.9	0.458
0.50	0.0982	2.454×10^{-2} 5.418×10^{-5}		8.2	0.572
0.60	0.1696	4.241×10^{-2} 9.362×10^{-5}		4.7	0.687
0.70	0.269	6.734×10^{-2} 1.487×10^{-4}		3.0	0.801
0.80	0.402	1.005×10^{-1} 2.219×10^{-4}		2.0	0.916
0.90	0.573	1.43×10^{-1} 3.15×10^{-4}		1.4	1.031
1.00	0.785	1.963×10^{-1} 4.33×10^{-4}		1.0	1.145

Fig. 3-7. Fuel pellet mass and geometry.

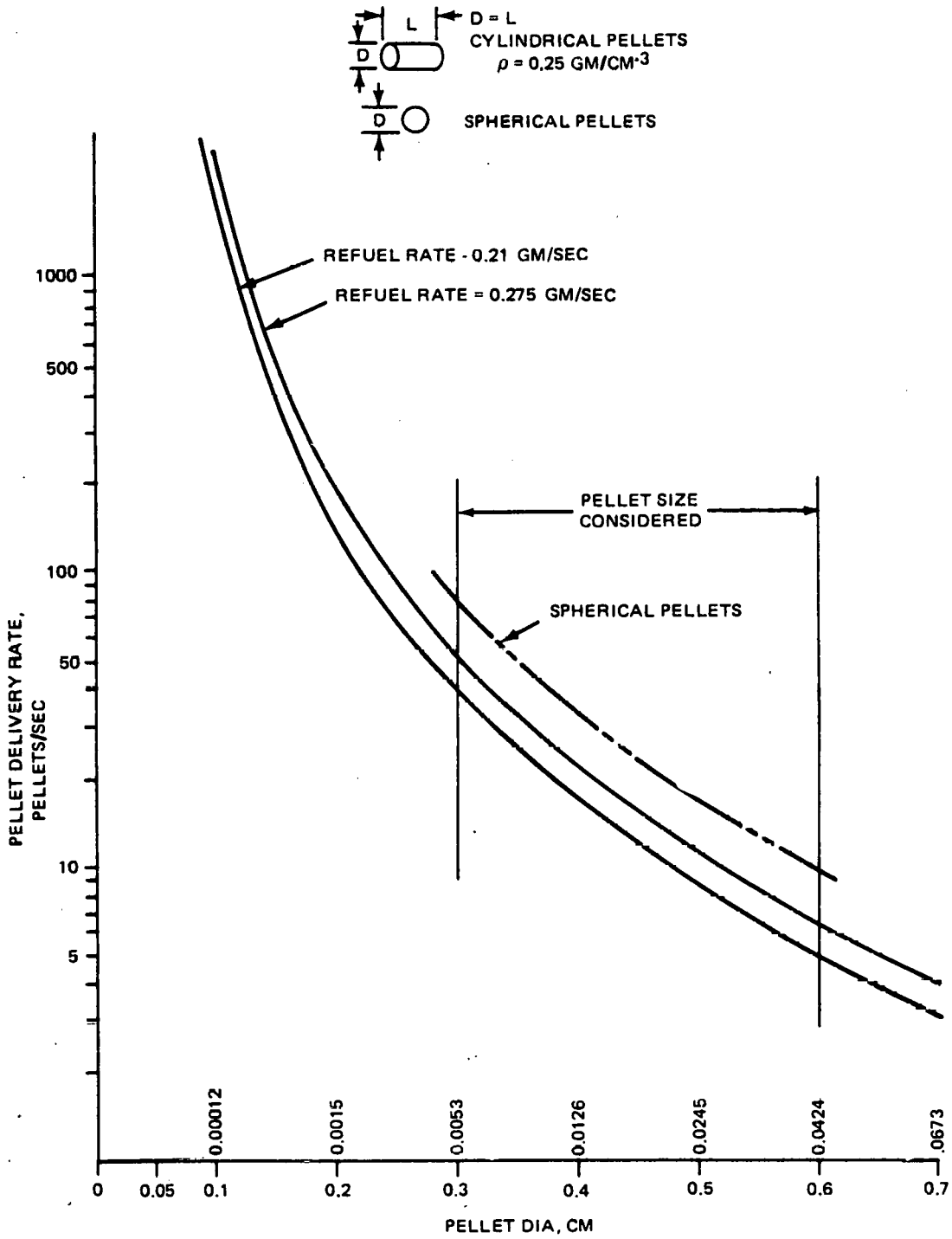


Fig. 3-8. Pellet delivery rate.

4. CANDIDATE INJECTORS

The TNS requirements established ranges for pellet parameters such as velocity, delivery rate, size, and, indirectly, mass. In addition to assessing the fueling concepts against these requirements, we also considered other factors necessary to successfully deliver the fuel to the plasma. These factors included the pellet formation technique and the ability to produce large pellets, the injection loads on the admittedly weak pellet, and the probability of the injection concept introducing contaminants into the plasma.

The fueling concepts are in an early stage of investigation and only the centrifugal pellet injector and pneumatic gun have progressed to the test hardware stage. Thus, the evaluation of some concepts was highly subjective, and the advantages and limitations of all of the concepts are not well defined. Several concepts (e.g., electrical methods charging the pellet or encasing it in a conducting carrier) were eliminated at the outset of the study since former studies^{2,15} had judged them impractical for tokamak fuel pellet injection.

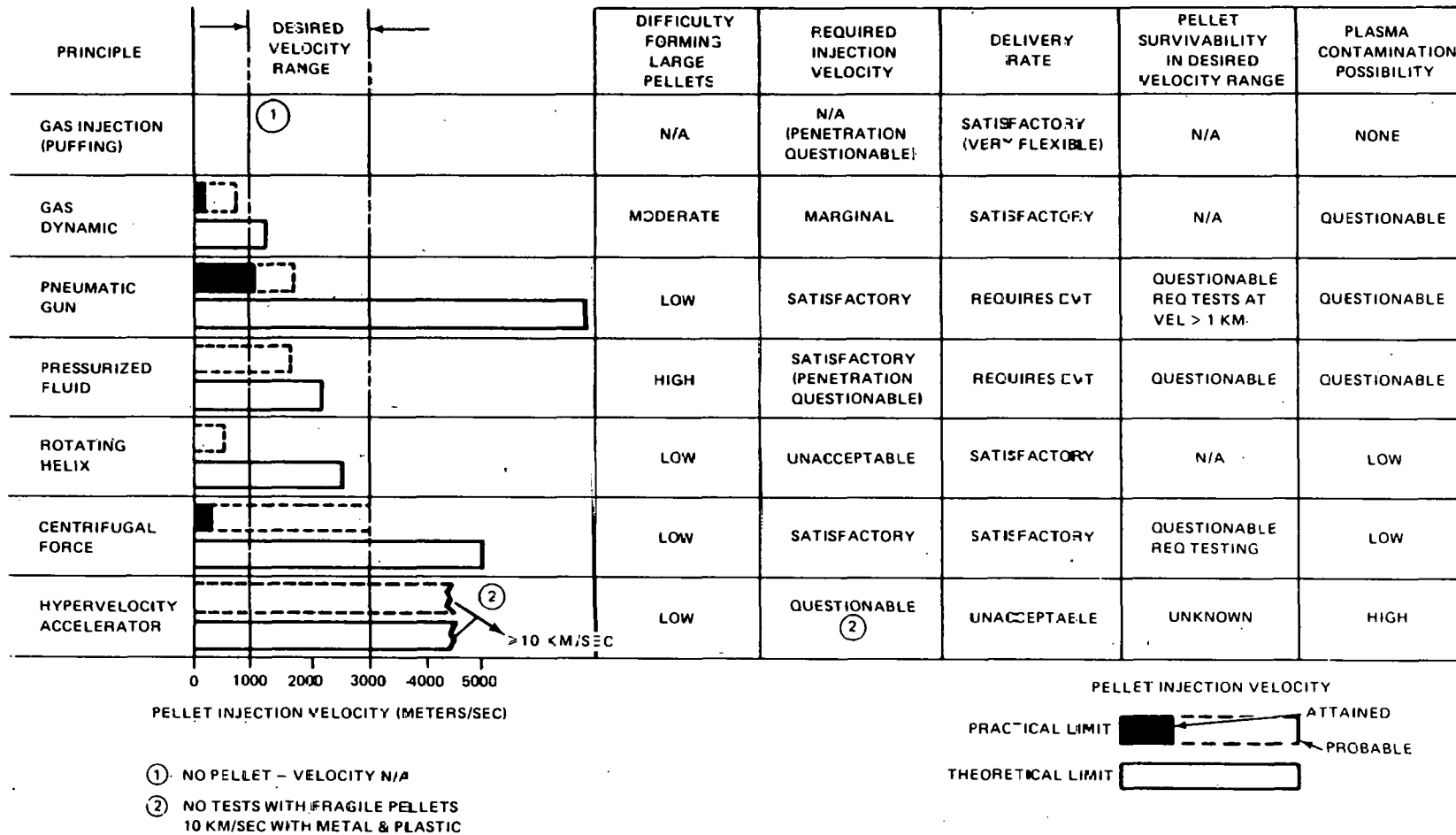
Figure 4-1 illustrates the categories used in the rating as well as the theoretical velocity limits. In addition, velocities attained in experiments are shown as are estimates of the probable operating limits.

Based on the rating, three methods were recommended for further investigation:

- centrifugal pellet injector
- pneumatic gun
- pressurized fluid.

Of the three, the centrifugal pellet injector has the inherent capacity for providing high velocity and delivery rate for a range of pellet sizes. A demonstration device has already yielded a repetition rate of 150 pellets/sec with 1-mm-diam pellets.

The pneumatic gun has already demonstrated the minimum required velocity for TNS. Engineering development is needed to improve delivery rate.



44

Fig. 4-1. Fuel injector comparisons.

Pressurized fluid injection seems promising, but there is no hardware for test evaluation. Delivery rate and the ability to handle pellets of TNS size are serious concerns.

Unfortunately, none of the recommended injectors is without developmental problems, and pellet survivability is a common concern.

Gas injection (puffing) appears to be the simplest method of fueling and is in use in present devices. As discussed earlier, it is questionable whether it will work in larger plasma devices such as TNS. A gas dynamic injector has the problem of producing large pellets, directing them accurately, and attaining the necessary velocity. The observed dispersion of 0.005-cm pellets in ORMAK indicates a large loss of pellets prior to injection with a consequent undesirably large tritium inventory.

Hypervelocity acceleration has never been used successfully with fragile pellets. In addition to the pellet survivability problem, there are problems of delivery rate and probable plasma contamination. An attempt was made to simplify the accelerating (rotating) helix injector (Fig. 4-2) by including a solid fuel extruder and modifying the rotor so that a cylindrical pellet could be used. Raised lands on the rotor push the aft end of the pellet while the cylindrical surfaces rest on the rotor surface and on the guide groove in the housing. Unfortunately, the permissible driving forces are low and therefore the acceleration times and distances are impractically long.

4.1 CENTRIFUGAL PELLET INJECTOR EVALUATION

The centrifugal pellet injector received a major share of analysis because it seemed to have the capability of accelerating both small and large pellets to an acceptable velocity range.

In evaluating the centrifugal injector we sought to calculate these effects:

- rotational velocity needed for a given pellet exit velocity by a straight radial track and a semicircular track
- effect of initial pellet injection velocity (V_{in}) on the exit velocity

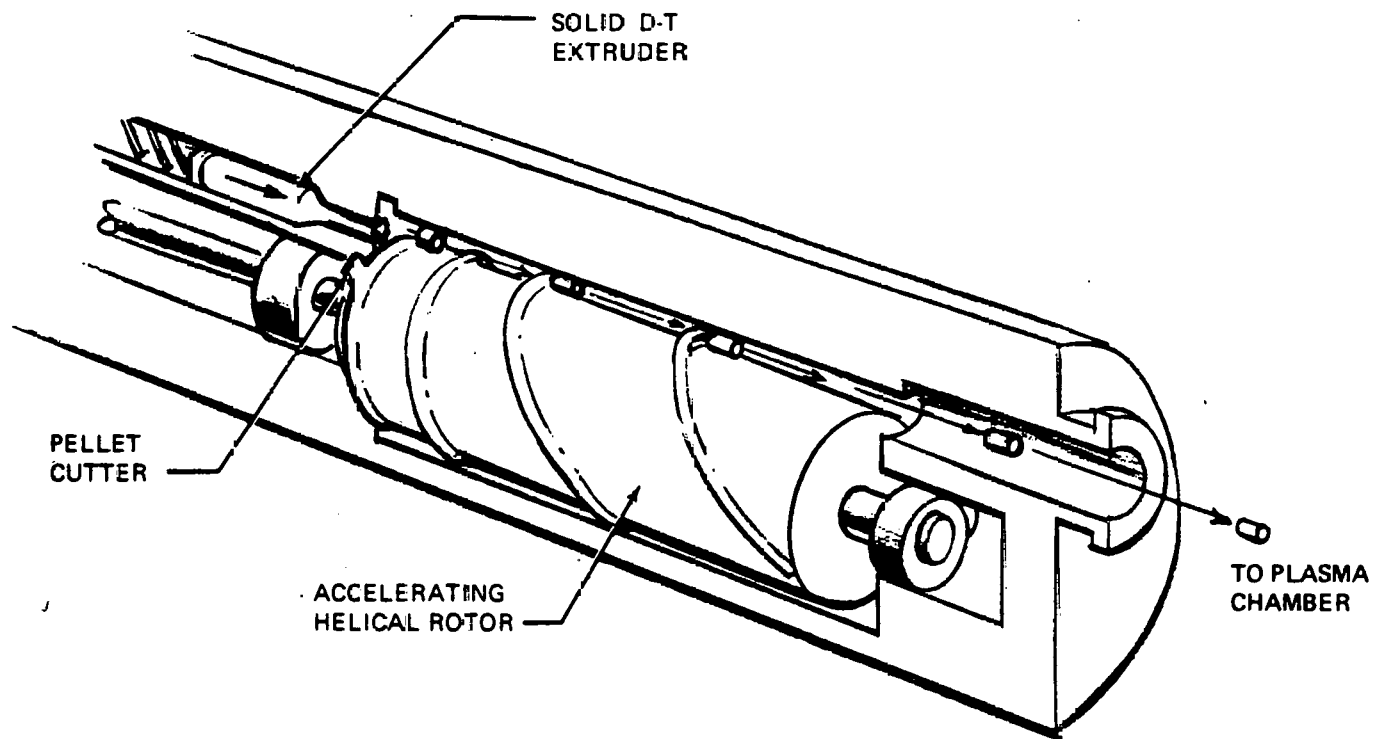


Fig. 4-2. Accelerating rotary helix.

- effect of track friction on the exit velocity
- effect of impeller radius and spin velocity on the exit velocity.

Appendix F details the analyses used to calculate these effects. It must be noted that early in the study we felt that subjecting the pellet to high dynamic forces was not desirable, and therefore we suggested geometry and injection methods that minimized such loading. Since necessary material properties were unavailable, these analyses were performed to provide sizing and trending data, rather than absolute answers.

The demonstration injector, shown in Fig. 4-3, is designed to provide a 940-m/sec exit velocity with 0.05-cm-diam cylindrical H pellets. Analyses indicated large pellet deformations and Hertzian stresses with hydrogen pellets. By expanding the diameter of the basic injector design we established that the pellet reaction force could be reduced by increasing the impeller diameter. Significant force reductions could also be obtained by changing from a straight radial track to a curved track, indicating that the tubular or straight radial track is not as efficient as the semicircular track. This conclusion is valid only for the case of coefficients of friction <0.1 .

Analyses to evaluate the effect of track shape on pellet exit velocity with the same diameter and impeller speed show the curved track yields a significantly higher exit velocity for cases with negligible friction. Moderate friction (coefficients of 0.2) reduces the exit velocity, and the effect on the curved track is more significant than on the straight track. For coefficients of friction >0.25 , the pellet does not leave the curved track.

For the curved track it was shown that increasing the injection velocity by 100 m/sec resulted in only a 40-m/sec exit velocity increase. This does not seem to warrant the use of higher initial velocities and would also tend to increase the dynamic pellet shock loading.

The problem of aligning the impeller exit point with the injection tube to the plasma chamber is highly sensitive to pellet friction. A variation in friction coefficient from 0.0-0.05 resulted in a 12% reduction in exit velocity, and the increase in exit time corresponds to a

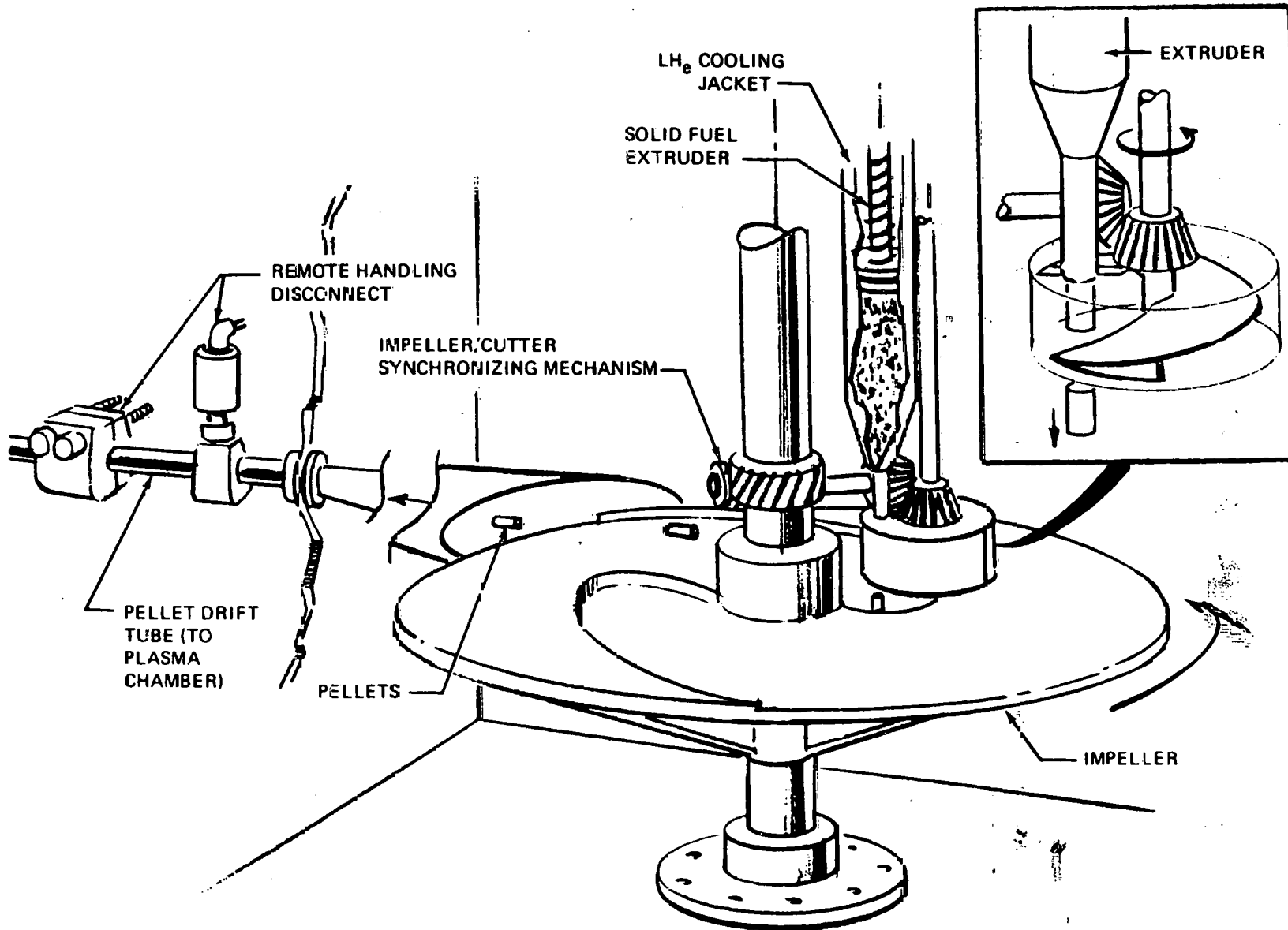


Fig. 4-3. Centrifugal force pellet injector.

variation in angular position of the impeller exit point of approximately 11° . Thus, any variation in pellet-to-pellet friction must be kept within small limits.

4.2 PNEUMATIC GUN INJECTOR EVALUATION

ORNL has constructed a pneumatically powered pellet injector⁶ that has achieved velocities of 1000 m/sec and has successfully injected 0.10-cm H pellets into the ISX.³ Figure 2-6 described the essential features of the system; Fig. 4-4 shows a section of the actual apparatus.

Pressurized liquid hydrogen gas is introduced into a chamber below the accelerator gun barrel. Liquid helium coils surround the mechanism, and the hydrogen is condensed and frozen into a solid pellet. The chamber into which the pellet has been frozen is designed to rotate. When rotated, it simultaneously shears the frozen hydrogen in the line, sizes the pellet, and locates the sized pellet in line with the gun barrel. A pneumatic pressure supply reservoir (helium) with a fast acting shut-off valve in line is connected to the pressure chamber of the gun which is upstream of the formed pellet. When commanded, the valve opens and admits driver gas to the pressure chamber, thus accelerating the pellet through the barrel until it reaches the muzzle of the gun.

The pellet passes through an evacuated chamber and then through a vacuum tight drift tube which permits the pellet to enter the plasma chamber and penetrate the plasma. The helium used for propelling the pellet is trapped by a series of baffles and valves so that none is admitted to the plasma chamber. This experimental apparatus is very flexible in its ability to propel pellets of various size by modification of barrel length and diameter and by varying the pressure of the driving gas. At present it has the capacity to fire only a single shot.

The pneumatic gun is bore sighted, so that its trajectory is well defined. At present the scatter is only 0.2° .

The ability to achieve the desired delivery rate of 20-30 pellets/sec is a design problem. A schematic of a system illustrating a way of providing multiple shots in rapid sequence is shown in Fig. 4-5. The

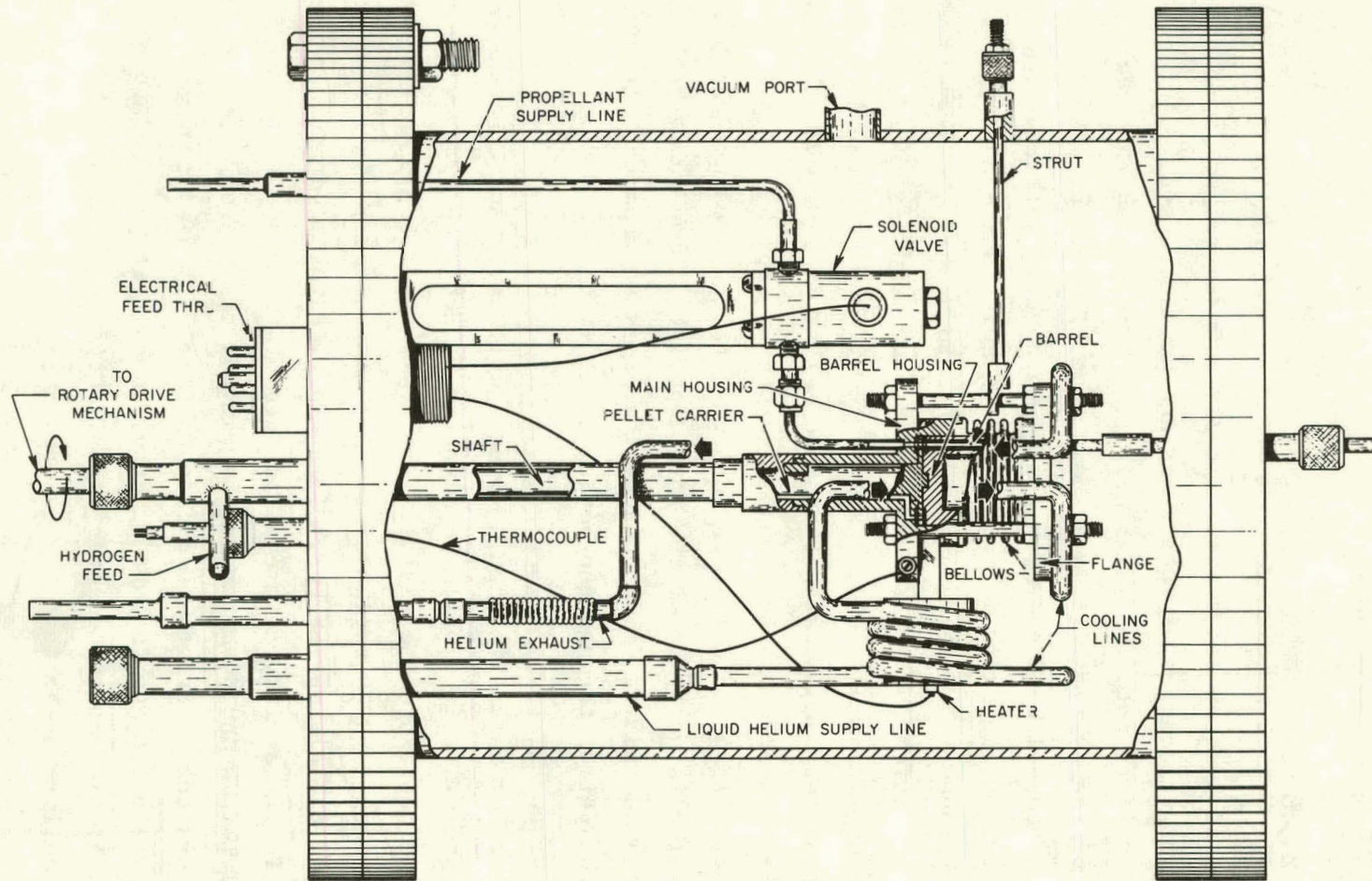


Fig. 4-4. Pneumatic pellet injector.

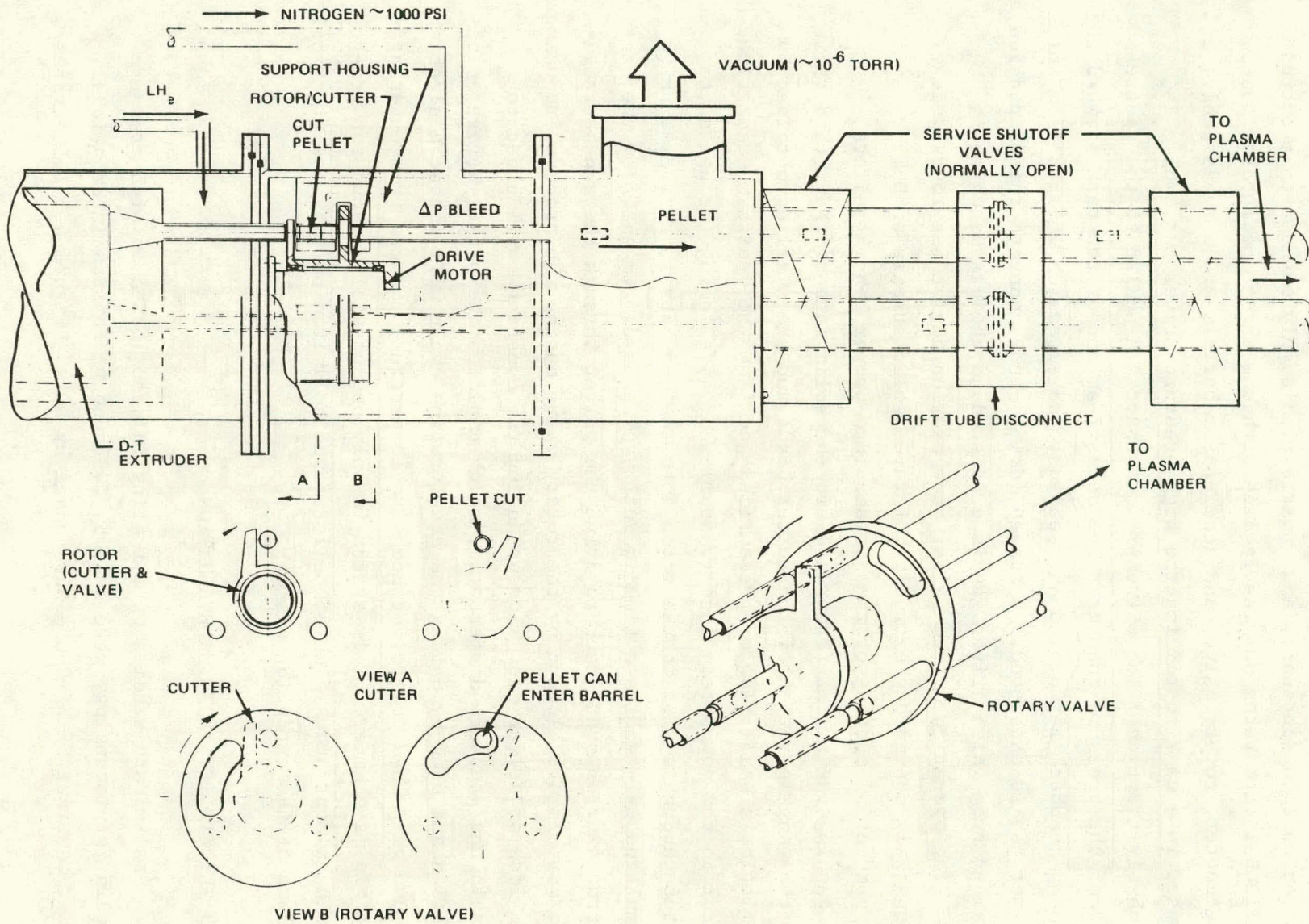


Fig. 4-5. Constant delivery rate pneumatic gun.

system consists of a three-barrelled gun tube, a rotary valve and pellet cutter on a common shaft, and, upstream, a supply chamber that extrudes solid D-T into three nozzles in line with the three accelerator tubes. The cutter, rotary valve, and accelerator barrels are a subassembly, all housed in a tank containing the high pressure driver gas, which is probably hydrogen. The extruder is mounted and sealed to the upstream end of the pressure chamber. The downstream end of the tank (toward the plasma chamber) is mounted and sealed to an expansion chamber from which driver gas is exhausted. A sealed (drift) tube connects this expansion chamber from which driver gas is exhausted to the plasma chamber.

The operation of the pellet acceleration device has four basic steps: 1) continuous extruding of three solid streams of D-T, 2) sequential cutting of the streams into proper length pellets, 3) pushing the pellet forward toward the solid face of the rotary valve by the wedging action of the cutter blade and the small Δp obtained by admitting a small flow of pressurized gas from the upstream face of the rotor to the downstream face (vacuum) and, 4) allowing the pellet to enter through a slot in the rotor into the gun barrel, a process which simultaneously admits a timed quantity of pressurized gas from the surrounding pressure tank to drive the pellet through the gun barrel. Two barrels are blocked by the rotary valve during the process, reducing the loss of driver gas. Losses during the constant small bleed to obtain the pressure differential which emplaces the pellet before acceleration and blow-by during the acceleration cycle will impose a sizable vacuum pump load to prevent undesirable gaseous products from entering the plasma chamber. This system is only one possible avenue for producing a continuous flow of pellets and is limited only by the practical volume of the extrusion chamber.

4.3 LIQUID JET INJECTOR EVALUATION

Preliminary studies of a fueling injector based on high pressure liquid jet technology were done by C. Bruno of Physics International under contract EF-77-C-03-1560 funded by DOE.⁸ Figure 4-6 illustrates

ORNL-DWG 79-2717 FED

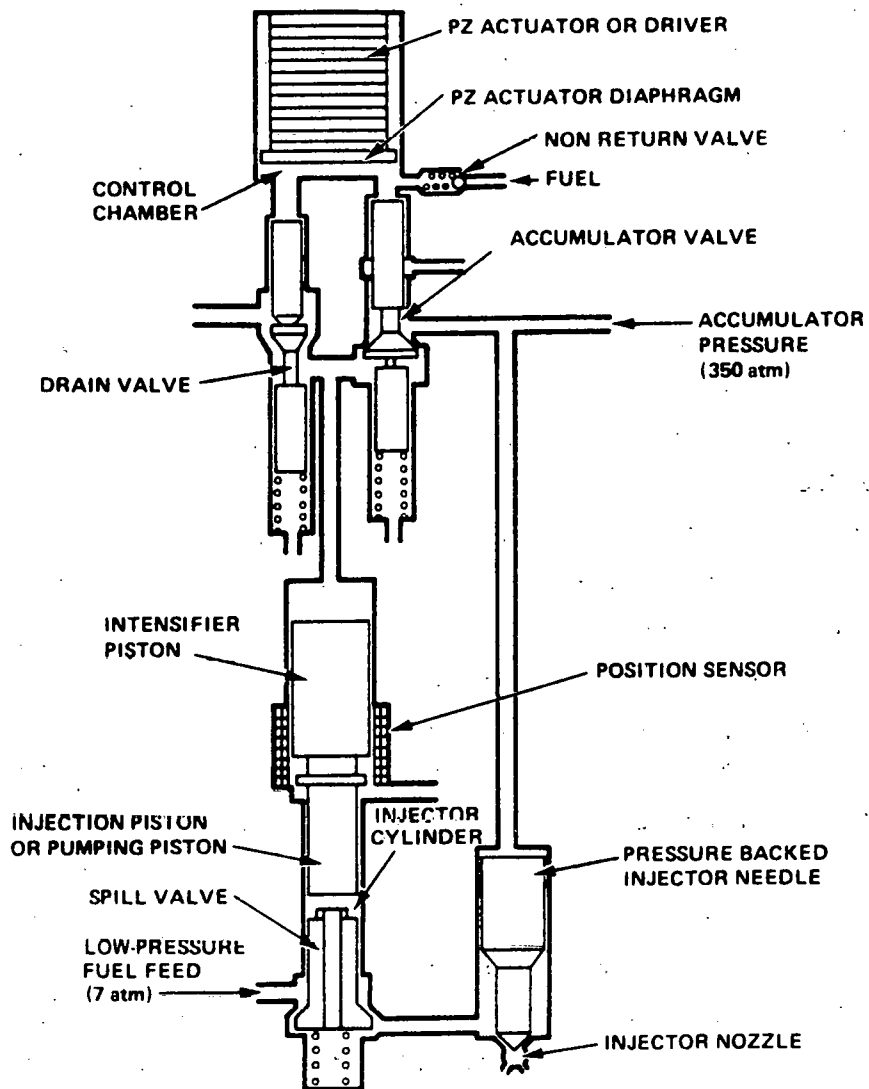


Fig. 4-6. Diagram of piezoelectric servo-valve fuel injector.

the initial concept; Figs. 4-7 and 4-8 illustrate the injector nozzle assembly and a schematic of the installation including identification of support subsystems.

The injection nozzle design is quite complex; therefore, the program is separating some of the components into more manageable development items. The nozzle high pressure system has higher priority; manufacture and test of the nozzle is planned for December 1978 with the pelletizer, the mechanism for breaking up the continuous liquid stream into droplets, to be started in early 1979.

The injector is presently designed to produce pellets of up to 0.1 cm, but at a low repetition rate (1/5 min). TNS requirements are for 0.5-cm-diam pellets at 20-30/sec. The present Physics International concept generates a stream of fuel (hydrogen), uses a vibrating nozzle to break up the stream, then subjects the droplets to a high vacuum where they freeze by evaporation. Because of the nozzle motion necessary to develop droplets, they fan out or disperse. Several methods might be employed for selecting pellets having the desired trajectory, but all of these methods either involve loss of quantities of pellets or very precise timing methods to accurately synchronize the pressure pulses and nozzle position to provide a desired trajectory. Loss of H pellets is of little consequence, but any substantial loss of D-T is highly undesirable because of the increase in tritium inventory.

If the engineering problems of controlling pressure and precise timing to control pellet trajectory can be solved, fluid injection could be a clean, flexible system. Personnel of Physico International⁹ feel that providing large pellets (0.5 cm) will be a rather difficult job, and the behavior difference of hydrogen and D-T must be investigated. A possible solution of providing rapid rates might involve use of an array of nozzles sequentially injecting a metered quantity of fuel. Such a system might simplify solenoid or piezoelectric valve design.

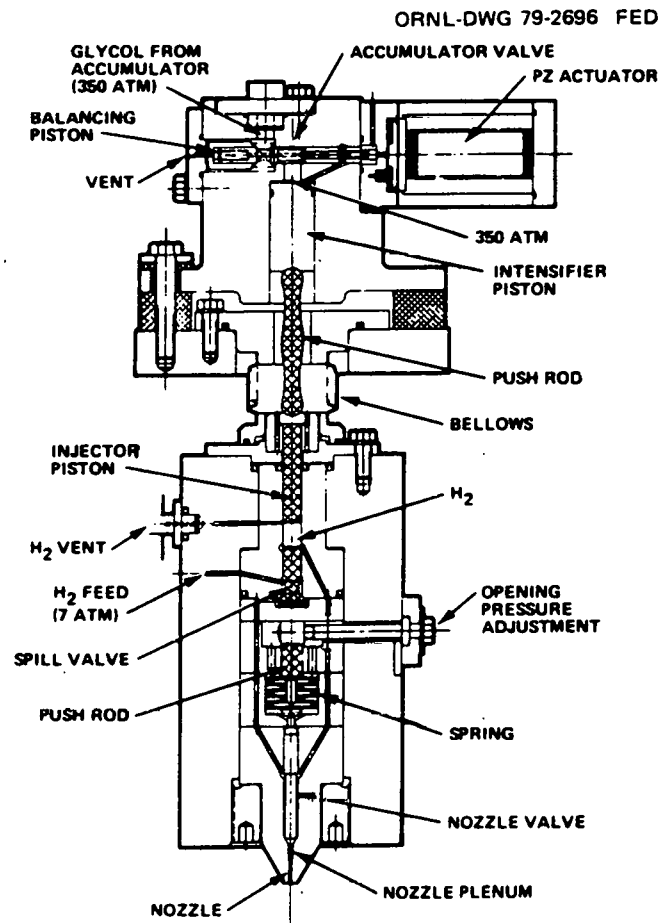


Fig. 4-7. Tokamak fueling injector conceptual design.

ORNL-DWG 79-2695 FED

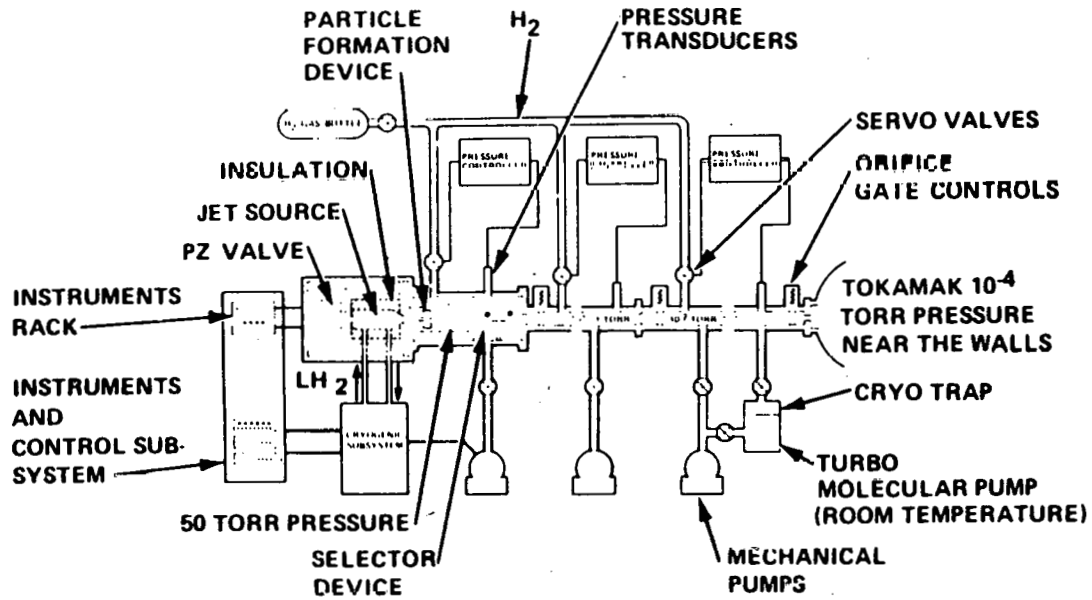


Fig. 4-8. Tokamak fueling subsystems schematic.

4.4 MAINTENANCE

It is highly desirable that maintenance concepts be developed in a manner such that TNS operating procedures and experience can be transferred directly to prototype commercial installations. Downtime on commercial reactors must be minimized; therefore, any subsystems that could malfunction between scheduled maintenance times must be designed for ease of repair or replacement. On-line repair is time consuming and may not meet operating guidelines. The environment in the reactor building is hazardous for manual maintenance; therefore, semiremote or remote equipment must be used.

It is proposed that each pellet injector be designed as a self-sufficient assembly with a minimum number of interface connections. Although the three candidate injector systems are dissimilar, there is a great deal of commonality in their reactor and building interfaces and their supporting system requirements. The common subsystems are:

- electrical power
- pneumatic pressure
- vacuum pump outlets
- D-T supply
- LH_e supply
- structural supports.

The interface of the injector is a drift tube assembly, possibly housing a group of tubes and two vacuum tight shut-off valves, one to protect the plasma chamber vacuum and the other to close off the injector assembly for events like D-T leakage. Between the valves is a quick-disconnect coupling designed for remote handling to break the drift tube assembly. All connections except vacuum lines should be gathered into a single quick-opening assembly to facilitate removal. Vacuum pump lines should be connected with hard valves and quick-disconnect couplings in the manner described for the pellet drift tube assembly.

The concept provides for breaking three quick couplings: the drift tube, the vacuum pump line, and the ganged subsystem umbilical assembly. With removal of these couplings, the entire injector assembly can be transported to a hot cell for repair.

4.5 RELIABILITY

The TNS is a complex experimental machine composed of one-of-a-kind prototype installations. While reliability goals must be set and certainly approached as the machine matures and systems are refined, past experience shows it to be unrealistic to expect firm maintenance schedules to prevail at the outset.

Reliability begins initially with good design, selection of quality components, careful fabrication, and a reasonable amount of preliminary testing to eliminate unsuspected faults and infant mortality. Considering the complexity and difficulty of maintenance in a hostile environment, redundancy of critical components should be seriously considered. Even if budgets do not permit duplication of whole assemblies such as an entire injector subsystem, provisions for redundant assembly installations on the machine should be made. The trade-off of downtime costs vs cost of redundant equipment is difficult to make on an experimental machine, but the ability to demonstrate burn during a malfunction using a redundant unit can provide invaluable operating experience for future technology transfer.

With only concepts available for analysis, prediction of the MTBF of a system is unrealistic at this time. A goal of 100 h of operation before breakdown or major disassembly would be a reasonable goal at the outset, with a three-month disassembly and maintenance operation a future goal.

4.6 OPERATING REDUNDANCY

There are many single point failures that can result in machine shut-off in the event of malfunctions. This study scope does not permit a detailed evaluation of optimum redundancy features, but it is able to suggest some obvious elements of pellet injector systems that benefit operations. For example, the pneumatic gun has multiple barrels. Jamming of fuel in one barrel reduces the required flow to the plasma chamber and degrades performance, but will not result in immediate catastrophic shutdown. Our suggestion is an installation having three injector assemblies, two operational and the third on standby. The

three units should be exercised sequentially in rotating pairs in order to provide constant operational readiness and reduce the wear of high delivery rates by sharing the demand. If a malfunction occurs in one injector (like the single jamming of a barrel described above), sensing systems would switch on the standby unit with a minimal impact on the pellet delivery rate. All units should feature quick removal and reassembly methods.

While the pneumatic pellet injector was used as an example, the centrifugal injector or fluid injection systems should also be designed for a similar redundancy of operation and installation.

4.7 SAFETY

Safety is a key consideration in two areas. The first is the design of the machine to avoid operational failures due to component or other malfunctions. Second, radiation shielding should be installed to maintain the integrity of injector materials exposed to high energy neutrons or thermal radiation; this prevents the activation of materials that generate radioactive compounds emitting gamma radiation harmful to personnel. The type and thickness of material used for shielding is dependent on the injector and the particular installation. All of the injectors have a common problem. The drift tube which permits the pellet to enter the plasma chamber also permits thermal radiation and neutrons to penetrate the interior of the injector system. This situation triggers activation of injector materials, possibly degradation due to tritium permeation, and ultimately requires shielded or remote handling means for service of components. A further safeguard which should be included in all installations is a second pressure tight container to prevent tritium escape into the test chamber environment. This will entail a separate pumping system to evacuate the protective jacket or additional valves and piping leading to the main plasma chamber vacuum pumping system.

THIS PAGE
WAS INTENTIONALLY
LEFT BLANK

5. RECOMMENDATIONS

Section 4 described the three recommended concepts as potentially meeting TNS requirements and briefly touched on what appear to be shortcomings or design areas requiring deeper concentration.

5.1 CENTRIFUGAL PELLET INJECTOR

1. Analysis of the demonstration injector indicates that the 940-m/sec ejection design velocity will produce pellet stresses high enough to question their physical integrity. For TNS application, an analysis should be made to define an optimum track geometry, length of track (disc diameter), and rotational velocity consistent with the D-T pellet strength.
2. A mechanism should be designed which will accurately deposit the pellet onto the impeller with minimum initial impact load.
3. A test should be devised which will define the coefficient of friction of a large pellet (weight of 0.5-cm D-T pellet) on a long track under varying loads and track temperatures. Consistency of travel time, exit location, and pellet weight loss are the principal test objectives.

5.2 PNEUMATIC GUN

1. The pneumatic gun should be tested with a longer barrel and higher pressure to verify the maximum velocity attainable.
2. The pneumatic gun should be designed with a mechanism permitting delivery rates consistent with TNS requirements and pellet mass. For the purposes of proposed redundancy requirements described previously, there should be a reduction of the delivery rate to a fraction of the total by increasing the number of injectors to be installed. Better definition of detail design, materials, and reliability requirements is required.

5.3 FLUID INJECTOR

1. A proof-of-principle device should be developed and tested.
2. If the device proves successful, the following should be undertaken.
 - a. Design for 0.5-cm cylindrical pellets (D-T mass).
 - b. Use multiple nozzles to reduce piezoelectric valve rate requirements.
 - c. Design nozzles to bore-sight pellet droplets. Investigate precisely metered impulsive injection rather than droplet production by vibrating nozzles on a continuous stream.
 - d. Investigate a long cold plate drift tube (a jacket of flowing LH_2) to freeze pellet and combat effect of heat emanating from plasma chamber.

These recommendations are the results of design analyses, contact with the various originators of the proposed hardware, and open discussions of some anticipated problems and development requirements. Many of these potential solutions of anticipated problems may prove to be inappropriate when forthcoming tests are performed and results evaluated.

5.4 MATERIALS TESTING

Throughout this study, the weak link in any analysis or firm recommendation was lack of material properties which limit mechanical device performance.

1. A program should be generated to test those material properties which are critical to injector performance. These tests must be conducted in vacuum at cryogenic temperatures. The principal information desired is the compressive and bearing allowable stress at close to static loading and at high applied strain rates (~ 5000 in./in./lb) and the coefficient of friction on smooth metallic or plastic composite surfaces. Tests should first be performed with hydrogen or deuterium and later verified with D-T.

2. Tests should be proposed using existing or modestly modified hardware (centrifugal injector or pneumatic gun) to deduce properties such as friction or compression deformation and to determine effects of varying operating parameters such as pressure, barrel length and diameter, rotational speed, and pellet mass.

5.5 TEST PROGRAM

DOE should prepare or delegate to a national laboratory the preparation of a test program to coordinate the development of the recommended injectors and define the supplementary analyses and physical tests consistent with TNS development objectives. A screening and monitoring system should be provided to narrow the candidate injector field to the one to be chosen for TNS.

The recommendations of this report do not appear to be consistent with present DOE funding levels.

THIS PAGE
WAS INTENTIONALLY
LEFT BLANK

REFERENCES

1. A. T. Mense, W. A. Houlberg, S. E. Attenberger, and S. L. Milora, *Effects of Fueling Profiles on Plasma Transport*, ORNL/TM-6026, Oak Ridge, Tennessee (1978).
2. R. J. Turnbull, "Review of Pellet Fueling," in *Proc. Fusion Fueling Workshop*, CONF-771129, Princeton, New Jersey (1978).
3. S. L. Milora, C. A. Foster, P. H. Edmonds, and G. L. Schmidt, *Hydrogen Pellet Fueling Experiment on the ISX-A Tokamak*, ORNL/TM-6496, Oak Ridge, Tennessee (1978); to be published in *Phys. Rev. Lett.*
4. S. L. Gralnick, "Gas Blanket Fueling of a Tokamak Reactor," in *Proc. Fusion Fueling Workshop*, CONF-771129, Princeton, New Jersey (1978).
5. C. A. Foster, K. Kim, R. J. Turnbull, and C. D. Hendricks, *Rev. Sci. Instrum.* 48, 625 (1977).
6. S. L. Milora and C. A. Foster, *Pneumatic Hydrogen Pellet Injection System for the ISX Tokamak*, ORNL/TM-6598, Oak Ridge, Tennessee (1978).
7. R. F. Flagg, "A Review of Gas Gun Technology With Emphasis on Fusion Fueling Applications," in *Proc. Fusion Fueling Workshop*, CONF-771129, Princeton, New Jersey (1978).
8. C. Bruno, "Fueling by Liquid Jets," in *Proc. Fusion Fueling Workshop*, CONF-771129, Princeton, New Jersey (1978).
9. J. Knowles (Physics International), private communication, 1978.
10. T. Shannon (Oak Ridge National Laboratory), private communication, 1978.
11. D. N. Bolshutkin, Y. E. Stetsenko, L. A. Indan, and A. A. Khudoteplaya, *Sov. Phys. - Solid State* 120, 29 (1971); 121, 150 (1972).
12. P. C. Souers, "Cryogenic Hydrogen Data Pertinent to Magnetic Fusion Energy," Lawrence Livermore Laboratory, Livermore, California, to be published.
13. D. N. Bolshutkin, Y. K. Stetsenko, and L. A. Alekseeva, *Sov. Phys. - Solid State* 12, 119 (1970).

14. A. A. Illyushin and V. S. Lensky, *Strength of Materials*, translated by J. K. Lusher, Pergamon Press, New York (1971).
15. S. L. Milora, C. A. Foster, and G. D. Kerbel, *Bull. Am. Phys. Soc.* 21, 1052 (1976).

APPENDIX A
BIBLIOGRAPHY OF HYPERVELOCITY ACCELERATORS

Initial library searches indicated approximately 2000 different listings on hypervelocity accelerators and hypervelocity testing impact data. However, closer evaluation indicated that applicability to pellet fueling was limited to a very small percentage of these listings.

The documents with the most pertinent information are:

1. *Advanced Experimental Techniques for Study of Hypervelocity Flight*, Hypervelocity Techniques Symposium, University of Denver, Denver, Colorado, March 1967.
2. *Proceedings of the Fifth Symposium on Hypervelocity Impact*, Vols. I and II, Denver, Colorado, October 30, 1961.
3. *Proceedings of the Sixth Symposium on Hypervelocity Impact*, Vols. I and III, Cleveland, Ohio, April 30, 1963.
4. *Hypervelocity Impact Fourth Symposium*, Sponsored by U.S. Army, Navy, and Air Force, Vols. I, II, & III, April 1960.
5. *Proceedings of Seventh Hypervelocity Impact Symposium*, Vol. III, Tampa, Florida, November 17, 1964.

THIS PAGE
WAS INTENTIONALLY
LEFT BLANK

APPENDIX B
CRYOGENIC PROPERTIES OF H, D, AND T

The following tables have been supplied by Dr. P. C. Souers of the Lawrence Livermore Laboratory, Livermore, California. They are a part of his study entitled "Cryogenic Hydrogen Data Pertinent to Magnetic Fusion Energy," which is to be published this year. The latest tables include saturated properties of solid and liquid nH_2 , nD_2 , D-T (estimated), and nT_2 (estimated <104K).

In the tables the symbols are:

- Q^0 = vapor pressure solid
- P^0 = vapor pressure liquid
- ρ = vapor pressure liquid
- ρ_s, ρ_l = solid, liquid density
- Z = gas compressibility
- H_s, H_v = heat of sublimation, vaporization

Table B-1. Properties of nH₂

Solid T(K)	Q ⁰ (Pa)	Q ⁰ (torr)	ρ (mole/m ³)	Z	ρ_s (mole/m ³)	H _S (J/mole)
4.2	1.3(-4)	9.7(-7)	3.7(-6)	1.0000	44300	823
6	1.8(-1)	1.3(-3)	3.6(-3)	1.0000	44230	863
8	1.5(1)	1.1(-1)	2.3(-1)	0.9999	44090	908
10	2.4(2)	1.8	2.9	0.9988	43850	952
12	1.72(3)	1.29(1)	1.73(1)	0.9945	43500	993
14	7.41(3)	5.55(1)	6.47(1)	0.9836	43000	1025
16	2.33(4)	1.74(2)	1.82(2)	0.962	42340	1043
18	5.88(4)	4.41(2)	4.25(2)	0.925	41490	1039
20	1.27(5)	9.56(2)	8.81(2)	0.867	40430	1001
21	1.79(5)	1.34(3)	1.24(3)	0.828	39810	965
Liquid T(K)	P ⁰ (Pa)	P ⁰ (torr)	ρ (mole/m ³)	Z	ρ_L (mole/m ³)	H _V (J/mole)
14	7.38(3)	5.54(1)	6.45(1)	0.9837	38280	908
16	2.04(4)	1.53(2)	1.59(2)	0.9669	37430	922
18	4.60(4)	3.45(2)	3.26(2)	0.9426	36460	926
20	8.99(4)	6.74(2)	5.94(2)	0.9109	35380	917
22	1.58(5)	1.19(3)	9.92(2)	0.8711	34190	894
24	2.57(5)	1.93(3)	1.57(3)	0.8222	32890	853
26	3.93(5)	2.95(3)	2.38(3)	0.764	31270	792
28	5.73(5)	4.30(3)	3.56(3)	0.691	29350	702
30	8.04(5)	6.03(3)	5.40(3)	0.597	26890	567

Table B-2. Properties of nD₂

Solid T(K)	Q^0 (Pa)	Q^0 (torr)	ρ (mole/m ³)	Z	ρ_s (mole/m ³)	H_s (J/mole)
4.2	5.6(-9)	4.2(-11)	1.6(-10)	1.0000	50700	1219
6	2.2(-4)	1.7(-6)	4.4(-6)	1.0000	50660	1254
8	1.3(-1)	9.8(-4)	2.0(-3)	1.0000	50570	1293
10	6.7	5.1(-2)	8.1(-2)	1.0000	50430	1332
12	1.0(2)	7.6(-1)	1.0	0.9996	50220	1370
14	7.36(2)	5.52	6.34	0.9979	49930	1406
16	3.41(3)	2.56(1)	2.58(1)	0.9932	49540	1438
18	1.16(4)	8.71(1)	7.89(1)	0.9828	49030	1459
20	3.18(4)	2.38(2)	1.98(2)	0.9635	48410	1464
21	4.93(4)	3.70(2)	2.97(2)	0.950	48040	1459
Liquid T(K)	P^0 (Pa)	P^0 (torr)	ρ (mole/m ³)	Z	ρ_L (mole/m ³)	H_v (J/mole)
14	9.99(2)	7.49	8.61	0.9972	45200	1241
16	4.07(3)	3.06(1)	3.08(1)	0.9918	44410	1257
18	1.22(4)	9.13(1)	8.30(1)	0.9819	43520	1265
20	2.93(4)	2.20(2)	1.82(2)	0.9666	42520	1265
22	6.05(4)	4.54(2)	3.50(2)	0.9452	41420	1253
24	1.11(5)	8.36(2)	6.06(2)	0.9181	40210	1230
26	1.89(5)	1.41(3)	9.90(2)	0.8835	38890	1191
28	2.99(5)	2.24(3)	1.52(3)	0.843	37470	1138
30	4.50(5)	3.37(3)	2.27(3)	0.795	35950	1065

Table B-3. Properties of D-T (estimated)

Solid T(K)	Q^0 (Pa)	Q^0 (torr)	ρ (mole/m ³)	Z	ρ_s (mole/m ³)	H_s (J/mole)
4.2	3.6(-10)	2.7(-12)	1.0(-11)	1.0000	51980	1326
6	3.6(-5)	2.7(-7)	7.2(-7)	1.0000	51950	1360
8	3.6(-2)	2.7(-4)	5.4(-4)	1.0000	51870	1398
10	2.6	1.9(-2)	3.1(-2)	1.0000	51760	1436
12	4.7(1)	3.5(-1)	4.7(-1)	0.9998	51580	1473
14	3.90(2)	2.99	3.42	0.9988	51330	1509
16	2.06(3)	1.54(1)	1.56(1)	0.9957	51000	1542
18	7.62(3)	5.72(1)	5.15(1)	0.9883	50570	1567
20	2.23(4)	1.67(2)	1.38(2)	0.9738	50040	1578
21	3.56(4)	2.67(2)	2.12(2)	0.963	49730	1576
Liquid T(K)	p^0 (Pa)	p^0 (torr)	ρ (mole/m ³)	Z	ρ_L (mole/m ³)	H_v (J/mole)
14	6.42(2)	4.82	5.53	0.9981	46870	1345
16	2.75(3)	2.07(1)	2.08(1)	0.9942	46080	1356
18	8.67(3)	6.50(1)	5.87(1)	0.9866	45170	1362
20	2.02(4)	1.65(2)	1.36(2)	0.9742	44160	1359
22	4.74(4)	3.56(2)	2.71(2)	0.9563	43040	1347
24	9.08(4)	6.81(2)	4.88(2)	0.9323	41820	1322
26	1.58(5)	1.19(3)	8.10(2)	0.9025	40490	1284
28	2.57(5)	1.93(3)	1.28(3)	0.866	39050	1231
30	3.92(2)	2.94(3)	1.91(3)	0.824	37510	1163

Table B-4. Properties of nT₂ (estimated <104K)

Solid T(K)	Q ⁰ (Pa)	Q ⁰ (torr)	ρ (mole/m ³)	Z	ρ _S (mole/m ³)	H _S (J/mole)
4.2	2.9(-11)	2.2(-13)	8.3(-13)	1.0000	53110	1424
6	6.7(-6)	5.0(-8)	1.3(-7)	1.0000	53090	1458
8	1.1(-2)	8.2(-5)	1.7(-4)	1.0000	53030	1495
10	1.0	7.7(-3)	1.2(-2)	1.0000	52930	1532
12	2.3(1)	1.7(-1)	2.3(-1)	0.9999	52780	1569
14	2.22(2)	1.67	1.91	0.9993	52570	1605
16	1.27(3)	9.53	9.57	0.9972	52290	1638
18	5.09(3)	3.81(1)	3.43(1)	0.9919	51930	1665
20	1.58(4)	1.19(2)	9.69(1)	0.9809	51490	1681
21	2.59(4)	1.94(2)	1.52(2)	0.9725	51230	1683
Liquid T(K)	P ⁰ (Pa)	P ⁰ (torr)	ρ (mole/m ³)	Z	ρ _L (mole/m ³)	H _V (J/mole)
14	3.51(2)	2.63	3.02	0.9989	48410	1448
16	1.73(3)	1.31(1)	1.31(1)	0.9962	47610	1456
18	6.07(3)	4.55(1)	4.10(1)	0.9903	46690	1458
20	1.65(4)	1.24(2)	1.01(2)	0.9801	45670	1453
22	3.74(4)	2.80(2)	2.12(2)	0.9649	44540	1438
24	7.41(4)	5.56(2)	3.93(2)	0.9443	43300	1417
26	1.33(5)	9.95(2)	6.70(2)	0.9180	41960	1374
28	2.19(5)	1.65(3)	1.06(3)	0.887	40510	1324
30	3.41(5)	2.56(3)	1.61(3)	0.850	38950	1258

THIS PAGE
WAS INTENTIONALLY
LEFT BLANK

APPENDIX C

FUEL PELLETT INJECTION IMPACT FORCE

- ASSUME: a. A single degree of freedom pellet
 b. Cylindrical shape (see Fig. C-1)
 c. Strikes blade at relative impact, V_r , parallel to cylinder axis, and coefficient equal to zero (plastic impact-stick condition)
 d. Pellet velocity of 14.0 m/sec arriving at disc.
1. Relative displacement of pellet

$$x = \frac{V_r}{\omega_n} \sin \omega_n t$$

where

$$\omega_n = \sqrt{k/m} = \frac{1}{L} \sqrt{\frac{E}{\rho}}$$

2. Max impact force in pellet

$$Kx_{\max} = \frac{kV_r}{\omega_n} = V_r \sqrt{mk}$$

3. Max impact stress

$$\sigma_{\max} = \frac{kx_{\max}}{A} = V_r \sqrt{\frac{mk}{A^2}} = V_m \sqrt{E}$$

(See Fig. C-2.)

ORNL-DWG 79-2689 FED

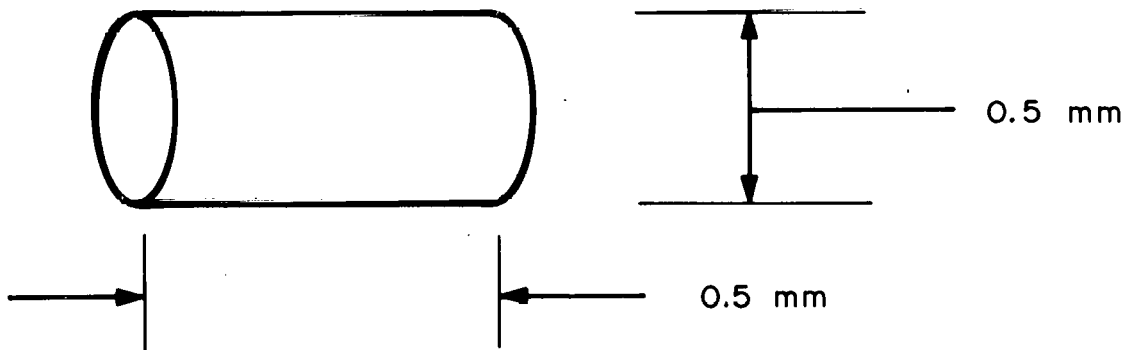


Fig. C-1. Cylindrical shape.

ORNL-DWG 79-2690 FED

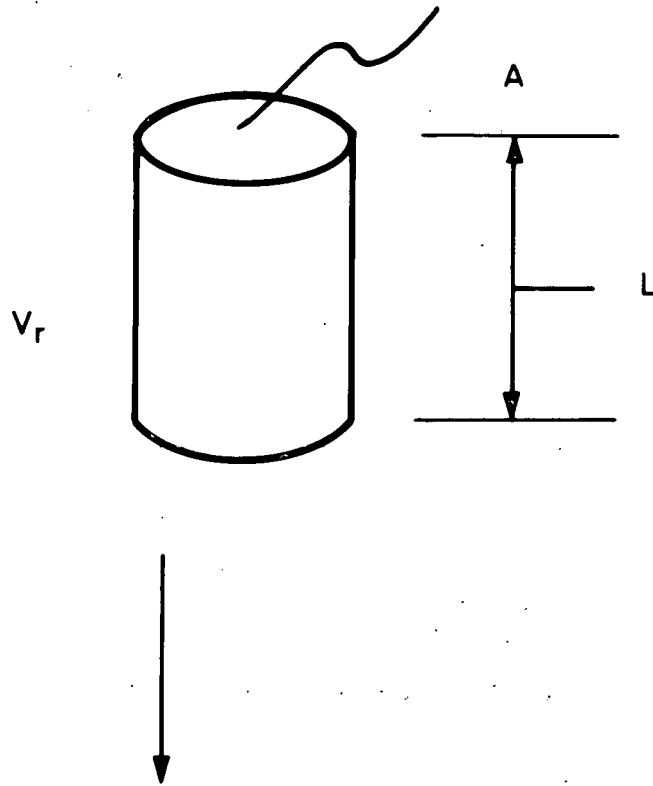


Fig. C-2. Max impact stress.

$$A = \frac{\pi}{4} d^2 = \frac{\pi}{4} (0.5)^2$$

$$\rho = 0.175 \text{ gm/cm}^3 \text{ (H)}$$

$$E \cong 60,000 \text{ psi}$$

$$\begin{aligned} \rho &= 0.175 \text{ gm/cm}^3 = \frac{1.75(16)}{28(16) \cdot (386H)} \times \frac{(2.54)^3}{\text{in.}^3} \\ &= 16.5662 \times 10^{-6} \text{ lb-sec}^2/\text{in.}^4 \end{aligned}$$

$$m = A(1)$$

$$k = \frac{AE}{L}$$

CASE I — PELLET "MISSES" HUB BY 10 mm = 0.01 m

Using the measured geometry of the ORNL demonstration injector as shown in Fig. C-3(a) in the computation of V_r , the velocity of the pellet is reduced by $\sqrt{2}$ because V_p makes an angle $\cong 45^\circ$ with plane of disc.

$$\theta = \cos^{-1} \frac{0.0675}{0.0775} = 29.43^\circ$$

$$\phi = \tan^{-1} \frac{0.0775}{0.0850} \sin \theta = 24.13^\circ$$

To compute the velocity of the pellet and the disc normal to the impact surface, the geometry shown in Fig. C-3(b) was used.

$$V_p = 14 \text{ m/sec}$$

$$V_{P_n} = \frac{14}{\sqrt{2}} \cos (14^\circ + 29.43^\circ) \cong 21 \text{ m/sec}$$

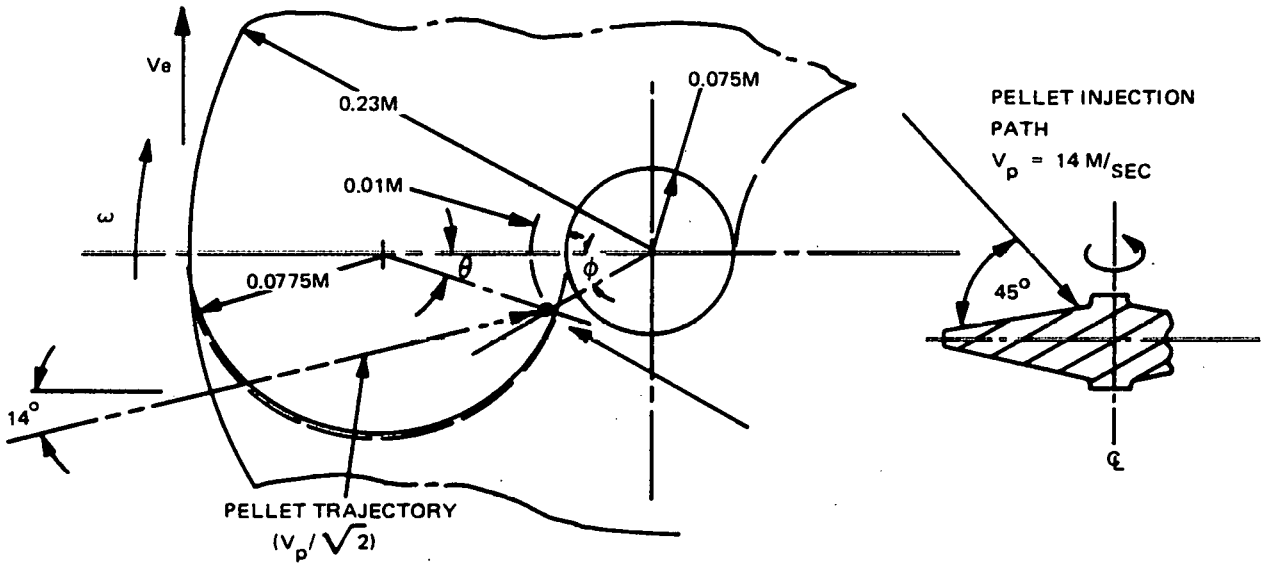


Fig. C-3.(a) Computation of relative impact velocity.

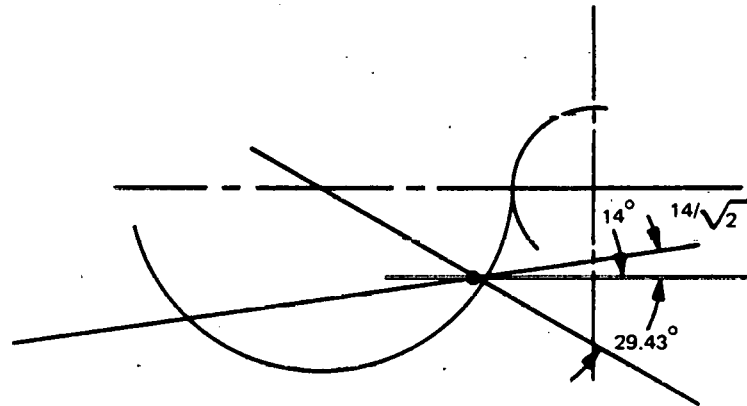


Fig. C-3.(b) Computation of velocity of pellet and disc normal to impact surface.

CASE II — PELLET "MISSES" HUB BY 5 mm = 0.005 m

$$\theta = \cos^{-1} \left(\frac{0.0675 + 0.005}{0.0775} \right) = 20.69^\circ .$$

$$\phi = \tan^{-1} \left(\frac{0.0775 \sin 20.69^\circ}{0.080} \right) = 18.90^\circ .$$

$$V_{P_n} = 14/\sqrt{2} \cos (14^\circ + 20.69^\circ) = 8.14 \text{ m/sec}$$

$$= 320.47 \text{ in./sec} .$$

$$r_2 = \sqrt{(0.0775 \sin 20.69^\circ)^2 + (0.080)^2} = 0.084556 .$$

$$V_{n_2} = r_2 \omega \cos (90^\circ - 20.69^\circ - 18.90^\circ)$$

$$= r_2 \omega \cos 50.41 = 110.1 \text{ m/sec} = 4335 \text{ in./sec} .$$

$$\sigma_{\text{max impact}} = 4665 \sqrt{E_p} = 4665 \sqrt{6 \times 10^5 \times 0.165662 \times 10^6}$$

$$= 4651 \text{ psi} .$$

CASE III — PELLET INITIAL "MISS" IS ZERO (INSIDE HUB GROOVE)

$$V_{P_n} = 14/\sqrt{2} = 9.9 \text{ m/sec} = 389.74 \text{ in./sec} .$$

$$V_{n_2} = 0, V_r = \sqrt{(9.9)^2 + (9.9)^2} = 14 \text{ m} = 551 \text{ in./sec} .$$

$$\sigma_{\text{max impact}} = 551 \sqrt{(6 \times 10^5) \times 0.165662 \times 10^6} = 549 \text{ psi} .$$

APPENDIX D
STRAIN RATE ASSESSMENT

Given here are approximations of strain rates and stresses of solid deuterium subjected to impact loading based on information given in Appendix B and by D. N. Bolshutkin, Yu. E. Stetsenko, and L. A. Alekseeva.¹³ The low temperature range (1.4-4K) is characterized by a brittle condition; at higher temperatures the sample is plastic.

Let us consider solid deuterium at 8K.

$$\sigma_y = 30 \text{ psi .}$$

$$E_1 = 19 \times 10^3 \text{ psi; } E_2 = 4.5 \times 10^3 \text{ psi .}$$

$$\rho = 0.08 \text{ g/cm}^3 = 7.6 \times 10^{-6} \text{ lb-sec}^2/\text{in.}^4 \text{ .}$$

For $\frac{\dot{u}}{\sqrt{E/\rho}} \leq e_y$ we have elastic impact

where

\dot{u} = particle velocity

$c = \sqrt{E/\rho}$ = wave velocity

e_y = yield strain .

For elastic impact,

$$\sigma = \rho c \dot{u} = \sqrt{E\rho} \dot{u} \text{ .}$$

Assuming a bilinear stress-strain law (see Fig. D-1),

E_1 = elastic modulus

E_2 = linear hardening modulus .

For plastic impact, stress at impact

$$\sigma = E_1 \sqrt{\frac{E_2}{E_1}} \frac{\dot{u}}{c} + E_1 \left(1 - \sqrt{\frac{E_2}{E_1}} \right) e_y$$

$$e_y = \sigma_y / E = 1.6 \times 10^{-3} .$$

Design impact velocity, $V_1 = 14 \text{ m/sec} = 551 \text{ in./sec.}$

Wave speed, $c = \sqrt{E/\rho} = 5 \times 10^4 \text{ in./sec.}$

$$\frac{\dot{u}}{c} = \frac{V_1}{c} = \frac{551}{5 \times 10^4} = 1.1 \times 10^{-2} = \frac{\dot{u}}{\sqrt{E/\rho}} .$$

$$e_y = 1.6 \times 10^{-3} .$$

$$\frac{\dot{u}}{\sqrt{E/\rho}} > e_y .$$

Impact stress for plastic impact

$$\sigma = E_1 \sqrt{\frac{E_2}{E_1}} \frac{\dot{u}}{c} + E_1 \left(1 - \sqrt{\frac{E_2}{E_1}} \right) e_y .$$

ORNL-DWG 79-2691 FED

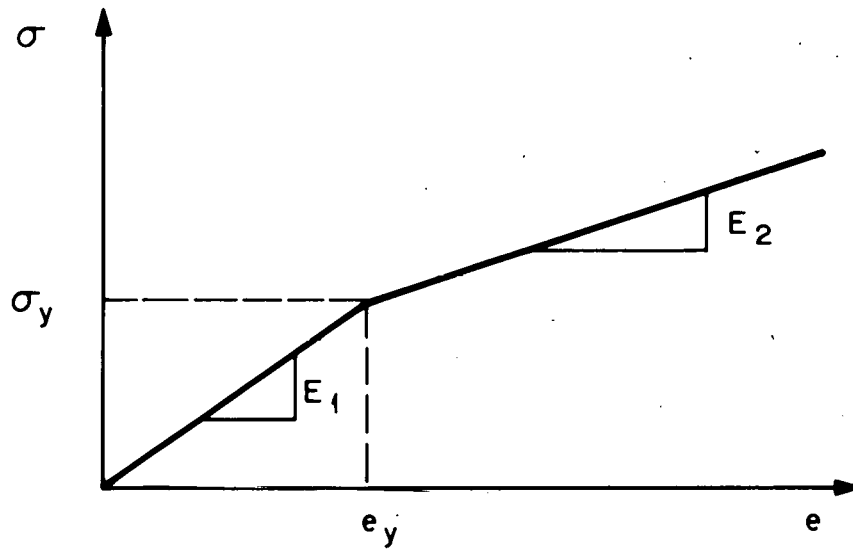


Fig. D-1. Strain rate assessment.

If elastic

$$\sigma = \sqrt{E\rho} \dot{u} = 210 \text{ psi .}$$

$$\frac{\dot{u}}{\sqrt{E/\rho}} / e_y \approx 7; \text{ therefore plastic impact.}$$

If plastic

$$\begin{aligned} \sigma_I &= \sqrt{E_1\rho} \dot{u} \sqrt{\frac{E_2}{E_1}} + E_1 \left(1 - \sqrt{\frac{E_2}{E_1}} \right) e_y \\ &= 210 \times (0.5) + (0.5) (1.57 \times 10^{-3}) (19 \times 10^3) \\ &= 118 \text{ psi .} \end{aligned}$$

Impact stress is reduced approximately 50% in plastic range.

Consider dynamic properties; assume

$$E_1 = 4E_1 \text{ (static)}$$

$$E_2 = 4E_2 \text{ (static)}$$

$$\sigma_I = 256 \text{ psi .}$$

Still highly plastic, the impact is partially absorbed by plastic deformation.

Force-strain curve.

Measure time of impact (see Fig. D-2).

$$\sigma = \bar{\sigma} \left(1 - \cos \frac{\pi}{2t} t \right) .$$

The minimum time of impact is the time it takes a wave to traverse back and forth across specimen.

ORNL-DWG 79-2692 FED

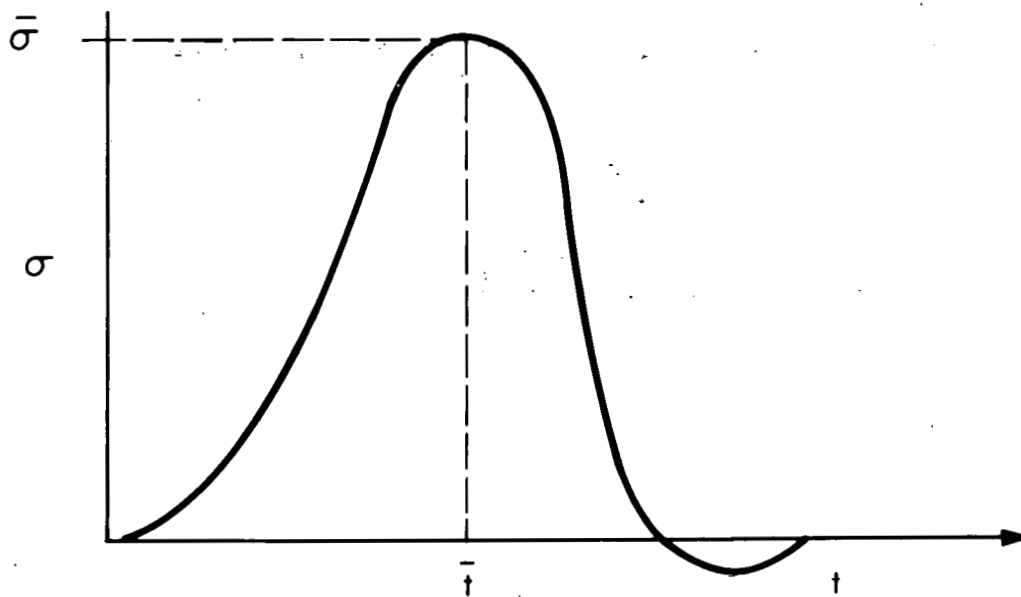


Fig. D-2. Impact time.

Let $l = 0.5 \text{ cm} = 0.197 \text{ in.}$

The time for wave to travel $l = \frac{l}{c} = 3.92 \times 10^{-6} \text{ sec} = \bar{t}$

$$\bar{\sigma} = 256 \text{ psi .}$$

$$\bar{t} \geq 3.92 \times 10^{-6} \text{ sec .}$$

$$|\dot{\sigma}|_{\max} = \bar{\sigma} \frac{\pi}{2\bar{t}} , \quad |\dot{\sigma}|_{\max} < 10 \times 10^7 \text{ psi/sec .}$$

$$\dot{\epsilon} < 2.5 \times 10^3 .$$

$$\text{Strain rate} \approx (10^3 - 10^4) \frac{\text{in./in.}}{\text{sec}} .$$

APPENDIX E
STATIC PELLET LOADS

The injection devices impart forces by various methods: mechanically, by viscous gas drag force, by shock or explosive, by rocket reaction, or by techniques using a gas medium. The pellet is subjected to impact loads, friction, or compressive loads with forces produced by mechanical loads — probably the most severe.

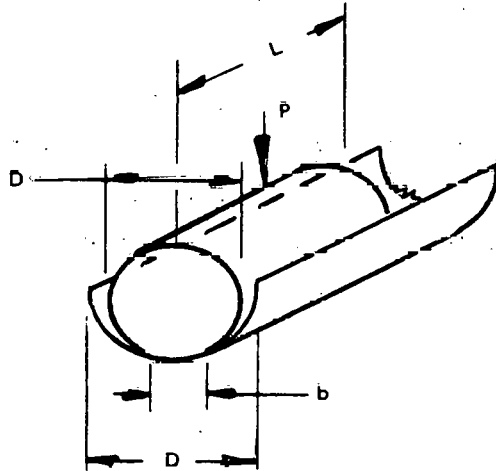
Mechanical devices are usually fabricated of metallic materials or composite plastics. If the effect of the material deformation were to be examined, it is apparent that deflection effects of the other materials on the pellet are insignificant in relation to the pellet behavior. The values of elastic properties (E) of various possible materials contacting a pellet are listed below:

Steel	$E = 30 \times 10^6$
Titanium	$E = 20 \times 10^6$
Aluminum	$E = 10 \times 10^6$
Kevlar (plastic)	$E = 1 \times 10^6$
D-T (estimated)	$E = 6 \times 10^4$

For example, the interaction of a hydrogen pellet in contact with a semicircular track in a centrifugal accelerator of Kevlar plastic composite with cylinder pellet proportions and groove dimensions is shown in Fig. E-1. The relation of both the deformed area of the pellet (b) and the compression stress (σ_c) on the pellet is given by Eqs. (E.1) and (E.2).

$$b = 1.6 \sqrt{P \frac{D_1 D_2}{D_1 + D_2} \left(\frac{1 - \nu_1^2}{E_1} + \frac{1 - \nu_2^2}{E_2} \right)} \quad (\text{E.1})$$

ORNL-DWG 79-2707 FED



- P = Load on Cylinder
- D = Pellet Dia
- D = Groove Dia
- L = Pellet Length
- E = (Pellet)
- E = Mtl Track
- b = footprint width

Fig. E-1. Pellet/track geometry.

where

$$p = P/L D_1, E_1, \nu_1 \text{ (track)}$$

$$= 0.3 D_2, E_2, \nu_2 \text{ (pellet)}$$

b = width developed by mutual deformation.

$$\sigma_c = 0.798 \sqrt{\frac{D_1 + D_2}{D_1 D_2} \frac{P}{\frac{1 - \nu_1^2}{E_1} + \frac{1 - \nu_2^2}{E_2}}} \quad (\text{E.2})$$

$\sigma_{c_{\max}}$ = max unit stress developed in the pellet.

If calculated for the track (0.00000091) or for the pellet (0.000016), it governs both the stress and deformation. The pellet is so soft in relation to any reasonable material surface that it has minimal influence on other surfaces. It is also shown that fitting a pellet closely to a mating surface geometrically reduces both pellet deflection and stress.

THIS PAGE
WAS INTENTIONALLY
LEFT BLANK

APPENDIX F
DYNAMIC ANALYSES FOR TWO ROTATING
PARTICLE ACCELERATING DEVICES

Dynamic analyses were conducted to determine the performance of two rotating types of centrifugal injectors. This Appendix contains the analytical details, the FORTRAN computer coding, and the numerical results which were summarized in Sect. 4.1.

ROTATING STRAIGHT TRACK ACCELERATOR

Consider a straight tube which rotates with angular velocity ω (see Fig. F-1). In the absence of all other forces, a particle of mass m contained within the tube will move radially outward, impeded only by the contact force of the tube. This force is decomposed into a friction component, F_f , and a normal component, F_n , which rotate, together with a polar coordinate system (r, θ) , at angular speed, ω . The friction component is related to the normal force component through the coefficient of friction, μ . Thus,

$$F_f = \mu F_n \quad (F.1)$$

Newton's second law of mechanics applied to the particle relates these force components through the equations

$$F_n = 2m\dot{r}\omega \quad (F.2)$$

and

$$F_f = m(r\dot{\omega}^2 - \ddot{r}) \quad (F.3)$$

where $\dot{(\)}$ denotes $d(\)/dt$ and t is time.

ORNL-DWG 79-2727 FED

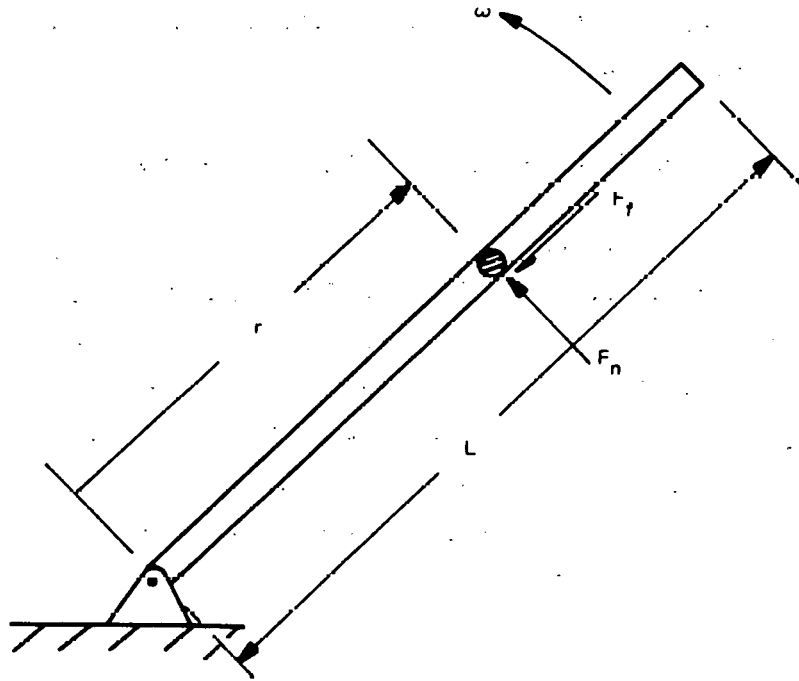


Fig. F-1. Rotating straight track particle accelerator parameters.

Combining Eqs. (F.1), (F.2), and (F.3) yields the differential equation

$$\ddot{r} + 2\mu\omega\dot{r} - \omega^2 r = 0 . \quad (F.4)$$

The solution to Eq. (F.4), subject to the initial conditions

$$r(t = 0) = r_0 \quad (F.5)$$

and

$$\dot{r}(t = 0) = v_0 \quad (F.6)$$

is

$$r = e^{-\mu\omega t} r_1$$

where

$$r_1 = r_0 \cosh \alpha t + B \sinh \alpha t . \quad (F.7)$$

$$\alpha = \omega(1 + \mu^2)^{1/2} \quad (F.8)$$

and

$$B = (v_0 + \mu\omega r_0)/\alpha . \quad (F.9)$$

A computer program based upon these equations was written in FORTRAN with the following symbol equivalences:

$\omega = W$
 $r_0 = \text{DISP}$
 $v_0 = \text{VEL}$
 $\mu = \text{FR}$
 $t = \text{TIME}$
 $\alpha = \text{ALPHA}$
 $B = \text{BETA}$
 $r = \text{RHO}$
 $r_1 = \text{PI}$.

The solution logic used in the computer program was to increment time (DTIME) in steps of $\pi/(50\omega)$ until the particle exits the rotating tube as governed by the relationship $r \geq L$. A listing of the computer program is shown in Fig. F-2.

ROTATING SEMICIRCULAR TRACK ACCELERATOR

The kinematics of a particle moving on a semicircular track which rotates about an eccentrically offset center (see Fig. F-3) with angular velocity, ω , are derived in terms of a compound rotating coordinate system. The position vector, \vec{r} , of the particle is given in terms of unit polar, \vec{e}_ρ and \vec{e}_θ , and cartesian vectors, \vec{e}_x and \vec{e}_y , as

$$\vec{r} = \rho \vec{e}_\rho + \epsilon \vec{e}_y \quad (\text{F.11})$$

The corresponding velocity, \vec{V} , and acceleration, \vec{a} , vectors are given by

$$\vec{V} = \dot{\vec{r}} = \dot{\rho} \vec{e}_\rho + \rho(\dot{\theta} + \omega) \vec{e}_\theta + \epsilon \dot{\vec{e}}_y \quad (\text{F.12})$$

and

$$\begin{aligned} \vec{a} = \dot{\vec{V}} = & [\ddot{\rho} - \rho(\dot{\theta} + \omega)^2] \vec{e}_\rho \\ & + [\rho\ddot{\theta} + 2\dot{\rho}(\dot{\theta} + \omega)] \vec{e}_\theta + \epsilon \ddot{\vec{e}}_y \quad (\text{F.13}) \end{aligned}$$

LEVEL 2,2,1 (DEC 77)

09/360 FORTRAN M EXTENDED

DATE 78,200/08,30,21

PAGE 1

REQUESTED OPTIONS: NUDECK,OPT(2)

OPTIONS IN EFFECT: NAME(MAIN) OPTIMIZE(2) LINECOUNT(55) SIZE(MAX) AUTOOBL(NONE)
 SOURCE EBCDIC NOLIST NUDECK OBJECT MAP NOFORMAT GUSTHY NOXREF ALC NUANSF TERM FLAG(1) DUMP

```

ISN 0002      NR2044
ISN 0003      L=9.0551
ISN 0004      DT=90.2
ISN 0005      V=180.0
ISN 0006      FR=0.2
ISN 0007      PI=1.4159265
ISN 0008      DTIME=PI/(W*50.)
ISN 0009      PLOTZ=1.001
ISN 0010      ALPHA=PI*(1+FR**2)**0.5
ISN 0011      BETA=(VEL+FR**2*DISP)/ALPHA
ISN 0012      WRITE(6,10)
ISN 0013      WRITE(6,15)
ISN 0014      WRITE(6,20)
ISN 0015      DO 400 I=1,1000
ISN 0016      TIME=(I-1)*DTIME
ISN 0017      AT=ALPHA*TIME
ISN 0018      P1=(DISP+COSH(AT))*(BETA+SINH(AT))
ISN 0019      P2=(DISP*SINH(AT))*(BETA+COSH(AT))
ISN 0020      FATE=(FR*TIME)
ISN 0021      ZEXP(FATE)
ISN 0022      RHOZ=PI
ISN 0023      RHO=Z*(ALPHA**2+FR**2)
ISN 0024      RHO=Z*((ALPHA**2*(FR**2)**2)*PI-(2.*FR**ALPHA**2))
ISN 0025      VTH=RHO**0.5
ISN 0026      AN=2.*RHO**0.5
ISN 0027      WRITE(6,30)I,TIME,RHO,RHOZ,RHODD,VTH,AN
ISN 0028      WRITE(6,40)
ISN 0029      IF (RHO .GT. PLOTZ) GO TO 500
ISN 0030      15 FORMAT(1X,STEP,TIME,ANI,RHO,RHO*,RHO*)
ISN 0031      20 FORMAT(2X,/)
ISN 0032      30 FORMAT(2X,13.6E14.4)
ISN 0033      40 FORMAT(2X,/)
ISN 0034      IF (RHO .GT. PLOTZ) GO TO 500
ISN 0035      400 CONTINUE
ISN 0036      500 CONTINUE
ISN 0037      STOP
ISN 0038      END
    
```

NAME TAG TYPE ADD				/ MAIN /				SIZE OF PROGRAM 000444 HEXADECIMAL BYTES						
AN	SF	R#4	000150	NAME	TAG	TYPE	ADD	NAME	TAG	TYPE	ADD	NAME	TAG	TYPE
P1	SF	R#4	000160	L	SF	R#4	000154	H	SF	R#4	000158	Z	SF	R#4
RHO	SF	R#4	000170	AT	SFA	R#4	000164	FR	SF	R#4	000168	PI	SF	R#4
DISP	SF	R#4	000000	VEL	SF	R#4	000174	EXP	SF	XF	R#4	FATE	SFA	R#4
				DISP	SF	R#4	000180	VTH	SF	R#4	000184	BETA	SF	R#4
							00018C	RHOZ	SF	R#4	000190	SINH	SF	XF

Fig. F-2. FORTRAN listing - rotating straight track accelerator.

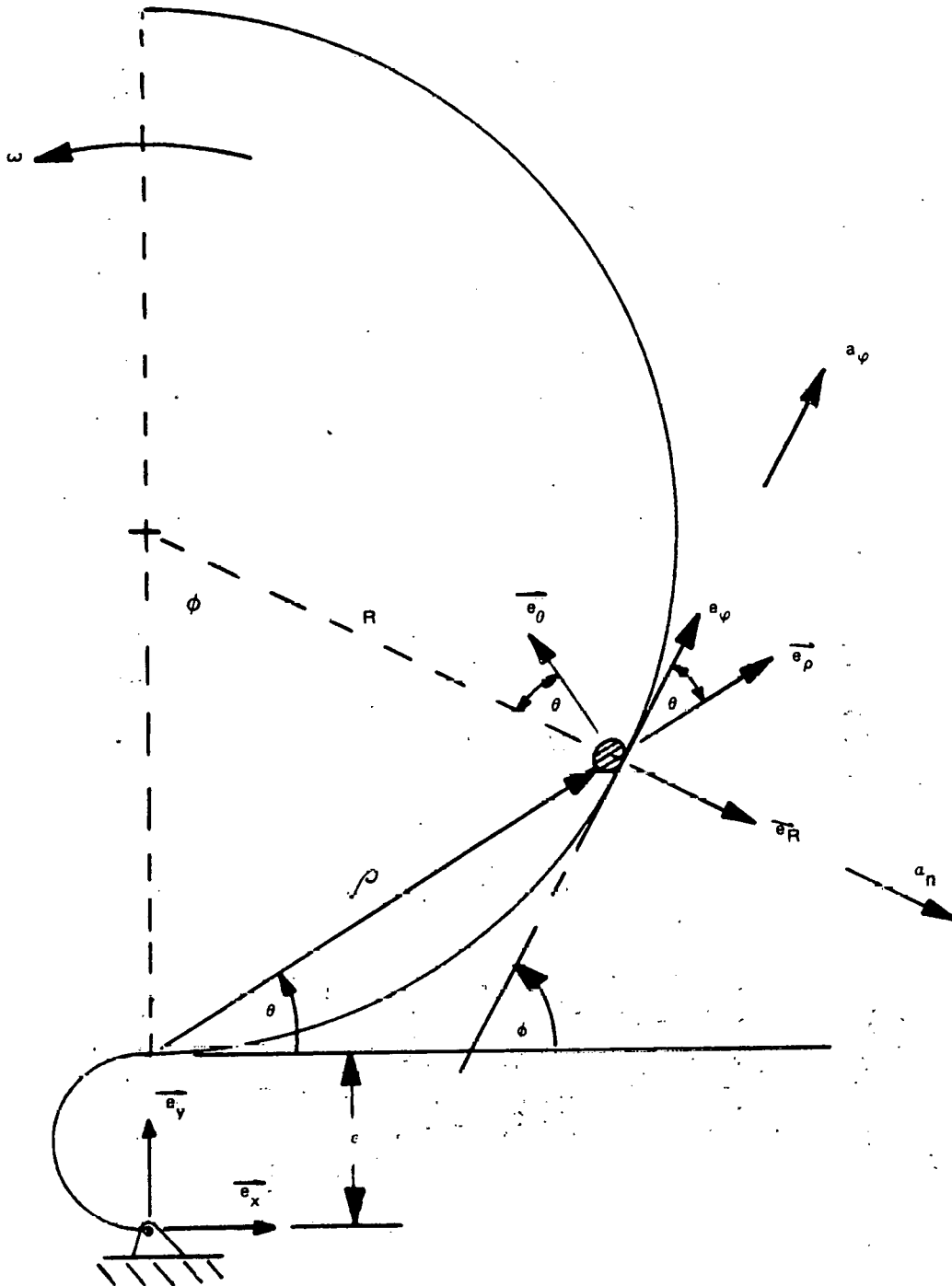


Fig. F-3. Rotating semicircular track accelerator parameters.

Noting that

$$\begin{aligned}
 \dot{\vec{e}}_y &= -\omega \vec{e}_x \\
 \ddot{\vec{e}}_y &= -\omega \dot{\vec{e}}_x = -\omega^2 \vec{e}_y \\
 \vec{e}_y &= \sin \theta \vec{e}_\rho + \cos \theta \vec{e}_\theta \\
 \vec{e}_x &= -\sin \theta \vec{e}_\theta + \cos \theta \vec{e}_\rho ,
 \end{aligned}
 \tag{F.14}$$

the rotating radial and tangential components of the acceleration, a_ρ and a_θ , respectively, become

$$\begin{aligned}
 a_\rho &= \ddot{\rho} - \rho(\dot{\theta} + \omega)^2 - \omega^2 \epsilon \sin \theta \\
 a_\theta &= \rho \ddot{\theta} + 2\dot{\rho}(\dot{\theta} + \omega) - \omega^2 \epsilon \cos \theta .
 \end{aligned}
 \tag{F.15}$$

From Fig. F-3 it is seen that

$$\rho = 2R \sin \theta
 \tag{F.16}$$

which upon repeated differentiation yields

$$\begin{aligned}
 \dot{\rho} &= 2R \cos \theta \dot{\theta} \\
 \ddot{\rho} &= -2R \sin \theta \dot{\theta}^2 + 2R \cos \theta \ddot{\theta} .
 \end{aligned}
 \tag{F.17}$$

Combining these last three equations with the geometric conditions

$$\begin{aligned}
 a_n &= a_\rho \sin \theta - a_\theta \cos \theta \\
 a_\phi &= a_\rho \cos \theta + a_\theta \sin \theta
 \end{aligned}
 \tag{F.18}$$

gives

$$a_n = -4R\dot{\theta}(\dot{\theta} + \omega) - 2R\omega^2 \sin^2 \theta - \omega^2 \epsilon (\cos^2 \theta - \sin^2 \theta) \quad (\text{F.19})$$

and

$$a_\phi = 2R\ddot{\theta} - 2R\omega^2 \sin \theta \cos \theta - 2\omega^2 \epsilon \sin \theta \cos \theta .$$

Applying Newton's second law and the friction condition, Eq. (1), once again yields

$$\mu a_n = -a_\phi . \quad (\text{F.20})$$

Upon substitution of Eq. (F.19) into Eq. (F.20), the following differential equation is obtained:

$$\begin{aligned} \ddot{\theta} + 2\mu\dot{\theta}^2 + 2\mu\omega\dot{\theta} + \omega^2 \sin \theta (\mu \sin \theta - \cos \theta) \\ + \frac{\epsilon\omega^2}{2R} [\mu(1 - 2 \sin^2 \theta) - 2 \sin \theta \cos \theta] = 0 . \end{aligned} \quad (\text{F.21})$$

Since Eq. (F. 21) is highly nonlinear, it was solved by numerical integration. The FORTRAN program written for this purpose employs the following equivalence symbols with reference to those used above:

ω = W
 ϵ = E
 μ = FR
 θ = DISP
 $\dot{\theta}$ = VEL
 $\ddot{\theta}$ = ACCEL
 t = TIME
 a_n = AN
 a_ϕ = AP .

The initial velocity condition for $\dot{\theta}$, required for a solution, follows from the tangential velocity component, V_ϕ [see Eqs. (F.12), (F.14), and (F.18)].

$$V_\phi = 2R\dot{\theta} + 2\omega R \sin^2 \theta - \epsilon\omega(\cos^2 \theta - \sin^2 \theta) \quad (\text{F.22})$$

and the initial position condition

$$\theta(t = 0) = 0 .$$

Thus,

$$\dot{\theta}_0 = \frac{v_0}{2R} + \frac{\epsilon\omega}{2R} \quad (\text{F.23})$$

where

$$v_0 = V_\phi(t = 0) .$$

The solution logic used in the computer program was to increment the time (DTIME) in steps of $\pi/(50\omega)$ until the particle exits the rotating semicircle as governed by the relationship $\theta \geq \pi/2$. A computer listing of the program is shown in Fig. F-4.

NUMERICAL RESULTS

The centrifugal injector received a major share of analysis because it seemed to have the capability of accelerating both small and large pellets to an acceptable velocity range.

In evaluating the centrifugal injector we sought to calculate these effects:

- rotational velocity needed for a given pellet exit velocity by a straight radial track and a semicircular track,
- effect of initial pellet injection velocity (V_{in}) on the exit velocity,

LEVEL 2,2,1 (DEC 77)

DS360 FORTRAN M EXTENDED

DATE 7A,216/12,00,20

PAGE 1

REQUESTED OPTIONS: NNODECK,OPT(2)

OPTIONS IN EFFECT: NAME(MAIN) OPTIMIZE(2) LINECOUNT(55) SIZE(MAX) AUTOJDL(NONE)
SOURCE EBCDIC MHLIST NNODECK REJECT MAP MFORMAT GHOST MHLREF ALC MANSF TERM FLAG(1) DUMP

```

ISN 0002      N=2044.
ISN 0003      E=0.
ISN 0004      R=4.52755
ISN 0005      FR=0.1
ISN 0006      DISP=0.
ISN 0007      VEL=645.
ISN 0008      PI=3.14159265
ISN 0009      DTIME=PI/(N*50.)
ISN 0010      PLOTZ=PI/2.*1.001
ISN 0011      WRITE(6,10)
ISN 0012      WRITE(6,15)
ISN 0013      WRITE(6,20)
ISN 0014      DO 400 I=1,1000
ISN 0015      TIME=(I-1)*DTIME
ACCEL=(N**2*SIN(DISP)+(COS(DISP)-(FR*SIN(DISP))))-(2.*FR*(VEL**2+
1*VEL))+(N**2*E/(2.*R))*(SIN(2.*DISP)+FR*2*(SIN(DISP)**2)-FR)
IF(TIME .EQ. 0.) GO TO 200
DISP=DISP+VEL*DTIME+2.*ACCEL*DTIME**2/3.-AOLD*DTIME**2/6.
VEL=VEL+3.*ACCEL*DTIME/2.-0.5*AOLD*DTIME
100 CONTINUE
GO TO 300
200 DISP=DISP+VEL*DTIME+0.5*ACCEL*DTIME**2
VEL=VEL+ACCEL*DTIME
300 CONTINUE
ANN=(4.*R*VEL*(VEL+N)+2.*R*N**2*SIN(DISP)**2)
ANN=-ANN
AP=2.*R*ACCEL.-2.*R*N**2*SIN(DISP)*COS(DISP)
VN=-2.*R*N*SIN(DISP)*COS(DISP)
VP=2.*R*VEL*COS(DISP)**2+2.*R*(N+VEL)*SIN(DISP)**2
AOLD=ACCEL
WRITE(6,30) I, TIME, DISP, VEL, ACCEL, ANN, AP, VN, VP
WRITE(6,40)
10 FORMAT(1-1)
15 FORMAT(1X,1STEP      TIME      ANNA      VN      VP)
1 **
20 FORMAT(2X,/)
30 FORMAT(2X,13,8E14,4)
40 FORMAT(2X,/)
IF(DISP .GT. PLOTZ) GO TO 500
400 CONTINUE
500 CONTINUE
STOP
END

```

100

NAME	TAG	TYPE	ADD.	NAME	TAG	TYPE	ADD.	NAME	TAG	TYPE	ADD.	NAME	TAG	TYPE
				MAIN				SIZE OF PROGRAM	000540	HEXADECIMAL	BYTES			

Fig. E-4. FORTRAN listing - rotating semicircular track accelerator.

- effect of track friction on the exit velocity,
- effect of impeller radius and spin velocity on the exit velocity.

It must be noted that early in the study we felt that subjecting the pellet to high dynamic forces was not desirable, and therefore we suggested geometry and injection methods that minimized such loading. Since necessary material properties were unavailable, these analyses were performed to provide sizing and trending data rather than absolute answers.

The demonstration injector, shown in Fig. 4-3, is designed to provide a 940-m/sec exit velocity with 0.05-cm-diam cylindrical H pellets. Analyses indicated large pellet deformations and Hertzian stresses with these hydrogen pellets. The density and mass of a D-T pellet of similar configuration yielded stress and deflections approximately three times higher (since the ratio of D-T density to hydrogen density is 3 to 1). By expanding the diameter of the basic injector design we established, as shown in Fig. F-5, the effect of varying impeller speed and diameter on pellet exit velocity. Figure F-6 illustrates the maximum pellet forces which occur at the point the pellet leaves the injector for both a curved (ORNL) and straight radial track. One conclusion drawn is that very large impellers are required to reduce pellet forces to a tolerable level. It also shows that the tubular or straight radial track is not as efficient as the semicircular track. This conclusion is valid only for the case of coefficients of friction less than 0.1.

Figure F-7 shows the effect of track shape on pellet exit velocity with the same diameter and impeller speed, as well as the reduction of exit velocity if moderate friction (coefficients of 0.2 or higher) is involved. The analysis shows that at coefficients of friction $\mu \geq 0.25$, the pellet does not leave the loop track. The phenomenon underlines the importance of friction in any device in which the pellet slides, like the impeller, for a substantial length of a pneumatic gun barrel. The results also show that the time to reach the exit point is very short, leaving little time to ablate or generate a gas dynamic blanket that could reduce sliding friction effects.

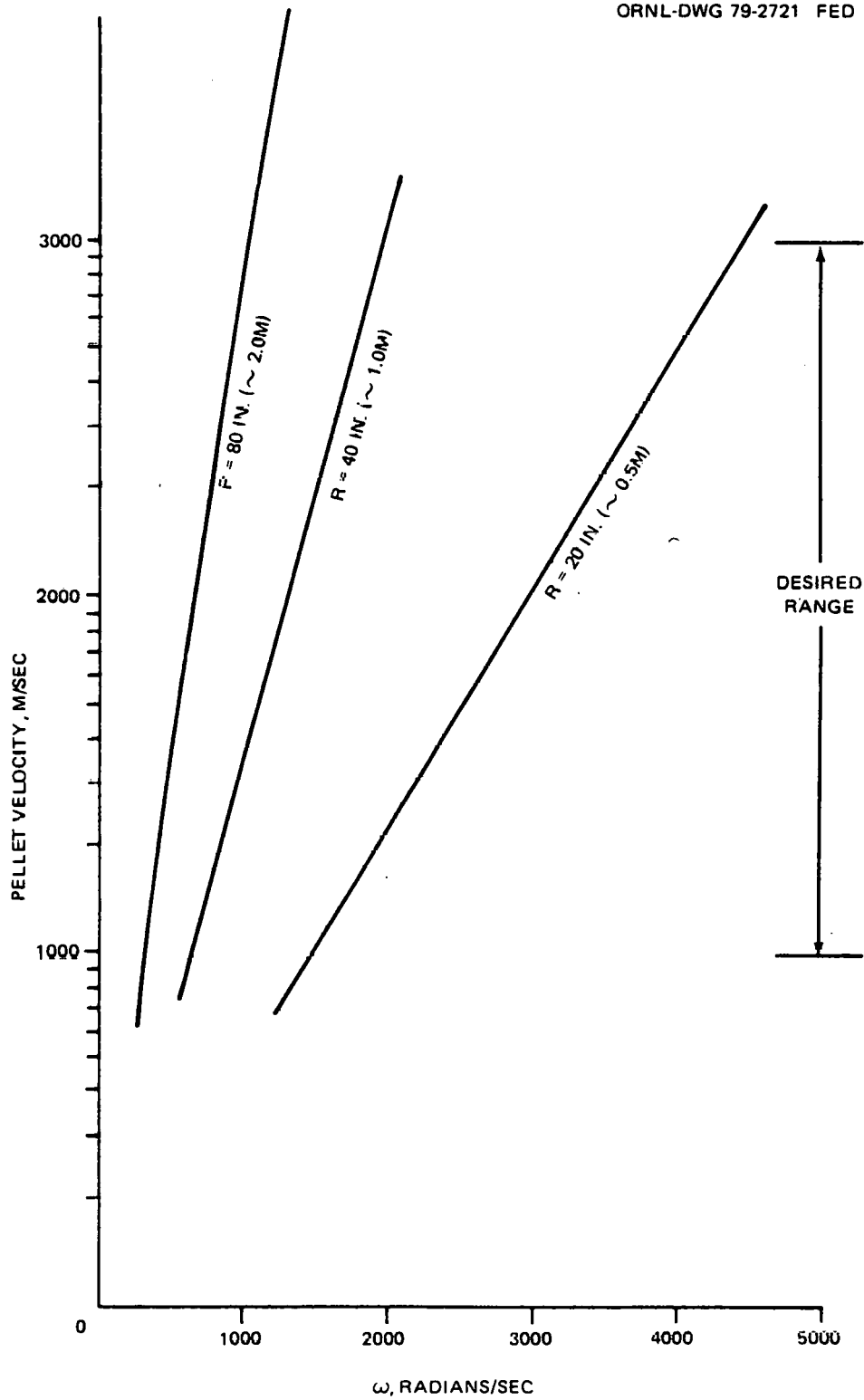


Fig. F-5. Pellet velocity vs impeller speed ORNL geometry - expanded.

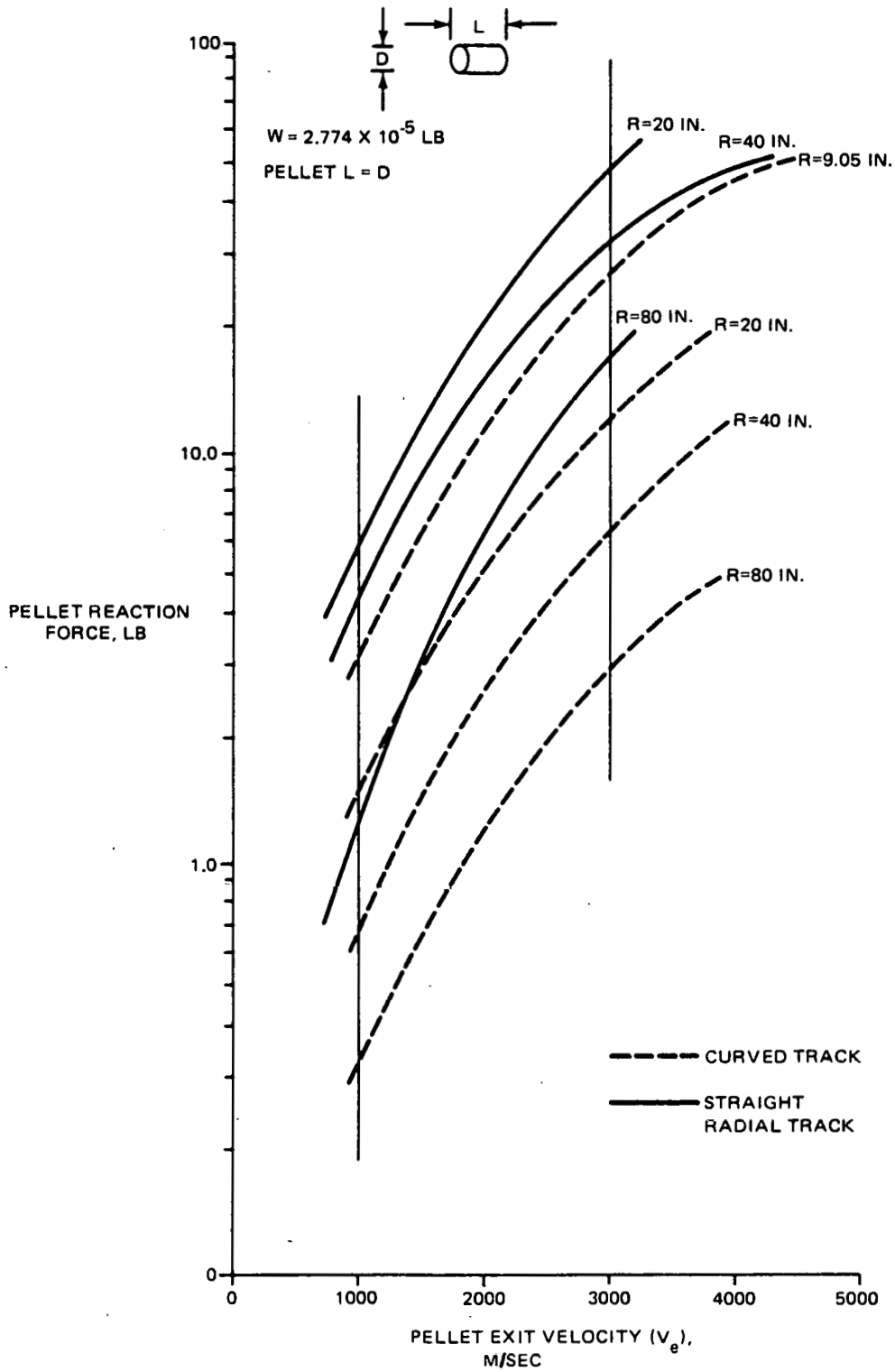


Fig. F-6. Pellet reaction forces — straight vs curved track centrifugal impeller.

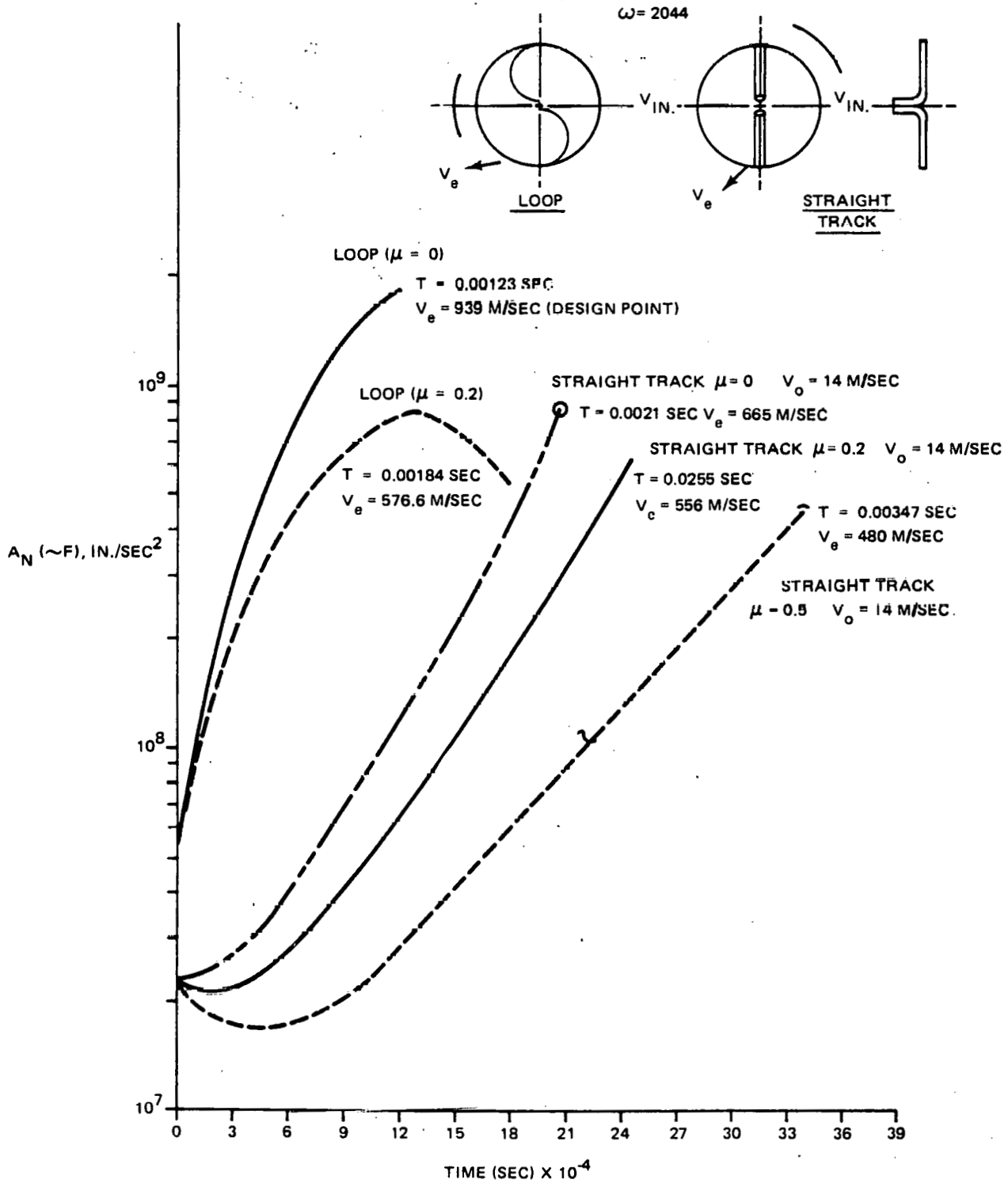


Fig. F-7. Pellet acceleration forces — loop vs straight track.

Figure F-8 shows the pellet velocity vs time for the curved track and the loop track. The initial velocities of the pellet injection to the curved track were 150 m/sec and 250 m/sec. This computation was made to compare the effect of injection velocity and to see if higher injection velocities would improve the performance of the injector. It was shown that increasing the injection velocity by 100 m/sec resulted in only a 40-m/sec exit velocity increase. This does not seem to warrant the use of higher initial velocities and would also tend to increase the dynamic pellet shock loading.

The loop originates at the center of the impeller and has a longer track length than the curved track, permitting the pellet to be accelerated over a longer distance. This results in a higher exit velocity for the loop as well as a greater time for the pellet to exit for the frictionless cases considered.

We examined the results of a computer analysis for a 40-in. radius, ORNL configuration type disc spinning at 492 rad/sec with an initial injection velocity of 100 m/sec to further evaluate the effects of friction. For $\mu = 0$, the exit velocity was 1041 m/sec, and the exit time was 0.00338 sec. For $\mu = 0.05$, the exit velocity was 921 m/sec, and the exit time was 0.00377 sec. At a rotational speed of 492 rad/sec and a time difference of 0.00039 sec (0.00377-0.00338 sec), the variation in angular position of the impeller exit point is approximately 11° (0.192 rad). The variation in distance along the circumference of the impeller is 7.5 in. Thus, the problem of aligning the impeller exit point with the injection tube to the plasma chamber is highly sensitive to pellet friction. It also is apparent that any variation in pellet-to-pellet friction must be kept within very small limits.

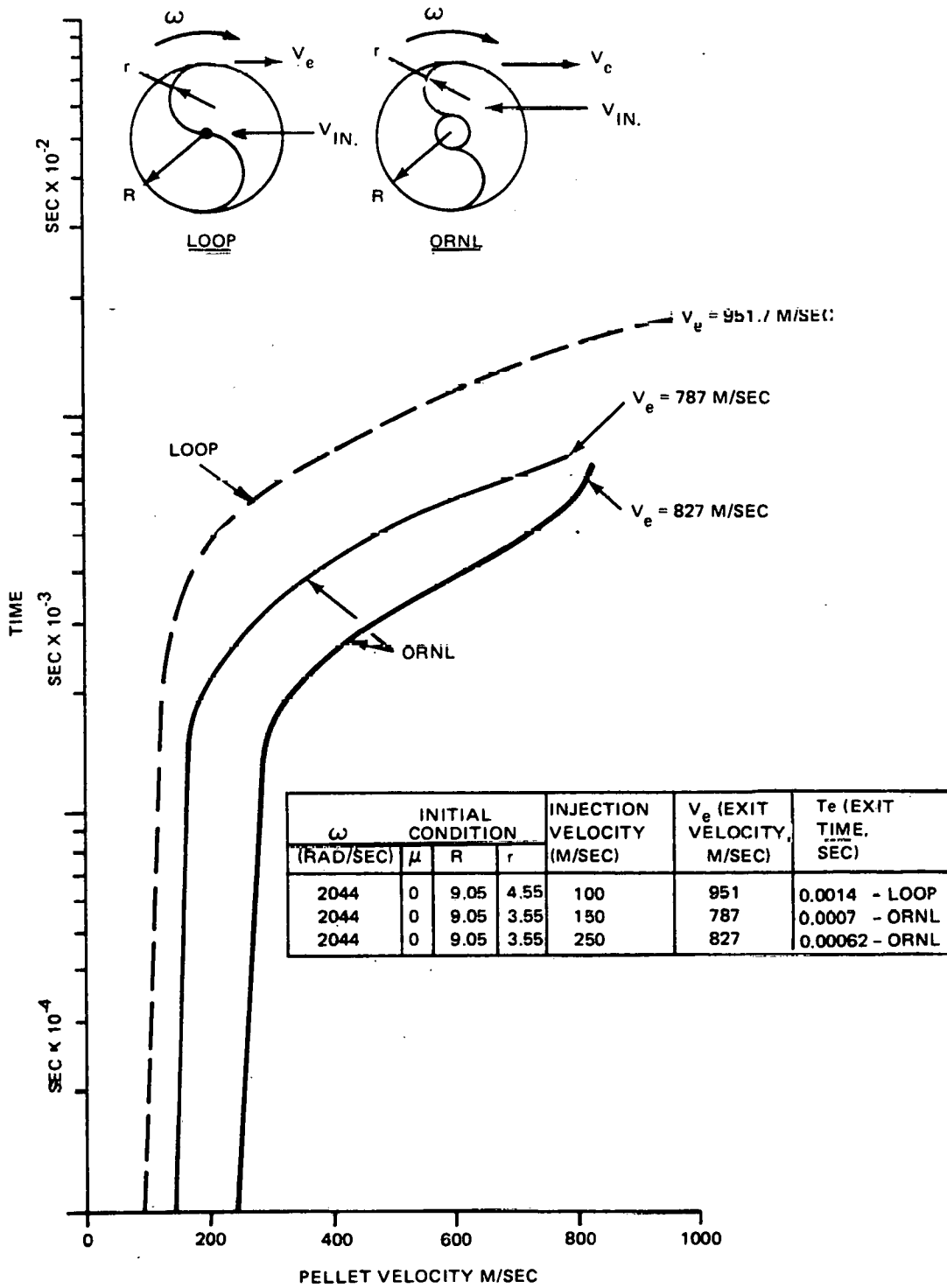


Fig. F-8. Pellet velocity comparison - ORNL modified injector vs loop.

INTERNAL DISTRIBUTION

- | | | | |
|--------|----------------|--------|---|
| 1. | W. R. Becraft | 61. | J. S. Watson |
| 2. | T. G. Brown | 62. | G. W. Wiseman |
| 3. | E. H. Bryant | 63-64. | Central Research Library |
| 4. | J. D. Callen | 65-66. | Fusion Energy Division
Library |
| 5. | W. A. Houlberg | 67. | Fusion Energy Division
Communications Center |
| 6. | R. L. Reid | 68-69. | Laboratory Records Department |
| 7. | J. A. Rome | 70. | Laboratory Records, ORNL-RC |
| 8. | C. Sardella | 71. | ORNL Patent Office |
| 9. | T. E. Shannon | 72. | Document Reference Section |
| 10-59. | D. Steiner | | |
| 60. | N. A. Uckan | | |

EXTERNAL DISTRIBUTION

73. R. E. Aronstein, Bechtel, P.O. Box 3965, San Francisco, CA 94119
74. D. J. Anthony, General Electric Co., Bldg. 23, Rm. 290, 1 River Rd., Schenectady, NY 12345
75. J. E. Baublitz, Office of Fusion Energy, Department of Energy, Washington, DC 20545
76. D. S. Beard, Office of Fusion Energy, Department of Energy, Washington, DC 20545
77. G. Benedict, Department of Energy, Oak Ridge Operations, P.O. Box E, Oak Ridge, TN 37830
78. S. L. Bogart, Science Applications Inc., 8400 Westpark Drive, McLean, VA 22102
79. R. Boom, University of Wisconsin, Madison, WI 53706
80. R. Botwin, Grumman Aerospace Corp., Bethpage, NY 11714
81. R. N. Cherdack, Burns & Roe, Inc., 283 Highway 17, Paramus, NJ 07652
82. J. F. Clarke, Office of Fusion Energy, Department of Energy, Washington, DC 20545
83. F. E. Coffman, Office of Fusion Energy, Department of Energy, Washington, DC 20545
84. D. Cohn, Massachusetts Institute of Technology, Cambridge, MA 02139
85. J. W. Coursen, Grumman Aerospace Corp., Bethpage, NY 11714
86. J. G. Crocker, EG&G Idaho, Idaho National Engineering Laboratory, P.O. Box 1625, Idaho Falls, ID 83401
87. Library, Culham Laboratory, Abingdon, Oxon, OX14 3DB, United Kingdom
88. N. A. Davies, Office of Fusion Energy, Department of Energy, Washington, DC 20545

89. H. W. Deckman, Advanced Energy Systems Laboratory, Government Research Laboratories, Exxon Research and Engineering Co., P.O. Box 8, Linden, NJ 07036
90. A. Favale, Grumman Aerospace Corporation, Bethpage, NY 11714
91. J. J. Ferrante, Large Coil Program, Bldg. 2-708, General Electric, Co., 1 River Rd., Schenectady, NY 12345
92. F. Fickett, National Bureau of Standards, Boulder, CO 80302
93. C. A. Flanagan, Westinghouse Electric Corp., Fusion Power Systems, P.O. Box 10864, Pittsburgh, PA 15236
94. H. K. Forsen, Exxon Nuclear Co., Inc., 777 106th Ave., Bellevue, WA 98009
95. J. W. French, EBASCO Services, Inc., Princeton University, P.O. Box 451, Princeton, NJ 08540
96. G. M. Fuller, McDonnell-Douglas, Dept. E-450, Bldg. 10613, Rm. 370, St. Louis, MO 63166
97. H. P. Furth, Princeton Plasma Physics Laboratory, Princeton University, P.O. Box 451, Princeton, NJ 08540
98. A. Gaines, Combustion Engineering, 100 Prospect Hill Rd., Windsor, CT 06095
99. A. Gibson, Culham Laboratory, Abingdon, Oxon, OX14 3DB, United Kingdom
100. R. W. Gould, Mail Stop 116-81, California Institute of Technology, Pasadena, CA 91125
101. E. Gregory, Airco Inc., Murray Hill, NJ 07974
102. D. S. Hackley, Large Coil Program, General Dynamics-Convair Division, P.O. Box 80847, San Diego, CA 92138
103. R. Hancox, Culham Laboratory, Abingdon, Oxon, OX14 3DB, United Kingdom
104. C. R. Head, Office of Fusion Energy, Department of Energy, Washington, DC 20545
105. C. Henning, Lawrence Livermore Laboratory, P.O. Box 808, Livermore, CA 94550
106. R. L. Hirsch, Exxon Research and Engineering Co., P.O. Box 101, Florham Park, NJ 07932
107. Anthony Hsu, Office of Fusion Energy, Department of Energy, Washington, DC 20545
108. D. L. Jassby, Princeton Plasma Physics Laboratory, Princeton University, P.O. Box 451, Princeton, NJ 08540
109. D. L. Kummer, McDonnell-Douglas Astronautics Co., East, P.O. Box 516, St. Louis, MO 63166
110. D. G. McAlees, Manager, ETF Systems Interface, Exxon Nuclear Co., Inc., Research and Technical Center, 2955 George Washington Way, Richland, WA 99352
111. V. A. Maroni, Argonne National Laboratory, 9700 South Cass Ave., Argonne, IL 60439
112. D. M. Meade, Princeton Plasma Physics Laboratory, Princeton University, P.O. Box 451, Princeton, NJ 08540
113. R. L. Miller, General Atomic Co., P.O. Box 81608, San Diego, CA 92138
114. M. R. Murphy, Office of Fusion Energy, Department of Energy, Washington, DC 20545

115. J. G. Murray, Princeton Plasma Physics Laboratory, Princeton University, P.O. Box 451, Princeton, NJ 08540
116. L. K. Price, Department of Energy, Oak Ridge Operations, P.O. Box E, Oak Ridge, TN 37830
117. J. M. Rawls, General Atomic Co., P.O. Box 81608, San Diego, CA 92138
118. P. Reardon, Princeton Plasma Physics Laboratory, Princeton University, P.O. Box 451, Princeton, NJ 08540
119. T. Reuther, Office of Fusion Energy, Department of Energy, Washington, DC 20545
120. M. Roberts, Office of Fusion Energy, Department of Energy, Washington, DC 20545
121. D. J. Rose, Department of Nuclear Engineering, Massachusetts Institute of Technology, Cambridge, MA 02139
122. M. N. Rosenbluth, School of Natural Sciences, Princeton University, P.O. Box 451, Princeton, NJ 08540
123. C. Rosner, Intermagnetics General Corp., Charles Industrial Park, New Karner Rd., Guilderland, NY 12084
124. P. H. Sager, Jr., General Atomic Co., P.O. Box 81608, San Diego, CA 92138
125. G. Schilling, Princeton Plasma Physics Laboratory, Princeton University, P.O. Box 451, Princeton, NJ 08540
126. Z. M. Shapiro, Westinghouse Electric Corp., Fusion Power Systems Department, P.O. Box 10864, Pittsburgh, PA 15236
127. G. Siegel, Tennessee Vally Authority, 1360 Commerce Union Bank Bldg., Chattanooga, TN 37401
128. A. Simon, University of Rochester, Rochester, NY 14627
129. W. M. Stacey, Jr., School of Nuclear Engineering, Georgia Institute of Technology Atlanta, GA 30332
130. J. Stekly, Magnetic Corp. of America, 179 Bear Hill Rd., Waltham, MA 02154
131. L. D. Stewart, Princeton Plasma Physics Laboratory, Princeton University, P.O. Box 451, Princeton, NJ 08540
132. C. Taylor, Controlled Thermonuclear Research, Mail Code L-382, Lawrence Livermore Laboratory, P.O. Box 808, Livermore, CA 94550
133. F. Thomas, Grumman Aerospace Corp., Bethpage, NY 11714
134. T. C. Varljen, Westinghouse Electric Corp., Fusion Power Systems, P.O. Box 10864, Pittsburgh, PA 15236
135. S. S. Waddle, Department of Energy, Oak Ridge Operations, P.O. Box E, Oak Ridge, TN 37830
136. J. Willis, Office of Fusion Energy, Department of Energy, Washington, DC 20545
137. W. Wilkes, Mound Laboratories, Miamisburg, OH 45432
138. H. H. Woodson, Department of Electrical Engineering, University of Texas, Austin, TX 78712
139. W. W. Withee, Energy Systems, General Dynamics-Convair Division, P.O. Box 80847, San Diego, CA 92138
140. S. Yoshikawa, Princeton Plasma Physics Laboratory, Princeton University, P.O. Box 451, Princeton, NJ 08540
141. J. L. Young, Large Coil Program, Westinghouse Electric Corp., 1310 Beulah Road, Pittsburgh, PA 15235

142. E. Ziurys, Office of Fusion Energy, Department of Energy, Washington, DC 20545
143. K. Zwilsky, Office of Fusion Energy, Department of Energy, Washington, DC 20545
144. Office of Assistant Manager, Energy Research and Development, Department of Energy, Oak Ridge Operations, P.O. Box E, Oak Ridge, TN 37830
- 145-282. Given distribution as shown in TID-4500, Magnetic Fusion Energy (Distribution Category UC-20 d, Fusion Systems)